Technical University of Denmark

# Analysis of Cracks in Large Diesel Engines

**Lucht, Tore; Tvergaard, Viggo; Brøndsted, Povl**

Link back to DTU Orbit

**DTU Library**
Technical Information Center of Denmark

# Analysis of Cracks in Large Diesel Engines

Tore Lucht
PhD thesis
November 2007

# Analysis of Cracks in Large Diesel Engines

## by

## *Tore Lucht*

DEPT. OF MECHANICAL ENGINEERING

Solid Mechanics

## TECHNICAL UNIVERSITY OF DENMARK

DEPT. OF RESEARCH & DEVELOPMENT

New Design

## MAN DIESEL A/S

# Preface

This thesis is submitted in partial fulfillment of the requirements for obtaining the degree of Industrial PhD in mechanical engineering. The work was carried out at both the Department of Mechanical Engineering, Solid Mechanics, Technical University of Denmark and at the Department of Research & Development, MAN Diesel A/S, Two-stroke, Copenhagen in the period October 2004 to November 2007. Supervision was received from Professor Dr. techn. Viggo Tvergaard as university supervisor and from Senior Manager, Mechanical Engineer, MSc Søren Helmuth Jensen as industrial supervisor. The Industrial PhD study was financially supported by Danish Ministry of Science, Technology and Innovation and by MAN Diesel A/S.

I am very grateful to my two supervisors for their outstanding guidance during the project.

Part of this work was carried out with Professor M.H. Ferri Aliabadi, Imperial College London, during a three and a half month stay at Imperial College London, UK. I am very grateful to professor Aliabadi for making this stay possible.

I have had close collaboration with the BEASY development group at Southampton and I have been pleased with always to get a positive and quick response from the BEASY group when I have reported errors and suggested improvements.

I wish to thank my wife, Camilla, for all of her support and understanding during this period. I am also very grateful to our daughter, Clara, whose curiosity and strong will served as a truly inspiration.

Finally I wish to thank colleagues and fellow PhD students at the Department of Mechanical Engineering, Solid Mechanics and at MAN Diesel A/S for creating a friendly and stimulating environment.

Kgs. Lyngby, November 2007

Tore Lucht

## Abstrakt (in Danish)
## Analyse af revner i store diesel motorer

Denne afhandling omhandler numerisk modellering af revnevækst udført påforskellige tilfælde af revner. Der er foretaget analyse af et virkeligt tilfælde af udmattelsesrevnevækst i en stempelkrone, som er påvirket af både højre temperaturer og tryk. Analysen er foretaget ved at simplificere geometrien til en 2D boundary element model. Der er gennemført beregninger med flere 2D boundary element modeller for at studere modellering af revnevækst med lige elementer ud fra en udviklet metode og en reference metode til at korrigere revneudvidelsesretningen. Til at modellere ikke plan revnevækst i 3D er der udviklet en metode, der udnytter fordelene i både boundary element metoden og finite element metoden. Denne metode er evalueret ved at studere revnevækst i et testemne fra en stor dieselmotor. I studiet sammenlignes beregningerne afslutningsvis med et eksperiment. I afhandlingens sidste del benyttes den sidst udviklede metode til at analysere udmattelsesrevnevækst i en stor og kompleks model af en motorramme.

# Abstract
# Analysis of Cracks in Large Diesel Engines

Numerical modelling of crack growth has been used to analyze several cases of growing cracks. The analysis of a real case of fatigue crack growth in a piston crown exposed to both high temperatures and stresses has been performed by simplification of the problem to a 2D boundary element model. Furthermore several 2D boundary element models have been used to study the general modelling of crack growth by straight elements and by the use of a proposed and a reference procedure to correct the crack extension direction. To model non-planar 3D crack growth a new method is proposed which takes advantage of both the boundary element method and the finite element method. The method is evaluated by a study of fatigue cracks in a model of an engine test specimen and the calculations are finally compared to an experiment. Finally the proposed method is used to analyze fatigue crack growth in a large and complex model of an engine frame.

# Publications

The following publications are part of the thesis:

[P1] Lucht T., 2006. DBEM analysis of axisymetric crack growth in a piston crown. *16th European Conference of Fracture*, On CD.

[P2] Lucht T., Aliabadi M.H., 2007. Correction to the crack extension direction in numerical modelling of mixed mode crack paths. *International Journal of Fracture* **143**, 195-202.

[P3] Lucht T., Aliabadi M.H., 2007. A new correction procedure to correct the predicted crack extension direction of a mixed mode crack path. *Key Engineering Materials* **348-349**, 89-92.

[P4] Lucht T., 2007. Adaptive FE analysis of non-planar 3D crack growth by the use of a BE sub model. *Submitted*

# Contents

# Chapter 1
# Introduction

In analyses of crack growth several aspects of fracture mechanics are typically involved depending on the character of the crack. In an advanced engineering system as a large diesel engine all of the typical characters of cracks are assumed to exist. Two features of crack growth that include different aspects of fracture mechanics are either growth due to monotonic loading or growth due to cyclic loading. Crack growth in large diesel engines occurs due to monotonic loading or low cycle fatigue. In general these engines are exposed to a constant cyclic loading most of their life time as they produce power for the propulsion of ships or power for stationary power plants. Due to the loading of these engines through large numbers of load cycles the primary reason for the crack growth is small material defects located in critical areas of engine components. Experiments on fatigue crack growth suggest that the crack growth depends on material, load magnitude, initial crack tip conditions, ratio of different modes of loads and mean stress (Qian and Fatemi, 1996). Analysis and numerical modelling of fatigue crack growth is an active area of research in which several methods and parameters are defined. Qian and Fatemi (1996) have concluded that there is no single parameter which gives satisfactory correlations under all loading conditions. Thus numerical evaluation of fatigue crack growth must be based on extensive comparisons between calculations and experiments.

In numerical modelling of curved crack paths in two and three dimensions one of the main problems to be solved is that the manual discretization of the domain into elements often needs to be updated automatically after each crack extension so that the elements describe the shape of the arbitrary growing crack. Among several methods the dual boundary element method (DBEM) for two dimensional elasticity (Portela et al., 1992) and two dimensional thermoelasticity (Prasad et al., 1994) solves the problem in an elegant way as only the boundary is discretized. Thus in two dimensions the crack is extended by a straight element and for the three dimensional formulation (Mi and Aliabadi, 1994, 1995) the remeshing problem is reduced by an order of magnitude as only the part of the surface that contains the crack needs to be remeshed.

The limitation of the analyzed crack growth cases to high cycle fatigue enables a primary focus on the Linear Elastic Fracture Mechanics (LEFM) in which the stress field at the crack trip is described by the three stress intensity factors each representing a mode of fracture. The stress intensity factors can be calculated through several numerical methods by the use of the crack opening displacement in special crack tip elements. Several of these special crack tip elements are described in Aliabadi (2002). One of the most recognized methods to predict the stress intensity factors is however based on the path independent J-integral (Rice, 1968).

In the analysis of fatigue crack growth the relation between the stress intensity factor and the crack growth rate was first derived by Paris and Erdogan (1963) who's expression

can be used to describe a region of linear dependence in the logarithmic plot between the growth rate and the stress intensity factor. Other researchers as for example Erdogan and Ratwani (1970) have suggested related expressions by which all of the region between the threshold stress intensity factor and the critical stress intensity factor can be described. The expression by Erdogan and Ratwani (1970) also takes into account the R ratio which is expressed by $R = K_{min}/K_{max}$. Paris law was derived for cracks only exposed to mode I loading that is the opening mode. However in case of mixed mode loading several researchers have suggested an effective stress intensity factor which can replace the mode I factor. Among these some of the most used are the expressions by Tanaka (1974) and Gerstle (1985). In Mi and Aliabadi (1995) an expression is used that is similar to that of Gerstle (1985) with the empirical constant $B = 1$.

In the analysis of fatigue crack growth it is important to calculate not only the crack growth rate but also the direction of the propagating crack. For the prediction of the crack growth direction several expressions exist. The maximum principal stress criterion (Erdogan and Sih, 1963), is one of the most commonly used among several others which in case of a general curved crack predicts that the crack growth results in $K_{II} = 0$. In case of three dimensional modelling of crack growth the criterion of minimum strain energy (Sih, 1974), is one of the most commonly used. In the literature several examples of good correlations with experiments have been reported for these criteria, however cases exist in which the correlation is less good (Qian and Fatemi, 1996).

The papers [P1] to [P4] have been written during the author's PhD study and they are enclosed in the end of this thesis. In the first paper 'DBEM analysis of axisymmetric crack growth in a piston crown' a simplified model of a piston crown for a large diesel engine is analyzed by the thermoelastic formulation of the dual boundary element method (Prasad et al., 1994). In the evaluation of the crack growth direction the effect of non-proportional loading is addressed in which different crack growth directions are predicted during the load cycle by the maximum principal stress criterion (Erdogan and Sih, 1963).

The two dimensional dual boundary formulation (Portela et al., 1992) is used in the second and third paper 'Correction to the crack extension direction in numerical modelling of mixed mode crack paths' and 'A new correction procedure to correct the predicted crack extension direction of a mixed mode crack path'. In these papers the modelling of curved cracks with straight increments are studied by proposing a new correction procedure of the extension direction and comparing it to a reference procedure by Portela et al. (1993).

The final paper 'Adaptive FE analysis of non-planar 3D crack growth by the use of a BE sub model' proposes a new method to analyze non-planar 3D crack growth. The evaluation of the stress intensity factors is based on a solution of a sub model by a 3D boundary element formulation (Mi and Aliabadi, 1994, 1995). The main advantage of the proposed method is the ability to analyze crack growth by using previously developed FE models of complex engineering structures such as in a big diesel engine.

In the final part of the thesis analysis of a complex engineering problem is demonstrated by the proposed method. Several options and choices of configurations are given and discussed. References are drawn to the papers [P1] to [P4] as the same type of prob-

lems are handled in these papers by simpler examples. Thus the papers [P1] to [P4] form a basis for the last advanced example of a crack growth analysis.

# Chapter 2
# Thermoelasticity

In components of large diesel engines as in many other engineering structures it is important to consider the effect of both mechanical and thermal loading. In many of these engineering structures the material can be assumed to be isotropic and homogeneous and the material properties can be assumed to be independent of the temperature. If these assumptions hold the basic equations of thermoelasticity can be applied. This chapter summarizes the basic equations used in the derivation of the boundary element method treated in the later chapters.

Hooke's law can be used to calculate the strains for a given point in a structure in which the stress state $\sigma_{ij}$ and the temperature change $\theta$ at the point is known

$$\varepsilon_{ij} = \frac{1+\nu}{E}\sigma_{ij} - \frac{\nu}{E}\sigma_{kk}\delta_{ij} + \alpha\theta\delta_{ij} \tag{2.1}$$

where $E$ is Young's modulus, $\nu$ is the Poisson's ratio and $\alpha$ is the coefficient of linear thermal expansion. From (2.1) it can be seen that the thermal components do not contribute to any shear strains because the free thermal expansion does not produce angular distortion in an isotropic material.

Hooke's law can also be expressed in terms of stresses by rewriting (2.1)

$$\sigma_{ij} = \frac{E}{1+\nu}\left[\varepsilon_{ij} + \frac{\nu}{1-2\nu}\varepsilon_{kk}\delta_{ij}\right] - \frac{E}{1-2\nu}\alpha\theta\delta_{ij} \tag{2.2}$$

In the formulation of the boundary element method traction is one of the main variables. In case the stress tensor is given at a point the tractions at this point are defied by

$$t_i = \sigma_{ij}n_j \tag{2.3}$$

where $n_j$ are the components of a unit normal.

Navier's equations express the conditions of equilibrium in terms of displacements. These equations can be considered as the governing equations of elasticity and they are central equations in the derivation of the boundary element method. These equations can be derived from substituting the stress-strain relation (2.2) into the equation of equilibrium given as

$$\sigma_{ij,j} + b_i = 0 \tag{2.4}$$

using the Cauchy's strain displacement relation given by

$$\varepsilon_{ij} = \frac{1}{2}(u_{i,j} + u_{j,i}) \tag{2.5}$$

where $b_i$ are the components of the body force. The final expression of Navier's equation in terms of displacements is

$$\frac{E}{2(1+\nu)}u_{i,kk} + \frac{E}{2(1+\nu)(1-2\nu)}u_{k,ik} - \frac{E}{(1-2\nu)}\alpha\theta_{,i} + b_i = 0 \qquad (2.6)$$

In the derivation of the above equations it is assumed that the temperature is known in all the points of a given domain. This will not be the case in general and thus the heat conduction equation has to be used expressed by

$$\lambda\theta_{,ii} = \bar{\theta}\frac{E}{(1-2\nu)}\alpha\delta_{ij}\dot{\varepsilon}_{ij} + c\dot{\theta} \qquad (2.7)$$

as in dell'Erba (1999), where $\bar{\theta}$ denotes the reference absolute temperature for the state of zero stress and strain, $\lambda$ is the conductivity and $c$ is the specific heat. In equation (2.7) the temperature and strain field are coupled and that is because, the cooling and heating are associated with a change of volume. Equation (2.7) can in general be used in a much more simple form, steady state heat conduction, as the the loads are applied slowly to a domain and as all of the resulting diffusive processes are completed, the time dependency vanishes. Thus the equation is reduced to the Laplace's equation

$$\theta_{,ii} = 0 \qquad (2.8)$$

# Chapter 3
# Fracture mechanics

In the present chapter some of the basic definitions of fracture mechanics are summarized which form the grounding in the presented crack growth analyses of this thesis. The summary is based on Kanninen and Popelar (1985) and Anderson (1995) together with the references given in the chapter.

## 3.1 Origin of Linear Elastic Fracture Mechanics

In the formulation of the fracture mechanical theories some of the first work is done by Inglis (1913) in a study of stress concentrations at the end of an elliptical hole in tension loaded plates. For a perfectly circular hole Inglis showed that the relation between the most highly stressed point on the edge of the hole $\sigma$ and the stress action at boundary of the plate $\sigma_{norm}$ is $\sigma = 3\sigma_{norm}$. When the length of an ellipse is kept constant and the width is close to zero the ellipse becomes flat and it describes the shape of a sharp crack. For the crack shaped elliptical hole Inglis showed that infinite stress was predicted at the tip of the crack.

At the time when Inglis published these results it was quite a paradox since no material can sustain infinite stress. The paradox motivated Griffith in the development of a fracture theory based on energy rather than stresses. Thus postulating that a crack can initiate or grow only if such a process causes the total energy to decrease or remain constant. Griffith defined the total energy by the sum of, the work required by the crack to create a new surface and the potential energy available from both internal strain energy and external forces. For an elastic brittle material like glass, the energy balance can be expressed by

$$\frac{dW}{dA} - \frac{dU}{da} = \gamma \tag{3.1}$$

where $W$ is external work done on the domain, $U$ is the internal strain energy, $\gamma$ is the surface energy of the material, $a$ is the crack length and $A$ is the crack surface area. The right hand side of equation (3.1) was later used to define a parameter called the strain energy release rate, expressing the driving force on the crack. Based on the energy balance Griffith derived an expression of the remote stress that was required for the crack to grow in an infinitely wide plate for an ideally brittle solid

$$\sigma_f = \left(\frac{2E\gamma_s}{\pi a}\right)^{\frac{1}{2}} \tag{3.2}$$

where $E$ is Young's modulus, $2a$ is the length of the crack and $\gamma_s$ is the surface energy of the material which for an ideally brittle solid reflects the total energy of broken bonds.

Griffith was able to show good agrement between (3.2) and the experimental fracture strength of glass. The Griffith equation however underestimates the fracture strength of metal. When a crack propagates in a metal an additional energy dissipation is obtained from the dislocation motion which occurs in the vicinity of the crack tip. A modified expression of the Griffith equation for materials that are capable of plastic flow was suggested independently by Irwin (1948) and Orowan (1948)

$$\sigma_f = \left(\frac{2E(\gamma_s + \gamma_p)}{\pi a}\right)^{\frac{1}{2}} \tag{3.3}$$

In this expression $\gamma_p$ is the plastic work per unit area of created surface and it is typically much larger than $\gamma_s$. The two fracture criteria suggest that as the ductility of a brittle material is increased one needs to take into account the plastic flow in front of the crack.

The Griffith theory, its extension to metals by Irwin (1948) and Orowan (1948) and later the connection between Griffith's global crack parameter and the quantifiable local crack tip parameters (Irwin, 1957) were such important contributions to Linear Elastic Fracture Mechanics that the theory is also know as Griffith-Irwin fracture mechanics or less often Griffith-Irwin-Orowan theory.

Prediction of infinite stress at the crack tip by the linear elastic fracture is in practice known to create a plastic zone at the crack tip. As long as the size of the plastic zone is sufficiently small the assumption of LEFM is valid. As it will be shown in the following section the size of the plastic zone can be estimated. Thus elastic analyses can be shown to be valid for many engineering problems like fatigue crack growth in large diesel engines.

## 3.2   Some basic definitions in LEFM

Westergaard was among the first to publish a technique to analyze stresses and displacements ahead of a sharp crack tip (Westergaard, 1939). This approach was adopted by Irwin (1957) as Irwin showed that the stresses and displacements near the crack tip could be described by a single constant that was related to the energy release rate. If a polar coordinate system with origin at the crack tip is defined, the stresses $\sigma_{ij}$ at the point $P$ near the crack tip are given by

$$\sigma_{ij} = \left(\frac{k}{\sqrt{r}}\right)f_{ij}(\theta) + \sum_{m=0}^{\infty} A_m r^{\frac{m}{2}} g_{ij}^m(\theta) \tag{3.4}$$

where r and $\theta$ are defined in figure 3.1, k is a constant and $f_{ij}$ is a function of $\theta$. The second term of (3.4) is a higher order term that depends on the geometry of the domain. When the point $P$ is moved closer to the crack tip, $r$ approaches zero and the first term of (3.4) dominates as the second term gives values that are constant or tend to zero. Thus in the vicinity of the crack tip the stresses vary with $1/\sqrt{r}$ independently of the geometry of the cracked body. Furthermore the singular nature of the stresses is demonstrated from (3.4) as the stresses are asymptotic to $r = 0$. In addition it can be shown that the displacements near the crack tip vary with $\sqrt{r}$.
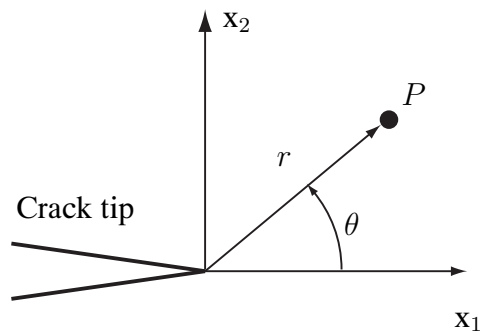
*Figure 3.1*    Local coordinates at the tip of a straight crack

To describe any cracked configuration three basic modes of fracture are considered as shown on figure 3.2. The first mode of fracture, mode I is the simplest and most studied mode of fracture. In mode I the load is applied normal to the plane of the crack and the resulting displacements describe an in-plane opening of the crack, figure 3.2.a. When a crack is subjected to Mode II the loading is applied in-plane and parallel to the crack surface and the displacements describe a slide of the two crack surfaces relative to each other, figure 3.2.b. In the last mode of fracture, Mode III the loading is applied out of the plane and parallel to the crack surface and the displacements describe a tearing of the crack surfaces relative to each other, figure 3.2.c.
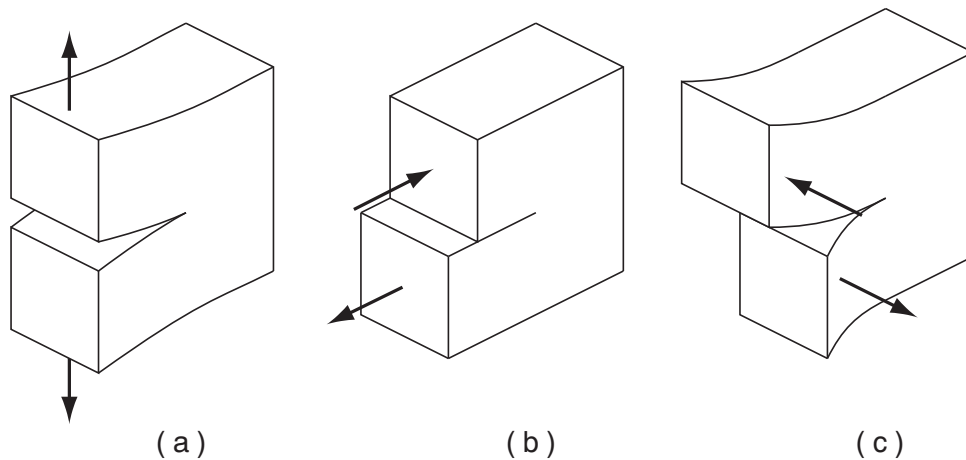


*Figure 3.2*    Definition of the three basic modes of loading and deformation . (a) Mode I, opening mode (b) Mode II, sliding mode (c) Mode III, tearing mode

For each of these modes of fracture the stress processes the $1/\sqrt{r}$ singularity. The stress intensity factor is more convenient to express as $K = k\sqrt{2\pi}$ and the trigonometric function $f_{ij}$ depends on the mode of fracture. Thus three different stress intensity factors exist that are $K_I$, $K_{II}$ and $K_{III}$. In a mixed mode problem the resulting stress state in the vicinity of the crack is the sum of each of the three modes. Irwin (1957) showed that in a general plane elastic crack problem the stress state in the vicinity of the crack can be

described using the local coordinate system illustrated in figure 3.1 as

$$
\sigma_{11} = \frac{K_I}{\sqrt{2\pi r}} \cos\frac{\theta}{2} \left[ 1 - \sin\frac{\theta}{2}\sin\frac{3\theta}{2} \right] - \frac{K_{II}}{\sqrt{2\pi r}} \sin\frac{\theta}{2} \left[ 2 + \cos\frac{\theta}{2}\cos\frac{3\theta}{2} \right]
$$

$$
\sigma_{22} = \frac{K_I}{\sqrt{2\pi r}} \cos\frac{\theta}{2} \left[ 1 + \sin\frac{\theta}{2}\sin\frac{3\theta}{2} \right] + \frac{K_{II}}{\sqrt{2\pi r}} \sin\frac{\theta}{2}\cos\frac{\theta}{2}\cos\frac{3\theta}{2} \tag{3.5}
$$

$$
\sigma_{12} = \frac{K_I}{\sqrt{2\pi r}} \sin\frac{\theta}{2}\cos\frac{\theta}{2}\cos\frac{3\theta}{2} + \frac{K_{II}}{\sqrt{2\pi r}} \cos\frac{\theta}{2} \left[ 1 - \sin\frac{\theta}{2}\cos\frac{3\theta}{2} \right]
$$

and for the displacements

$$
\begin{aligned}
u_1 = \frac{1}{4\mu}\sqrt{\frac{2r}{\pi}} \Bigg[ & K_I\left( (2\kappa - 1)\cos\frac{\theta}{2} - \cos\frac{3\theta}{2} \right) \\
& + K_{II}\left( (2\kappa + 3)\sin\frac{\theta}{2} + \sin\frac{3\theta}{2} \right) \Bigg]
\end{aligned}
$$

$$
\begin{aligned}
u_2 = \frac{1}{4\mu}\sqrt{\frac{2r}{\pi}} \Bigg[ & K_I\left( (2\kappa + 1)\sin\frac{\theta}{2} - \sin\frac{3\theta}{2} \right) \\
& + K_{II}\left( (2\kappa - 3)\cos\frac{\theta}{2} + \cos\frac{3\theta}{2} \right) \Bigg]
\end{aligned} \tag{3.6}
$$

Where $K_I$ and $K_{II}$ are the stress intensity factors of the opening and sliding modes. The constant $\mu$ is the shear modulus and $\kappa$ is given by $(3 - 4\nu)$ for plain strain and $(3 - 4\nu)(1 + \nu)$ for plain stress where $\nu$ is the Poisson's ratio. In this general plane elastic crack problem the stress intensity factor $K_{III}$ is not present since no out of plane loading or deformation is allowed.

As the size of the plastic zone is an important parameter to the validity of LEFM, expressions to estimate the size of the zone are summarized. In the first approximation it is assumed that the boundary between the elastic and plastic region occurs where the stress of an elastic analysis exceeds the yield stress. Thus for a mode I problem the radius of the plastic zone can be estimated as the stresses given by (3.5) satisfy the yield criterion. Inserting $r = r_y$, $\sigma_{22} = \sigma_{ys}$ and $\theta = 0$ into (3.5) yields

$$
r_y = \frac{1}{2\pi}\left( \frac{K_I}{\sigma_{ys}} \right)^2 \tag{3.7}
$$

The size of plastic zone $r_y$ is demonstrated in figure 3.3. A more precise estimate can be obtained as yielding is allowed and the stresses are allowed to redistribute in order to satisfy equilibrium. The plastic zone must increase in size in order to obtain the extra forces in the elastic material, illustrated by the area of the elastic curve $\sigma_{yy}$ above $\sigma_{ys}$ in figure 3.3. Thus a second estimate of the plastic zone is obtained by a simple force balance as the strain hardening of the material is neglected

$$
\sigma_{ys}r_p = \int_0^{r_y} \sigma_{yy}\,dr = \int_0^{r_y} \frac{K_I}{\sqrt{2\pi r}}\,dr \tag{3.8}
$$

by integration and rewriting the expression for $r_p$

$$r_p = \frac{1}{\pi}\left(\frac{K_I}{\sigma_{ys}}\right)^2 \tag{3.9}$$

From the expression it is seen that the value of $r_p$ is twice the value of the first order estimate $r_y$.
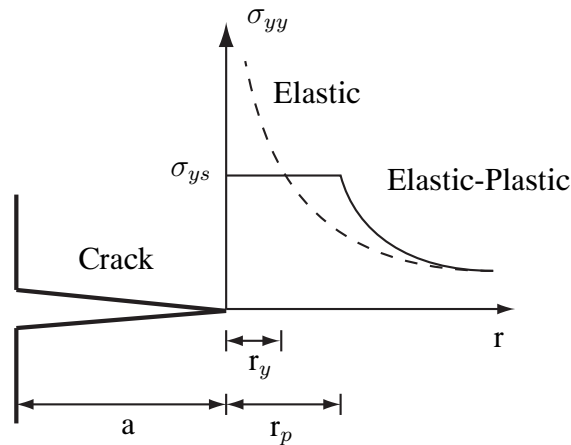


*Figure 3.3* Estimate of plastic zone size (Elastic estimate $r_y$ and elastic-plastic estimate $r_p$) calculated for mode I loading and in the plane of the crack $\theta = 0$

## 3.3 The J-integral

The integral was first derived by Eshelby (1956), and Rice (1968) was the first to recognize its potential use in fracture mechanics where it has been used to analyze crack growth for LEFM problems as well as for elastic-plastic deformations in non-linear elastics.
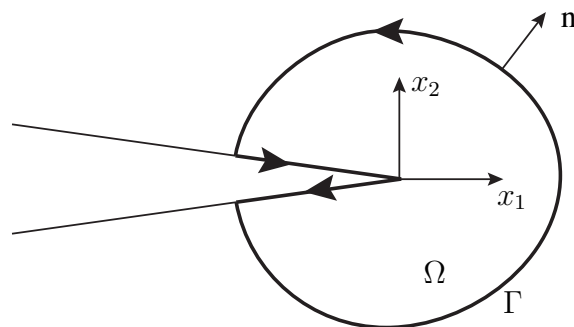


*Figure 3.4* Definition of the path independent J-integral

For a general contour around the crack front as illustrated in figure 3.4 the integral is

expressed by

$$J = \int_{\Gamma}(Wn_1 - t_iu_{i,1})d\Gamma \tag{3.10}$$

where $\Gamma$ is an arbitrary closed contour around the crack front, oriented in an anti clockwise direction, $n_1$ is the component of the outward normal along the crack axis $x_1$, $t_i$ are the traction components, $u_{i,1}$ are the derivatives of the displacement components with respect to $x_1$ and $W$ is the strain energy density given by

$$W = \int_0^{\varepsilon} \sigma_{ij}d\varepsilon_{ij} \tag{3.11}$$

The J-integral can be related to the stress intensity factors and for a linear elastic material the relations is

$$J = \frac{1 - \nu^2}{E}K_I^2 + \frac{1 - \nu^2}{E}K_{II}^2 \tag{3.12}$$

Other path independent integrals have been proposed in the literature in applications of other fields like for example thermal effects. The path independent integral $\hat{J}$ proposed by Kishimoto et al. (1980) for thermoelasticity can be written as

$$\hat{J} = \int_{\Gamma}(Wn_1 - t_iu_{i,1})d\Gamma + \int_{\Omega}\alpha\sigma_{kk}\theta_{,1}d\Omega \tag{3.13}$$

The thermoelastic integral has an additional term when compared to the integral by Rice. The additional term is defined in the domain enclosed by the contour $\Gamma$.

As it can be seen from (3.12) the J-integral is related to a combination of $K_I$ and $K_{II}$. It is however possible to decouple the relation by a division of displacements and stresses into symmetric and anti-symmetric components relative to the crack axis so that $K_I$ and $K_{II}$ can be calculated separately by the J-integral. The decomposition is demonstrated for a two dimensional dual boundary element formulation by Portela et al. (1992)

## 3.4   Fatigue crack growth

The growth of a crack during cyclic loading is characterized as fatigue crack growth. Due to the cyclic nature of the loading the magnitude of the loading required for the crack to grow is much less as compared to crack growth by monotonic loading. The relative low magnitude of the fatigue loading enables the use of LEFM in many analyses of fatigue crack growth.

Among the first crack growth laws of fatigue was the formulation by Paris et al. (1961) expressed by

$$\frac{da}{dN} = f(\Delta K) \tag{3.14}$$

where a is the length of the crack, N is the number of cycles and $\Delta K = K_{max} - K_{min}$. The crack growth law suggests that the crack growth rate $(da/dN)$ can be calculated by a function of the change in the stress intensity factor $\Delta K$ during one load cycle. By experiments the general relation between $(da/dN)$ and $\Delta K$ can be demonstrated by the curve illustrated in figure 3.5. The curve can be divided into three regions. In Region I the relation between the crack growth rate and $\Delta K$ is described near the threshold value where the crack is about to stop propagating. The curve is linear in Region II and in Region III $K_{max}$ is approaching the fracture toughness of the material and the crack growth rate accelerates.
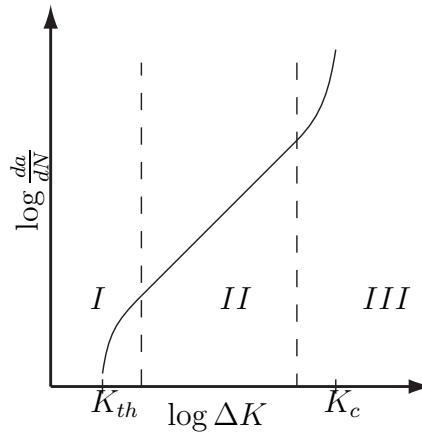


*Figure 3.5*    Typical relation between the fatigue load $\Delta K$ and the crack growth rate for metals

Several crack growth laws have been suggested in the form of (3.14). The simplest and most recognized is known as Paris law and it treats fatigue crack growth in Region II. This crack growth law was proposed by Paris and Erdogan (1963) and can be expressed by

$$\frac{da}{dN} = C(\Delta K)^m \tag{3.15}$$

where C and m are material constants. Other crack growth laws tend to describe fatigue crack growth in the two remaining regions and the effect of the R ratio given by $R = K_{max}/K_{min}$. This ratio has shown to be very important in fatigue crack growth and when this ratio is increased a tendency to a left shift of the curve has been observed.

## 3.5 Crack growth direction criteria

Several mixed mode fracture criteria have been proposed to determine the crack growth direction such as the well known maximum principal stress criterion proposed by Erdogan and Sih (1963) for two dimensional problems. Another well known criterion is the strain energy density criterion for both two dimensional problems (Sih, 1974) and for three dimensional problems (Sih and Cha, 1974).

*Maximum stress criterion*

This criterion predicts that the crack will grow perpendicular to the maximum principal stress. Thus transforming the stress near the crack tip (3.5) into the local coordinate system will result in

$$\sigma_{\theta\theta} = \frac{1}{\sqrt{2\pi r}} \cos\frac{\theta}{2}[K_I \cos^2\frac{\theta}{2} - \frac{3}{2}K_{II}\sin\theta]$$

$$\sigma_{r\theta} = \frac{1}{2\sqrt{2\pi r}} \cos\frac{\theta}{2}[K_I \sin\theta + K_{II}(3\cos\theta - 1)]$$

(3.16)

where $\sigma_{\theta\theta}$ is the stress perpendicular to the direction given by $\theta$ and $\sigma_{r\theta}$ is the shear stress in a given direction. The maximum principal direction is defined by zero shear stress and from (3.16) this condition is written as

$$\sigma_{r\theta} = K_I sin\theta + K_{II}(3\cos\theta - 1) = 0 \tag{3.17}$$

Thus the crack growth angle $\theta$ is defined by

$$\theta = 2\tan^{-1}\left(\frac{K_I}{4K_{II}} \pm \frac{1}{4}\sqrt{\left(\frac{K_I}{K_{II}}\right)^2 + 8}\right) \tag{3.18}$$

*Strain energy density criterion*

By the use of this criterion the crack extension angle is determined by the direction that gives the minimum strain energy density factor $S(\theta)$. The strain energy density factor can be calculated for any crack extension by

$$S(\theta) = a_{11}K_I^2 + 2a_{12}K_I K_{II} + a_{22}K_{II}^2 + a_{33}K_{III}^2 \tag{3.19}$$

Where

$$a_{11} = \frac{1}{16\pi\mu}(3 - 4\nu - \cos\theta)(1 + \cos\theta)$$

$$a_{12} = \frac{1}{8\pi\mu}\sin\theta(\cos\theta - 1 + 2\nu)$$

$$a_{22} = \frac{1}{16\pi\mu}\left(4(1-\nu)(1-\cos\theta) + (3\cos\theta - 1)(1 + \cos\theta)\right) \tag{3.20}$$

$$a_{33} = \frac{1}{4\pi\mu}$$

Three assumptions are connected to this criterion for three dimensions

- The direction of crack propagation at any point along the crack front is determined by the location on a spherical surface of the region with the minimum value of the strain energy density factor $S(\theta)$.

- Crack extension occurs when the strain energy density factor in the region determined by the first hypothesis, $S = S_{min}$, reaches a critical value $S_c$.

- The length, $r_0$, of the initial crack extension is assumed to be proportional to $S_{min}$ such that $S_{min}/r_0$ remains constant along the new crack front.

# Chapter 4
# Boundary integral equations

The two dimensional thermoelastic formulation of the Dual Boundary Element Method (DBEM) has been used to develop a program which is used to study several cases of cracks in thermal and mechanical loaded structures. The general boundary element formulation produces a singular system matrix when both coplanar surfaces of a crack are modelled, a problem DBEM solves by applying a different set of equations on each crack surface. Displacements and tractions are related by the displacement equations on one crack surface and the traction equations on the other crack surface. A detailed derivation of these equations are given in this chapter. In case of thermal exposure a body force term is present in these equations. The body force term can be calculated when the values of temperature change and flux are known. When the temperature equations are applied on one crack surface and flux equations are applied on the other crack surface it is possible to determine the values of temperature change and flux.

The boundary element method is all about solution of integral equations and in particular solution of singular boundary integral equations. The method consists of three main steps which will be described in the following two chapters. The first step is the formulation of integral equations based on the partial differential equations describing the behavior of the variables inside and on the boundary of the domain. The second step is the transformation of the integral equations to describe values on only the boundary of the domain. The third step is the numerical solutions of these equations.

## 4.1   Steady state heat conduction

This section treats the temperature and flux integral equations and the main focus will be on the transformation of the domain integrals to integrals relating only boundary values. The main references are Aliabadi (2002), Wrobel (2002), Becker (1992) and dell'Erba (1999)

The notation of points belonging to the domain $\Omega$ is $X$ and the points denoted by $x$ are the points on the boundary $\Gamma$ of the domain. Furthermore the source points in $\Omega$ and $\Gamma$ are denoted $X'$ and $x'$ respectively while the notation of the field points are $X$ and $x$ respectively.

The distance between the source point and field point is a central variable in the integral equation and this is the reason for the singular nature of the integral equations. The distance $r$ can be expressed by

$$r = \sqrt{r_i r_i} \qquad \text{where} \qquad r_i = X_i - X_i' \tag{4.1}$$

and the field points, source points and the distance $r$ are illustrated in figure 4.1.

### 4.1.1 Temperature equation for an internal point

The temperature integral equation can be derived from the Laplace equation for steady state heat conduction (2.8) by use of Green's second identity as in Wrobel (2002) or by using a weighted residual statement as in Brebbia and Dominguez (1977) to give

$$\theta(X') - \int_{\Gamma} q^*(X', x)\theta(x)d\Gamma(x) = -\int_{\Gamma} \theta^*(X', x)q(x)d\Gamma(x) \tag{4.2}$$

in which $\theta$ represents the temperature change and $q$ represents the flux. The unknown function $\theta$ satisfies the equation governing steady state thermoelasticity (2.8) and $\theta^*$ is known as the fundamental solution of the Laplace equation. The fundamental solution $\theta^*$ of the differential equation is the solution defined in an unbounded region for a point source of unit strength. The fundamental fields $\theta^*$ and $q^*$ can be expressed by (Prasad et al., 1994)

$$\theta^*(X', x) = -\frac{1}{2\pi\lambda}\ln r \tag{4.3}$$

and

$$q^*(X', x) = \frac{r_{,k}n_k}{2\pi r} \tag{4.4}$$

Where $\lambda$ is the thermal conductivity. By the temperature equation (4.2) the temperature of an internal point $X'$ can be calculated by the temperature and flux on the boundary of the domain.

### 4.1.2 Temperature equation for a boundary point

To derive the temperature equation for boundary points only the internal point $X'$ is moved to the boundary. As a result the source point and field point can coincide, $x = x'$, resulting in singular terms in the integrals including the fundamental functions $\theta^*$ and $q^*$ because of $r = 0$. To determine the values of the integrals they are each examined in a limiting process $x' \to X'$ where a small part of the surface ($\Gamma_\epsilon$) which contains the singular point is replaced by the semi circular surface ($\Gamma_\epsilon^*$) with radius $\epsilon$ shown in figure 4.1.b.

From the polar coordinate system in figure 4.1.b it is possible to derive the following relations for the semi circular boundary

$$\begin{aligned} r_1 &= \varepsilon\cos\phi & r_{,1} &= n_1 = \cos\phi \\ r_2 &= \varepsilon\sin\phi & r_{,2} &= n_2 = \sin\phi \\ r_{,i}n_i &= 1 & d\Gamma(\Gamma_\varepsilon^*) &= \varepsilon d\phi \end{aligned} \tag{4.5}$$

The definition of the new boundary $\Gamma = \lim_{\epsilon \to 0}(\Gamma - \Gamma_\epsilon + \Gamma_\epsilon^*)$ can be included in the integral equation to give

$$\theta(x') - \lim_{\varepsilon \to 0}\int_{\Gamma - \Gamma_\varepsilon + \Gamma_\varepsilon^*} q^*(x', x)\theta(x)d\Gamma(x) = -\lim_{\varepsilon \to 0}\int_{\Gamma - \Gamma_\varepsilon + \Gamma_\varepsilon^*} \theta^*(x', x)q(x)d\Gamma(x) \tag{4.6}$$

Since the integration of these integrals are not straight forward they are investigated separately in the remaining subsection. Both integrals can be regularized by the use of the
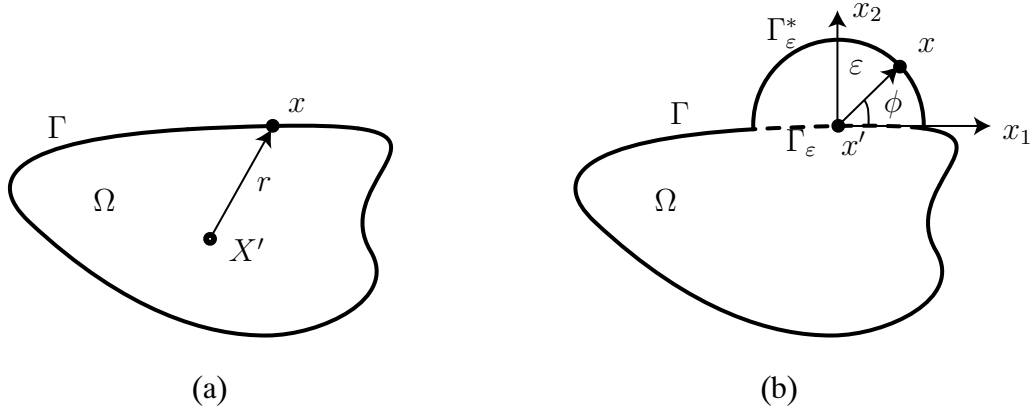
Figure 4.1   Two-dimensional domain (a) Internal source point $X'$ (b) Boundary source point $x'$ surrounded by a semi circular surface to determine values of singular integrals

first order Taylor expansion for which it is assumed that the temperature $\theta$ and flux $q$ are Hölder continuous on $\Omega + \Gamma$. The requirement can be expressed for the temperature field as

$$\theta \in C^{n=0,\alpha} \quad \text{if } C > 0 \text{ and } 0 < \alpha \leq 1 \text{ exist such that} \quad |\theta(x') - \theta(x)| \leq C|r|^\alpha \quad (4.7)$$

which applies to the derivatives of the fields up to the order of $n$. The integral on the right hand side of equation (4.6) can be rewritten by the use of the first term of a Taylor expansion of the integrand $q$ about the singular point $x'$

$$\lim_{\varepsilon \to 0} \int_{\Gamma - \Gamma_\varepsilon + \Gamma_\varepsilon^*} \theta^*(x', x) q(x) d\Gamma(x) = \lim_{\varepsilon \to 0} \int_{\Gamma_\varepsilon^*} \theta^*(x', x)[q(x) - q(x')] d\Gamma(x)$$

$$+ q(x') \lim_{\varepsilon \to 0} \int_{\Gamma_\varepsilon^*} \theta^*(x', x) d\Gamma(x) \qquad (4.8)$$

$$+ \lim_{\varepsilon \to 0} \int_{\Gamma - \Gamma_\varepsilon} \theta^*(x', x) q(x) d\Gamma(x)$$

$$= I_1 + I_2 + I_3$$

From which it can be seen that $I_1 \to 0$ as $\varepsilon \to 0$ due to the continuity of the flux function $q$ as $x$ goes to $x'$. Further since $\Gamma_\varepsilon \to 0$ for $\varepsilon \to 0$ and since the integration over $\Gamma - \Gamma_\varepsilon$ does not lead to any singular integrands, $I_3$ can be rewritten to give

$$I_3 = \lim_{\varepsilon \to 0} \int_{\Gamma - \Gamma_\varepsilon} \theta^*(x', x) q(x) d\Gamma(x) = \int_\Gamma \theta^*(x', x) q(x) d\Gamma(x) \qquad (4.9)$$

The integral $I_2$ can be solved using the polar coordinates

$$I_2 = q(x') \lim_{\varepsilon \to 0} \int_{\Gamma_\varepsilon^*} \theta^*(x', x) d\Gamma(x) = q(x') \lim_{\varepsilon \to 0} \int_{\phi_1}^{\phi_2} -\frac{1}{2\pi\lambda} \varepsilon \ln(\varepsilon) d\phi = 0 \qquad (4.10)$$

Thus the right hand side integral of equation (4.6) can be written as

$$\lim_{\varepsilon \to 0} \int_{\Gamma - \Gamma_\varepsilon + \Gamma_\varepsilon^*} \theta^*(x', x) q(x) d\Gamma(x) = \int_\Gamma \theta^*(x', x) q(x) d\Gamma(x) \qquad (4.11)$$

The left hand side of equation (4.6) is now investigated as the integrand is rewritten by the use of the first term of a Taylor expansion of the integrand $\theta$ about $x'$

$$\lim_{\varepsilon \to 0} \int_{\Gamma - \Gamma_\varepsilon + \Gamma_\varepsilon^*} q^*(x', x) \theta(x) d\Gamma(x) = \lim_{\varepsilon \to 0} \int_{\Gamma_\varepsilon^*} q^*(x', x) [\theta(x) - \theta(x')] d\Gamma(x)$$
$$+ \theta(x') \lim_{\varepsilon \to 0} \int_{\Gamma_\varepsilon^*} q^*(x', x) d\Gamma(x) \qquad (4.12)$$
$$+ \lim_{\varepsilon \to 0} \int_{\Gamma - \Gamma_\varepsilon} q^*(x', x) \theta(x) d\Gamma(x)$$
$$= I_1' + I_2' + I_3'$$

For which it can be seen that $I_1' \to 0$ as $\varepsilon \to 0$ due to the continuity of the temperature function $\theta$ as $x$ goes to $x'$. Since $\Gamma_\varepsilon \to 0$ for $\varepsilon \to 0$ and since the integration over $\Gamma - \Gamma_\varepsilon$ does not lead to any singular integrands, $I_3'$ can be rewritten to give

$$I_3' = \lim_{\varepsilon \to 0} \int_{\Gamma - \Gamma_\varepsilon} q^*(x', x) \theta(x) d\Gamma(x) = \int_\Gamma q^*(x', x) \theta(x) d\Gamma(x) \qquad (4.13)$$

Then $I_2'$ can be calculated using the definitions for the semi circular boundary in (4.5) to give

$$I_2' = \theta(x') \lim_{\varepsilon \to 0} \int_{\Gamma_\varepsilon^*} q^*(x', x) d\Gamma(x) = \theta(x') \lim_{\varepsilon \to 0} \int_{\phi_1}^{\phi_2} \left( \frac{1}{2\pi\varepsilon} \right) \varepsilon d\phi = \beta\theta(x') \qquad (4.14)$$

If the surface is smooth then $\phi_2 - \phi_1 = \pi$ and then $\beta = \frac{1}{2}$. The integral on the left hand side can now be written as

$$\lim_{\varepsilon \to 0} \int_{\Gamma - \Gamma_\varepsilon + \Gamma_\varepsilon^*} q^*(x', x) \theta(x) d\Gamma(x) = \int_\Gamma q^*(x', x) \theta(x) d\Gamma(x) + \beta\theta(x') \qquad (4.15)$$

By inserting (4.11) and (4.15) into (4.6) the temperature equation for a boundary point x' can now be written as

$$C(x')\theta(x') - \int_\Gamma q^*(x', x) \theta(x) d\Gamma(x) = - \int_\Gamma \theta^*(x', x) q(x) d\Gamma(x) \qquad (4.16)$$

Where $C(x') = \frac{1}{2}$ for a smooth surface. However as it will be discussed in the next chapter the constant $C$ does not need to be calculated explicitly for each boundary point.

### 4.1.3   Flux equation for a boundary point

The flux boundary integral equation is derived from the temperature equation for an internal point $X'$ (4.2) together with the definition of the flux, that is

$$q = -\lambda \frac{\partial \theta}{\partial X_i} n_i = -\lambda \theta_{,i} n_i \tag{4.17}$$

The temperature integral equation is differentiated to give

$$\frac{\partial \theta(X')}{\partial X_i'} - \int_\Gamma \frac{\partial q^*(X', x)}{\partial X_i'} \theta(x) d\Gamma(x) = - \int_\Gamma \frac{\partial \theta^*(X', x)}{\partial X_i'} q(x) d\Gamma(x) \tag{4.18}$$

where

$$\frac{\partial \theta^*(X', x)}{\partial X_i'} = -\frac{r_{,i}}{2\pi \lambda r}$$

and

$$\frac{\partial q^*(X', x)}{\partial X_i'} = \frac{1}{2\pi r^2} [2 r_{,i} r_{,j} n_j - n_i]$$

The integrands $\partial \theta^*(X', x)/\partial X_i'$ and $\partial q^*(X', x)/\partial X_i'$ are weakly singular $0(1/r)$ and strongly singular $0(1/r^2)$ respectively. A discussion on the continuity requirements for these integrals can be found in Krishnasmy et al. (1992). It is assumed in the following regulation of the integrals that $x'$ is on a smooth boundary and both $q$ and $\theta$ are $C^{0,\alpha}$ and $C^{1,\alpha}$ continuous respectively. The semi circular boundary formulation (4.5) of the integrals is now introduced

$$\frac{\partial \theta(x')}{\partial x_i'} - \lim_{\varepsilon \to 0} \int_{\Gamma - \Gamma_\varepsilon + \Gamma_\varepsilon^*} \frac{\partial q^*(x', x)}{\partial x_i'} \theta(x) d\Gamma(x) = - \lim_{\varepsilon \to 0} \int_{\Gamma - \Gamma_\varepsilon + \Gamma_\varepsilon^*} \frac{\partial \theta^*(x', x)}{\partial x_i'} q(x) d\Gamma(x) \tag{4.19}$$

The integral on the right hand side can now be rewritten using the definition of flux and the first term of the Taylor expansion of the integrand $q$ about $x'$, that is

$$\lim_{\varepsilon \to 0} \int_{\Gamma - \Gamma_\varepsilon + \Gamma_\varepsilon^*} \frac{\partial \theta^*(x', x)}{\partial x_i'} q(x) d\Gamma(x)$$

$$= \lim_{\varepsilon \to 0} \int_{\Gamma - \Gamma_\varepsilon} \frac{\partial \theta^*(x', x)}{\partial x_i'} q(x) d\Gamma(x) + \lim_{\varepsilon \to 0} \int_{\Gamma_\varepsilon^*} \frac{\partial \theta^*(x', x)}{\partial x_i'} [-\lambda \theta_{,k}(x) n_k(x)] d\Gamma(x)$$

$$= \lim_{\varepsilon \to 0} \int_{\Gamma - \Gamma_\varepsilon} \frac{\partial \theta^*(x', x)}{\partial x_i'} q(x) d\Gamma(x) - \lambda \lim_{\varepsilon \to 0} \int_{\Gamma_\varepsilon^*} \frac{\theta^*(x', x)}{\partial x_i'} n_k(x) [\theta_{,k}(x) - \theta_{,k}(x')] d\Gamma(x)$$

$$- \lambda \theta_{,k}(x') \lim_{\varepsilon \to 0} \int_{\Gamma_\varepsilon^*} \frac{\partial \theta^*(x', x)}{\partial x_i'} n_k(x) d\Gamma(x)$$

$$= I_1 + I_2 + I_3 \tag{4.20}$$

for which $I_2 \to 0$ as $\varepsilon \to 0$. The improper integral $I_1$ of (4.20) can be written in the Cauchy principal value sense

$$I_1 = \lim_{\varepsilon \to 0} \int_{\Gamma - \Gamma_\varepsilon} \frac{\partial \theta^*(x', x)}{\partial x_i'} q(x) d\Gamma(x) = \int_\Gamma \frac{\partial \theta^*(x', x)}{\partial x_i'} q(x) d\Gamma(x) \tag{4.21}$$

where $\fint$ is the Cauchy principal value integral. The last integral $I_3$ can be calculated by introducing polar coordinates, (4.5), to give

$$
\begin{aligned}
I_3 =& -\lambda\theta_{,k}(x')\lim_{\varepsilon\to 0}\int_{\Gamma_\varepsilon^*}\frac{\partial\theta^*(x',x)}{\partial x_i'}n_k(x)d\Gamma(x)\\
=& -\lambda\theta_{,k}(x')\lim_{\varepsilon\to 0}\int_0^\pi -\frac{r_{,i}n_k}{2\pi\lambda\varepsilon}\varepsilon d\phi\\
=& \frac{\theta_{,i}(x')}{4}
\end{aligned}
\tag{4.22}
$$

The right side of (4.19) can be rewritten by the use of equation (4.21) and (4.22) to give

$$
\lim_{\varepsilon\to 0}\int_{\Gamma-\Gamma_\varepsilon+\Gamma_\varepsilon^*}\frac{\partial\theta^*(x',x)}{\partial x_i'}q(x)d\Gamma(x) = \fint_\Gamma\frac{\partial\theta^*(x',x)}{\partial x_i'}q(x)d\Gamma(x) + \frac{\theta_{,i}(x')}{4}
\tag{4.23}
$$

The left hand side of (4.19) is now rewritten with the use of two terms of the Taylor expansion of the integrand $\theta$ about $x'$

$$
\begin{aligned}
&\lim_{\varepsilon\to 0}\int_{\Gamma-\Gamma_\varepsilon+\Gamma_\varepsilon^*}\frac{\partial q^*(x',x)}{\partial x_i'}\theta(x)d\Gamma(x)\\
=&\lim_{\varepsilon\to 0}\int_{\Gamma-\Gamma_\varepsilon}\frac{\partial q^*(x',x)}{\partial x_i'}\theta(x)d\Gamma(x)\\
&+\lim_{\varepsilon\to 0}\int_{\Gamma_\varepsilon^*}\frac{\partial q^*(x',x)}{\partial x_i'}[\theta(x)-\theta(x')-\theta_{,k}(x')(x_k-x_k')]d\Gamma(x)\\
&+\theta(x')\lim_{\varepsilon\to 0}\int_{\Gamma_\varepsilon^*}\frac{\partial q^*(x',x)}{\partial x_i'}d\Gamma(x)\\
&+\theta_{,k}(x')\lim_{\varepsilon\to 0}\int_{\Gamma_\varepsilon^*}\frac{\partial q^*(x',x)}{\partial x_i'}(x_k-x_k')d\Gamma(x)\\
=&I_1'+I_2'+I_3'+I_4'
\end{aligned}
\tag{4.24}
$$

Two integrals of (4.24) form a Hadamard principal value integral as stated below

$$
\begin{aligned}
I_1'+I_3' =&\lim_{\varepsilon\to 0}\int_{\Gamma-\Gamma_\varepsilon}\frac{\partial q^*(x',x)}{\partial x_i'}\theta(x)d\Gamma(x) + \theta(x')\lim_{\varepsilon\to 0}\int_{\Gamma_\varepsilon^*}\frac{\partial q^*(x',x)}{\partial x_i'}d\Gamma(x)\\
=&\dfint_\Gamma\frac{\partial q^*(x',x)}{\partial x_i'}\theta(x)d\Gamma(x)
\end{aligned}
\tag{4.25}
$$

where the symbol $\dfint$ refers to the evaluation of the improper integral in the Hadamard principal value sense. The integral $I_2'\to 0$ as $\varepsilon\to 0$. The last integral $I_4'$ of (4.24) can be

calculated using the polar coordinates, (4.6), to give

$$
\begin{aligned}
I'_4 &= \theta_{,k}(x') \lim_{\varepsilon \to 0} \int_{\Gamma^*_\varepsilon} \frac{\partial q^*(x', x)}{\partial x'_i}(x_k - x'_k) d\Gamma(x) \\
&= \theta_{,k}(x') \lim_{\varepsilon \to 0} \int_{\Gamma^*_\varepsilon} \frac{1}{2\pi r^2} \left[ 2r_{,i} r_{,j} n_j - n_i \right] (x_k - x'_k) d\Gamma(x) \\
&= \frac{\theta_{,k}(x')}{2\pi} \lim_{\varepsilon \to 0} \int_0^\pi \frac{2r_{,i} - n_i}{\varepsilon^2} \varepsilon n_k(x) \varepsilon d\phi \\
&= \frac{\theta_{,i}(x')}{4}
\end{aligned}
\tag{4.26}
$$

The left hand side of (4.19) can thus be written as

$$
\lim_{\varepsilon \to 0} \int_{\Gamma - \Gamma_\varepsilon + \Gamma^*_\varepsilon} \frac{\partial q^*(x', x)}{\partial x'_i} \theta(x) d\Gamma(x) = \frac{\theta_{,i}(x')}{4} + \fint_\Gamma \frac{\partial q^*(x', x)}{\partial x'_i} \theta(x) d\Gamma(x)
\tag{4.27}
$$

From equation (4.23) and (4.27) the derived temperature equation (4.18) can be rewritten to give

$$
\frac{1}{2} \frac{\partial \theta(x')}{\partial x'_i} - \fint \frac{\partial q(x')}{\partial x'_i} \theta(x) d\Gamma(x) = -\oint_\Gamma \frac{\partial \theta(x')}{\partial x'_i}(x', x) q(x) d\Gamma
\tag{4.28}
$$

The above equation is rewritten by the use of the flux definition (4.17) to give the flux integral equation for a boundary point x', that is

$$
\frac{1}{2} q(x') - n_i(x') \oint_\Gamma \theta^{**}(x', x) q(x) d\Gamma = -n_i(x') \fint q_i^{**}(x', x) \theta(x) d\Gamma(x)
\tag{4.29}
$$

where $\oint$ stands for a Cauchy value integral, $\fint$ stands for a Hadamard principal value integral and

$$
\begin{aligned}
\theta_i^{**} &= \frac{r_i}{2\pi r} \\
q_i^{**} &= -\frac{\lambda}{2\pi r^2} \left[ 2r_{,i} r_{,j} n_j - n_i \right]
\end{aligned}
\tag{4.30}
$$

## 4.2 The thermoelastic problem

The derivation of the boundary integral equations based on the governing thermoelastic equations described in chapter 2 are presented in this section. In order to limit the extend of the summary less attention will be paid on the transformation of the integral equations to describe only boundary values as demonstrated in the previous section.

The derivation of the boundary integral equations is the results of the efforts of several researchers. One of the first central works that contributed to the formulation of the boundary integral equations was by Betti in 1872. Betti (1872) formulated the reciprocal work theorem, which postulated an equilibrium between two sets of solutions by the two expressions of work that can be obtained from work done by the stresses of one set on the

strains at the opposite set. Based on the reciprocal theorem, Somigliana (1885) was the first to derive a representation of the integral equations in a form which today is known as Somigliana's identities. Since an analytical solution of these equations is only possible for simple problems the use of the integral equations to solve problems is very dependent on the discretization procedure. Thus the final formulations used in this thesis were first derived much later. The derivation of the integral equations can be done in several ways and examples of these derivations were obtained by Cruse and Rizzo (1968) who used Betti's reciprocal theorem, Jeng and Wexler (1977) employed a variational formulation similar to that used in the finite element method and Brebbia and Dominguez (1977) introduced the weighted residual concept.

Two basic approaches can be used in the formulation of boundary integral equations. In the indirect formulation, the unknowns are represented by fictitious density functions, which in most cases have no physical significance, but the physical unknowns can be derived from the density functions. Opposite is the direct formulation in which the unknowns are represented by the actual physical variables such as temperature, flux, displacements in the thermoelastic theory.

In this section the direct formulation of boundary integral equations for two dimensional thermoelasticity is summarized. The work of Prasad et al. (1994), Aliabadi (2002), Becker (1992) and dell'Erba (1999) represent the main references.

### 4.2.1 The boundary integral equation

The reciprocal work theorem can be used to consider a domain under equilibrium with two different sets of stress and strain. One set of stresses $\sigma_{ij}^a$ gives rise to a set of strains $\epsilon_{ij}^a$ and a second set b of stresses $\sigma_{ij}^b$ gives rise to another set of strains $\epsilon_{ij}^b$. Thus it follows from the reciprocal work theorem that the work done by the stresses of system a on the displacements of the system b is equal to the work done by the stresses of system b on the displacements of system a. The work equilibrium can be written as

$$\int_\Omega \sigma_{ij}^a \epsilon_{ij}^b d\Omega = \int_\Omega \sigma_{ij}^b \epsilon_{ij}^a d\Omega \tag{4.31}$$

which can be rewritten using the expression of strains in terms of the displacements (2.5), Einstein's summation convention and the equilibrium equations (2.4) to give

$$\int_\Omega (\sigma_{ij}^a u_i^b)_{,j} d\Omega + \int_\Omega b_i^a u_i^b d\Omega = \int_\Omega (\sigma_{ij}^b u_i^a)_{,j} d\Omega + \int_\Omega b_i^b u_i^a d\Omega \tag{4.32}$$

The divergence theorem allows the transformation of an area integral to a boundary integral. If $f_i$ is a vector field defined with continuous first derivatives on a neighborhood of the closed volume $\Omega$, it can be stated that

$$\int_\Omega \frac{\partial f_i}{\partial x_i} d\Omega = \int_\Gamma f_i n_i d\Gamma \tag{4.33}$$

where $\Gamma$ is the boundary of $\Omega$ with the outward pointing normals $n_i$. The divergence theorem can now be applied to (4.32) since the linear elastic stress and displacement fields have continuous first derivatives, thus

$$\int_\Gamma t_i^a u_i^b d\Gamma + \int_\Omega b_i^a u_i^b d\Omega = \int_\Gamma t_i^b u_i^a d\Gamma + \int_\Omega b_i^b u_i^a d\Omega \qquad (4.34)$$

where the traction is expressed as $t_i = \sigma_{ij} n_j$. The expression of (4.34) is known as Betti's reciprocal work theorem.

To be able to get to a system of linear independent algebraic equations with a unique solution, the definition of set a and b have to specified. If set a is considered as a set of unknown displacements, tractions and body force vectors then set b must represent a known set of displacements, tractions and body force vectors which are valid for any geometry in equilibrium.

For a known set b, the body force $b_i^b$ is defined as a point force in an infinite domain represented by the Dirac delta function $\Delta(X - X')$ as

$$b_i^b = \Delta(X - X')e_i \qquad (4.35)$$

where the unit vector $e_i$ corresponds to a unit positive force per unit thickness in the i direction applied at $X'$. The two points $X$ and $X'$ belongs to the domain $\Omega$. The expression of the body force $b_i^b$ is inserted into the last integral of (4.34) and by the special integration property of the Dirac delta function the integral becomes

$$\int_\Omega b_i^b u_i^a d\Omega = u_i^a(X')e_i \qquad (4.36)$$

The point force solution in an infinite medium was originally derived by Lord Kelvin and it is also know as Kelvin's fundamental solution. As already demonstrated the point force solution is very important in the derivation of the boundary element method and in the next sub section the point force solution is used to define a known traction field $T_{ij}$ and a known displacement field $U_{ij}$. The displacement and traction fields corresponding to the point force solution can be written as

$$u_i^b = U_{ij}(X', x)e_j \qquad (4.37)$$
$$t_i^b = T_{ij}(X', x)e_j$$

From (4.36) and (4.37) it can be seen that the reciprocal work theorem (4.34) can be rewritten as

$$u_i(X') = \int_\Gamma U_{ij}(X', x)t_j(x)d\Gamma - \int_\Gamma T_{ij}(X', x)u_j(x)d\Gamma + \int_\Omega U_{ij}(X', x)b_j(x)d\Omega \quad (4.38)$$

where $x \in \Gamma$. The above equation is known as Somigliana's identity for displacements. It is used to relate displacements at an internal point X' to boundary values of the displacements and tractions and to body forces.

### 4.2.2   The fundamental solutions

This section summarizes the derivation of the fundamental solutions of the temperature and displacement fields due to a point force. The fundamental solutions must satisfy the governing differential equations which in case of displacements are Navier's equations. Navier's equations in terms of displacements were presented in chapter 2. As the temperature change can be considered as a body force term, Navier's equation can now be written for a unit point force applied to the body at a point $X'$ as

$$\mu u_{i,jj} + \left( \frac{\mu}{1-2\nu} \right) u_{j,ji} + \Delta(X - X')e_i = 0 \tag{4.39}$$

where $\mu$ is the shear modulus and $\Delta(X - X')e_i$ is the body force corresponding to a point force in an infinite sheet represented by the Dirac delta function . The above equation is difficult to solve analytically but there is however several methods by which a solution can be obtained. In this thesis the method based on the Galerkin vector is used. The Galerkin method which is an approximated method incorporates the governing differential equation in its weak form and functions in principle, by restricting the possible solutions as well as the test functions to a smaller space than the original one. Thus the governing equation is not required to hold absolutely but only with respect to a certain test function. The displacements can be expressed in terms of a Galerkin vector as

$$u_i = G_{i,jj} - \frac{1}{2(1-\nu)} G_{i,ij} \tag{4.40}$$

By substituting this equation into (4.39) we end up with a biharmonic equation which in vector form is expressed as

$$\nabla^4 G_i = \nabla^2(\nabla^2 G_i) = \frac{-1}{\mu}\Delta(X - X')e_i \tag{4.41}$$

where $\nabla^2$ is the laplacian operator. The problem of a single concentrated force applied in the interior of an infinite domain is known as the Kelvin problem. Assume that a unit force is applied on an interior point $X'$ and we seek the effect of this force on another point $X$ anywhere in the domain. Two conditions can then be defined, firstly all stresses must vanish as the distance between $X'$ and $X$ tends to infinity and secondly the stresses must be singular at $X'$ itself (i.e. the stresses tend to infinity as the distance tend to zero). It can be verified that the following Galerkin vector is a solution of (4.40) and satisfies both the above mentioned physical conditions

$$G_i = \frac{1}{8\pi\mu} r^2 ln\left(\frac{1}{r}\right) e_i \tag{4.42}$$

where the function r is the physical distance between the two points $X'$ and $X$. The displacement vector can thus be obtained by substituting (4.42) into (4.40) to give

$$u_i = \frac{1}{8\pi\mu(1-\nu)} \left[ (3 - 4\nu)ln\left(\frac{1}{r}\right)\delta_{ij} + r_{,i}r_{,j} \right] \tag{4.43}$$

and by (4.37) the displacement field can be written as

$$U_{ij}(X', x) = \frac{1}{8\pi\mu(1-\nu)} \left[ (3-4\nu)ln\left(\frac{1}{r}\right)\delta_{ij} + r_{,i}r_{,j} \right] \qquad (4.44)$$

In the above equation $U_{ij}(X', x)$ represents the displacement in the $j$ direction at boundary point $x$ due to a unit force acting in the $i$ direction at the interior point $X'$. The traction field arising from the point force can be derived by differentiating the displacement vector, substituting it into the Hooke's law and rewriting the expression by the traction definition (2.3) to give

$$T_{ij}(X', x) = \frac{-1}{4\pi(1-\nu)r} \left[ \frac{\partial r}{\partial n}[(1-2\nu)\delta_{ij} + 2r_{,i}r_{j}] + (1-2\nu)[r_{,j}n_{i} - r_{,i}n_{j}] \right] \quad (4.45)$$

In the above equation $T_{ij}(X', x)$ represents the traction in the $j$ direction at boundary point $x$ due to a unit force acting in the $i$ direction at the interior point $X'$.

### 4.2.3 Displacement equation for a boundary point

In order to obtain the advantage of the BEM all integrals need to be expressed in terms of the boundary of the domain. Somigliana's identity for displacements already derived from the reciprocal theorem states

$$u_i(X') + \int_\Gamma T_{ij}(X', x)u_j(x)d\Gamma = \int_\Gamma U_{ij}(X', x)t_j(x)d\Gamma + \int_\Omega U_{ij}(X', X)b_j(X)d\Omega \quad (4.46)$$

where the fundamental solutions are given by (4.44) and (4.45). The second integral on the right hand side of (4.46) express the volume forces and it is still defined as an integral of the domain $\Omega$.

In case the body forces acting in the domain are only due to the temperature change the domain integral can now be rewritten into only a boundary integral . The total thermoelastic stresses (t) are first divided into an elastic contribution (e) and a contribution from the temperature change, that is

$$\sigma_{ij}^t = \sigma_{ij}^e + \frac{E\alpha}{1-2\nu}\theta\delta_{ij} \qquad (4.47)$$

By including the above expression in the derivation of the boundary integral equation from the reciprocal work theorem it can be shown as in Aliabadi (2002) that the domain integral can be written as

$$B_i = \int_\Omega U_{ij}(X', X)b_j(X)d\Omega(x) = \frac{E\alpha}{1-2\nu} \int_\Omega U_{ij,j}(X', X)\theta d\Omega \qquad (4.48)$$

The displacement fundamental solution given by (4.44) can now be inserted into the domain integral and the expression is rewritten by introducing the differential operator $\nabla^2$ to give

$$B_i = \frac{\alpha(1+\nu)}{8\pi(1-\nu)} \int_\Omega \nabla^2\{\frac{\partial}{\partial x_i}[r^2 ln(r)]\}\theta d\Omega \qquad (4.49)$$

The expression of (4.49) is given in a form which can be transformed into a boundary integral by the use of Green's second identity. The identity can be used to transform the domain integral of two harmonic functions $\psi$ and $\theta$ in the finite domain $\Omega$ to a boundary integral, expressed as

$$\int_\Omega [\theta \nabla^2 \psi^2 - \psi \nabla^2 \theta] d\Omega = \int_\Gamma [\theta \frac{\partial \psi}{\partial n} - \psi \frac{\partial \theta}{\partial n}] \theta d\Gamma \qquad (4.50)$$

where $\Gamma$ is the boundary of the domain and $n$ is the outward pointing normal of the boundary. By using the substitution

$$\psi = \frac{\partial}{\partial x_i} [r^2 ln(r)] \qquad (4.51)$$

along with the Laplace equation for steady state thermoelasticity $\nabla^2 \theta = 0$ the body force integral can be expressed as

$$B_i = \int_\Gamma \overline{P}_i(X', x)\theta(x)d\Gamma - \int_\Gamma \overline{Q}_i(X', x)q(x)d\Gamma \qquad (4.52)$$

where the fundamental fields for two dimensional problems are given as

$$\overline{P}_i(X', x) = \frac{(1+\nu)\alpha}{4\pi(1-\nu)} \left\{ \left[ ln\left(\frac{1}{r}\right) - \frac{1}{2} \right] n_i - r_{,i} r_{,k} n_k \right\} \qquad (4.53)$$

$$\overline{Q}_i(X', x) = -\frac{(1+\nu)}{4\pi\lambda(1-\nu)} \alpha r_i r \left[ ln\left(\frac{1}{r}\right) - \frac{1}{2} \right] \qquad (4.54)$$

The thermoelastic displacement of an internal point can now be derived by substituting (4.52) into Somigliana's identity (4.46) to give

$$u_i(X') + \int_\Gamma T_{ij}(X', x)u_j(x)d\Gamma(x)$$
$$= \int_\Gamma U_{ij}(X', x)t_j(x)d\Gamma(x) + \int_\Gamma \overline{P}_i(X', x)\theta(x)d\Gamma - \int_\Gamma \overline{Q}_i(X', x)q(x)d\Gamma \qquad (4.55)$$

The displacement boundary integral equation for a boundary point is now obtained by taking the internal point $X'$ to the boundary. This however leads to a singularity in the integrals containing the fundamental solution. By the use of the semi circular boundary in the limiting process, described in the previous section, it can be shown that

$$C_{ij}(x')u_i(x') + \int_\Gamma T_{ij}(x', x)u_j(x)d\Gamma(x) - \int_\Gamma \overline{P}_i(x', x)\theta(x)d\Gamma$$
$$= \int_\Gamma U_{ij}(x', x)t_j(x)d\Gamma(x) - \int_\Gamma \overline{Q}_i(x', x)q(x)d\Gamma \qquad (4.56)$$

where $C_{ij}(x') = \delta_{ij}/2$ for a smooth boundary.

### 4.2.4  Traction equation for a boundary point

The traction integral equation of a boundary point $x'$ can be calculated from the stress equation for a boundary point $x'$ by the use of the definition of tractions (2.3). The stress equation of the internal point $X'$ is firstly derived by differentiation of the displacement integral equations and by the thermoelastic definitions described in chapter 2. By differentiation of the displacement equation the following can be obtained

$$\frac{\partial u_i(X')}{\partial X'_j} + \int_\Gamma \frac{\partial T_{ik}(X',x)}{\partial X'_j}u_k(x)d\Gamma - \int_\Gamma \frac{\partial \overline{P}_i(X',x)}{\partial X'_j}\theta(x)d\Gamma$$

$$= \int_\Gamma \frac{\partial U_{ik}(X',x)}{\partial X'_j}t_k(x)d\Gamma - \int_\Gamma \frac{\partial \overline{Q}_i(X',x)}{\partial X'_j}q(x)d\Gamma \qquad (4.57)$$

the above expression can be rewritten to the stress integral equation by the use of Hooke's law for thermoelasticity (2.2) and the strain displacement relationship (2.5). Thus for an internal point the stress integral equation for an internal point $X'$ is given by

$$\sigma_{ij}(X') + \int_\Gamma T_{kij}(X',x)u_k(x)d\Gamma - \int_\Gamma \overline{P}_{ij}(X',x)\theta(x)d\Gamma + \frac{E}{1-2\nu}\alpha\theta(X')\delta_{ij}$$

$$= \int_\Gamma U_{kij}(X',x)t_k(x)d\Gamma - \int_\Gamma \overline{Q}_{ij}(X',x)q(x)d\Gamma \qquad (4.58)$$

Where the fundamental fields $T_{kij}$, $U_{kij}$, $\overline{P}_{ij}$ and $\overline{Q}_{ij}$ are obtained by insertion of the derivatives of the fundamental fields of the displacement integral equation into (4.57) to give

$$U_{kij}(X',x) = \frac{1}{4\pi(1-\nu)r}\left[(1-2\nu)(r_{,j}\delta_{ki} + r_{,i}\delta_{jk} - r_{,k}\delta_{ij}) + 2r_i r_j r_k\right]$$

$$T_{kij}(X',x) = \frac{\mu}{2\pi(1-\nu)}\frac{1}{r^2}\left\{2\frac{\partial r}{\partial n}\left[(1-2\nu)\delta_{ij}r_{,k} + \nu(r_{,j}\delta_{ik} + r_{,i}\delta_{jk}) - 4r_{,i}r_{,j}r_{,k}\right]\right.$$

$$+ 2\nu(n_i r_{,j}r_{,k} + n_j r_{,i}r_{,k}) + (1-2\nu)(2n_k r_{,i}r_{,j} + n_j\delta_{ik} + n_i\delta_{jk})$$

$$\left. - (1-4\nu)n_k\delta_{ij}\right\}$$

$$\overline{P}_{ij}(X',x) = \frac{\alpha\mu(1+\nu)}{2\pi(1-\nu)r}\left\{n_k r_{,k}\left[\frac{\delta_{ij}}{(1-2\nu)} - 2r_{,i}r_{,j}\right] + n_i r_{,j} + n_j r_{,i}\right\}$$

$$\overline{Q}_{ij}(X',x) = -\frac{\alpha\mu(1+\nu)}{2\pi\lambda(1-\nu)}\left\{r_{,i}r_{,j} + \frac{\delta_{ij}}{1-2\nu}\left[\frac{(1-2\nu)}{2} - ln\left(\frac{1}{r}\right)\right]\right\} \qquad (4.59)$$

Once more the limiting process of semi circular boundary, (4.5), can be used to evaluate the integral equation as the internal point $X'$ is moved to the boundary. If $n_j(x')$ are the components of the outward pointing normal on the boundary $\Gamma$ the traction integral

equation can be written as.

$$
\begin{aligned}
&\frac{1}{2}t_i(x') + n_j(x') \fint_\Gamma T_{kij}(x',x)u_k(x)d\Gamma(x) \\
&- n_j(x') \fint_\Gamma \overline{P}_{ij}(x',x)\theta(x)d\Gamma + \frac{E}{2(1-2\nu)}\alpha\theta(x')n_i(x') \\
&= n_j(x') \fint_\Gamma U_{kij}(x',x)t_k(x)d\Gamma(x) - n_j(x') \int_\Gamma \overline{Q}_{ij}(x',x)q(x)d\Gamma
\end{aligned}
\tag{4.60}
$$

the fundamental fields $T_{kij}$, $U_{kij}$, $\overline{P}_{ij}$ and $\overline{Q}_{ij}$ are given by (4.59), $\fint$ stands for a Cauchy value integral and $\fint$ stands for a Hadamard principal value integral.

# Chapter 5
# Dual boundary element method

Shortly after the first numerical solutions of the boundary integral equations were presented, a numerical formulation for potential problems was developed by Symm (1963) and for time independent elastic problems by Rizzo (1967). However the use of these first formulations of the boundary integral equations could not be applied directly to solve fracture mechanical problems in which both surfaces of the crack are discretized. Since the two surfaces of a crack will be coincided when no load is applied to the cracked domain a mathematical degeneration in the numerical formulation of the boundary element method is obtained (singular matrix) as showed by Cruse (1972) because the same equations are obtained for the two coincided surfaces

Several formulations of the integral equations have been used in order to overcome the problem of coincided crack surfaces. Among the most important formulations are the Green's function method presented by Snyder and Cruse (1975), the displacement discontinuity method by Crouch (1976), the multidomain or subregion modelling by Blandford et al. (1981) and finally the dual boundary element method (Portela et al., 1992).

The Green's function method incorporates an exact representation of the crack surface boundary conditions by the use of the Green's functions. The method is in general considered to be limited to two dimensional problems for which it can be used to obtain accurate results. The method is applied by mounting additional terms to the Kelvin fundamental solutions of the boundary integral equations and these additional terms result in zero stresses on the crack due to the point load.

In the displacement discontinuity method each pair of coincided source points on the crack surfaces is replaced by a single source point, and for each of these single points the unknowns are the displacement differences between the crack faces. Mukhopadhyay et al. (2000) refers to, that the approach does not work well in case of significant bending and in addition, problems with unknown tractions and displacements on the crack faces cannot be solved with this method. The method has however been used by several researchers.

The multi domain approach was first reported by Lachat and Watson (1976), but the first true multidomain fracture mechanical analysis for non-symmetric bodies was however presented by Raveendra and Banerjee (1992). The method overcomes the problem of the same integral equation on both crack surfaces as each crack surface belongs to different sub domains. Thus when this method is applied the crack surfaces are extended through the domain creating an artificial boundary. The part of the artificial boundary representing the crack is allowed to open while the remaining part of the boundary is kept closed. This method was the first widespread method to model coincided crack surfaces. Its main drawback is the creation of the extra boundaries ahead of the crack tip.

Finally the dual boundary element method can be used to model crack problems in case of coincided source points on the crack faces by introducing additional independent

boundary integral equations i.e. the flux and traction equations. The integral equations obtained for source points on both crack surfaces are thus able to be integrated in the whole boundary and thus the degeneration in the numerical formulation is avoided. The dual boundary element method was applied to two dimensional thermoelastic problems by Prasad et al. (1994) and to three dimensional thermoelastic problems by dell'Erba and Aliabadi (2000)

In this chapter the implementation of the thermoelastic dual boundary element formulation is described. To give an understanding of the method, the chapter focuses primarily on the modelling and discretization strategy rather than it gives another description of the full implementation of the boundary element method which is already covered in the literature by e.g. Prasad et al. (1994), dell'Erba and Aliabadi (2000) and Aliabadi (2002)

## 5.1   The integral equations

The temperature, flux, displacement and traction integral equations described in the previous chapter are now used to formulate the dual boundary element method.

A general cracked body is illustrated in figure 5.1 with open crack surfaces. The boundary of the cracked body $\Gamma$ has been devided into three different parts that is the non-crack boundary $\Gamma^n$, the upper crack surface $\Gamma^+$ and the lower crack surface $\Gamma^-$. The choice of integral equations used to describe the field variables at a source point will depend on the location of the point on one of the three sub boundaries.
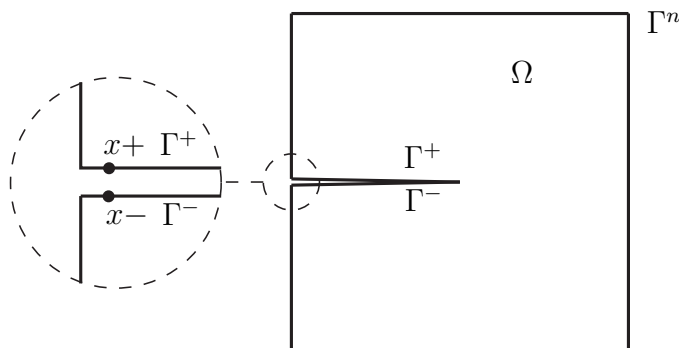


*Figure 5.1*   The boundary is divided into three sub boundaries in the formulation of the dual boundary element method. To illustrate the two crack surfaces the closed crack is sketched as opened

When the field variables of a point on the non-cracked boundary $\Gamma^n$ are to be found the temperature equation (4.16) and displacement equation (4.56) are used. To summarize the temperature integral equation it can be expressed by

$$C(x')\theta(x') - \int_\Gamma q^*(x',x)\theta(x)d\Gamma(x) = -\int_\Gamma \theta^*(x',x)q(x)d\Gamma(x) \qquad (5.1)$$

and the displacement integral equation

$$C_{ij}(x')u_i(X') + \int_\Gamma T_{ij}(x', x)u_j(x)d\Gamma(x) - \int_\Gamma \overline{P}_i(x', x)\theta(x)d\Gamma$$

$$= \int_\Gamma U_{ij}(x', x)t_j(x)d\Gamma(x) - \int_\Gamma \overline{Q}_i(x', x)q(x)d\Gamma \tag{5.2}$$

These integral equations are also used on one of the crack surfaces. When the integral equations are used to find the field variables of a point $x^+$ on the upper crack surface $\Gamma^+$, the temperature equation is written as

$$\frac{1}{2}\theta(x^+) + \frac{1}{2}\theta(x^-) - \int_\Gamma q^*(x^+, x)\theta(x)d\Gamma(x) = -\int_\Gamma \theta^*(x^+, x)q(x)d\Gamma(x) \tag{5.3}$$

and the displacement equation as

$$\frac{1}{2}u_i(x^+) + \frac{1}{2}u_i(x^-) + \int_\Gamma T_{ij}(x^+, x)u_j(x)d\Gamma(x) - \int_\Gamma \overline{P}_i(x^+, x)\theta(x)d\Gamma \tag{5.4}$$

$$= \int_\Gamma U_{ij}(x^+, x)t_j(x)d\Gamma(x) - \int_\Gamma \overline{Q}_i(x^+, x)q(x)d\Gamma$$

From (5.3) and (5.4) it is seen that an extra term $\frac{1}{2}\theta(x^-)$ and $\frac{1}{2}u_i(x^-)$ is added to each of the two equations because the source points $x^-$ and $x^+$ are coinciding.

When the source point is on the lower crack surface $\Gamma^-$ instead of $\Gamma^+$ an equivalent set of equations are obtained. Thus if the displacement equations are used on source points on both crack surfaces it leads to fewer independent equations than the number of unknowns. To be able to solve the total system of equations a different set of equations is needed on the opposite crack surface. The flux boundary equation (4.29) and traction boundary equation (4.60) are used for a source point on $x^-$. The flux boundary equation can be written as

$$\frac{1}{2}q(x^-) - \frac{1}{2}q(x^+) - n_i(x^-)\!\!\!\fint_\Gamma \theta^{**}(x^-, x)q(x)d\Gamma = -n_i(x^-)\!\!\!\fint q_i^{**}(x^-, x)\theta(x)d\Gamma(x) \tag{5.5}$$

and the traction equation as

$$\frac{1}{2}t_i(x^-) - \frac{1}{2}t_i(x^+) + n_j(x^-)\!\!\!\fint_\Gamma T_{kij}(x^-, x)u_k(x)d\Gamma(x)$$

$$- n_j(x^-)\!\!\!\fint_\Gamma \overline{P}_{ij}(x^-, x)\theta(x)d\Gamma + \frac{E}{2(1-2\nu)}\alpha\theta(x^-)n_i(x^-) \tag{5.6}$$

$$= n_j(x^-)\!\!\!\fint_\Gamma U_{kij}(x^-, x)t_k(x)d\Gamma(x) - n_j(x^-)\int_\Gamma \overline{Q}_{ij}(x^-, x)q(x)d\Gamma$$

where the relation $n_i(x^-) = -n_i(x^+)$ has been used.

The use of equations (4.16) and (4.56) for source points on $\Gamma^n$, equations (5.3) and (5.4) for source points on $\Gamma^+$ and equations (5.5) and (5.6) for source points on $\Gamma^-$ constitutes the dual boundary element method for thermoelastic crack problems.

## 5.2   Numerical formulation

By solution of the boundary integral equations the thermoelastic fields $\theta$, $q$, $u_i$ and $t_i$ can be determined for a given problem. Since an analytical solution of the integral equations is generally very difficult if not impossible, methods of weighted residuals can be used to obtain an approximative solution to the differential equations. Among these methods are the Galerkin Method and the Point Collocation Method. Several formulations of the Galerkin method have been applied to the boundary element method as for example by Polizzotto (1988), however the most straight forward and often used method is point collocation e.g. treated by Brebbia and Dominguez (1977) and because of that it is used in the present chapter.

In the point collocation method the boundary integral equations are derived for a number of locations of the source points on the boundary of the domain. The solution of thermoelastic fields satisfies the integral equations in each of these locations called the collocation points.

The first step in the use of the method is to discretize the boundary into a number of elements each described by the number and placements of nodes. In each of these elements the approximated thermoelastic fields can be described by the element shape functions and field values at the nodes. In the second step the boundary integrals related to each collocation point are evaluated by inserting the approximated thermoelastic fields and performing numerical integration element by element. As the procedure is repeated for all nodes a system of linear independent equations is obtained. Values of prescribed boundary conditions are inserted in the system of equations and by rearranging the system by knowns and unknowns it is finally possible to solve the system of equations obtaining all thermoelastic fields along the boundary.

In contrast to the point collocation method, the analytical solution satisfies the differential equations in all points. Thus intuitively the more discrete points are used the closer the approximated solution will be to the analytical solution.

The discretization of the integral equations are performed by dividing the domain into $N_e$ elements. For each of these elements the thermoelastic fields can be described by the expressions

$$\theta_j = \sum_{\alpha=1}^{m} N_\alpha(\eta)\theta_j^\alpha \quad q_j = \sum_{\alpha=1}^{m} N_\alpha(\eta)q_j^\alpha \qquad (5.7)$$

$$u_j = \sum_{\alpha=1}^{m} N_\alpha(\eta)u_j^\alpha \quad t_j = \sum_{\alpha=1}^{m} N_\alpha(\eta)t_j^\alpha$$

where $N_\alpha$ are the element shape functions, $m$ is number of nodes in the element and $\alpha$ refers to the current node on the element. In the general modelling of the dual boundary element method several types of quadratic elements can be used in the discretization of the domain as illustrated in figure 5.2

The crack surfaces are modelled with discontinuous quadratic elements as shown in figure 5.2. The discontinuous quadratic element has the special feature that the colloca-
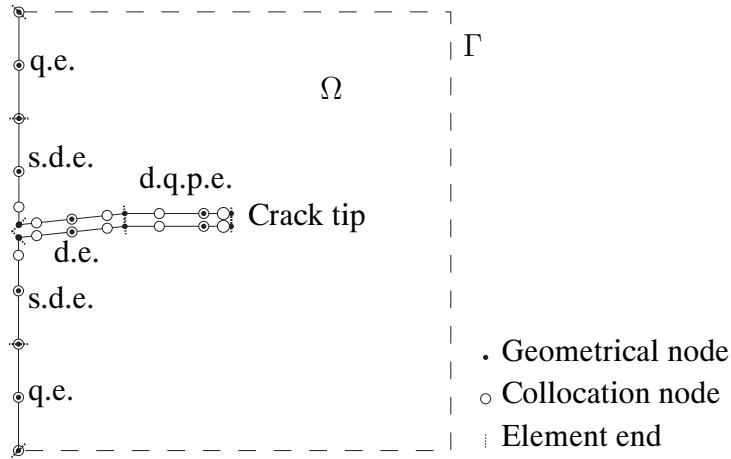
*Figure 5.2* Typical element used for modelling of crack problems by the dual boundary element method: Quadratic element (q.e.), semi discontinuous element (s.d.e.), discontinuous element (d.e.) and discontinuous quarter point element (d.q.p.e.)

tion nodes are located in a different position on the element than the geometrical nodes. The location of the collocation nodes within the element ensures the smoothness of the boundary at the source point. Therefore the requirements of continuity assumed in the derivation of the flux and the traction integral equations are satisfied for the boundary variables. Continuous quadratic elements as shown in figure 5.2 can be used along the remaining boundaries except at the intersection of the non-cracked boundary with the crack surfaces. At these corners semi discontinuous elements can be used to couple continuous and discontinuous elements.

The variation of the boundary variables within the elements are given by (5.7) expressed in terms of the values of the variables at the collocation nodes and the shape functions. For the continuous quadratic elements the shape functions can be expressed by

$$
\begin{aligned}
N_1 &= \frac{1}{2}\eta(\eta - 1) \\
N_2 &= 1 - \eta^2 \\
N_3 &= \frac{1}{2}\eta(1 + \eta)
\end{aligned}
\tag{5.8}
$$

and for the discontinuous elements

$$
\begin{aligned}
N_1 &= \eta(-\frac{1}{2\lambda} + \eta\frac{1}{2\lambda^2}) \\
N_2 &= 1 + \eta^2\frac{1}{\lambda^2} \\
N_3 &= \eta(\frac{1}{2\lambda} + \eta\frac{1}{\lambda^2})
\end{aligned}
\tag{5.9}
$$

where $\eta$ is the local element coordinate and $\lambda = \frac{2}{3}$ for the present discontinuous elements.

As the discretization procedure is carried out $N_e$ elements and $N_t$ nodes are placed along the boundary of the domain. Performing the numerical integration of the temperature and flux equations for each collocation node leads to a system of algebraic equations which can be expressed in matrix form as

$$[H_{\theta\theta}^{\theta,q}][\theta] = [G_{\theta\theta}^{\theta,q}][q] \qquad (5.10)$$

and for the displacement and traction equation

$$\begin{bmatrix} H_{11}^{u,t} & H_{12}^{u,t} & H_{1\theta}^{u,t} \\ H_{21}^{u,t} & H_{22}^{u,t} & H_{2\theta}^{u,t} \end{bmatrix} \begin{bmatrix} u_1 \\ u_2 \\ \theta \end{bmatrix} = \begin{bmatrix} G_{11}^{u,t} & G_{12}^{u,t} & G_{1\theta}^{u,t} \\ G_{21}^{u,t} & G_{22}^{u,t} & G_{2\theta}^{u,t} \end{bmatrix} \begin{bmatrix} t_1 \\ t_2 \\ q \end{bmatrix} \qquad (5.11)$$

These two matrix equations can be solved separately by inserting the temperature and flux results of (5.10) into (5.11) when the displacements and tractions are calculated. Alternatively the equations can be coupled as suggested in Prasad et al. (1994).

When applying boundary conditions it is possible to rearrange the equations to the well known configuration such that the unknowns are on left hand side and the knows are on the right hand side, that is

$$\mathbf{Ax} = \mathbf{b} \qquad (5.12)$$

## 5.3   Numerical integration

A general integration scheme can be applied to most of the integrals as the singular terms of the integral only occur when the collocation point is coinciding with the element in which the integration is performed. The Gauss quadrature formula can be applied to the non-singular cases in which the integration of the function f in the one dimension element can be expressed by

$$\int_{-1}^{1} f(\eta)d\eta = \sum^{S} A_s f(\eta_s) \qquad (5.13)$$

where $A_s$ are the weighting factors and $\eta$ the local element coordinate.

The main difficulty in the implementation of the dual boundary integral equation is related to the numerical integration of the singular integrals. In this sections the three types of singular integrals and the solution of these are only briefly discussed as a detailed derivation does not contribute to the understanding of the dual boundary element method.

*Hyper singular integrals*

The singularity of the order $O(1/r^2)$ is present for the flux and traction boundary equations used on the crack surface. These integrals give rise to the main difficulty in the numerical integration of the dual boundary element method. The hyper singular integration has been treated in several papers on the boundary element method e.g. Portela et al. (1992). These papers deals with the general approach that allows the integration to be

carried out by transformation of the hyper singular integrals into regular integrals. These integrals are evaluated by the standard quadratures and simple singular integrals which are integrated analytically. Saez and Gallego R. (1995) followed the same basic idea and derived the actual expressions for the hyper singular and strong singular integrals of the displacement and traction boundary integral equations. The expressions of Saez and Gallego R. (1995) are used in this thesis and the approach have been extended to the flux boundary element equation.

*Strongly singular integrals*

The $0(1/r)$ singularity characterizes these integrals and the singularity occurs in the temperature and displacement integral equations for the coefficients of $u_i$ and $\theta_i$. The evaluation of these integrals are however easily performed using rigid body approach for the non-cracked boundary.

Consider a body for zero temperature, zero flux and in the absence of body forces. Then a unity rigid body displacement in the direction of one of the cartesian coordinates the traction and body force vector must be zero and thus in according to (5.11)

$$\mathbf{H}^{u,t}\mathbf{I} = 0 \tag{5.14}$$

where $I$ represents the unitary displacement. Since equation (5.14) has to be satisfied for any rigid body displacement the following expression can be written

$$\mathbf{H}_{ii}^{u,t} = -\sum_{j=1}^{2N_T} \mathbf{H}_{ij}^{u,t} \quad \text{for } j \neq i \tag{5.15}$$

the above expressions avoid the calculations of the strongly singular integrals and the $C_{ij}$ term. Analog to the rigid body consideration for the elastic problem, equivalent considerations can be made for potential problems. If the temperature is constant in the domain this condition will lead to zero temperature gradients and as a consequence zero flux, and thus

$$\mathbf{H}_{ii}^{\theta,q} = -\sum_{j=1}^{N_T} \mathbf{H}_{ij}^{\theta,q} \quad \text{for } j \neq i \tag{5.16}$$

For the strongly singular integrals collocated at the crack surfaces, the rigid body considerations can not be applied because of the dual nodes at the crack faces. For these cases the integrals are evaluated directly by the same method used for the hyper singular integrals as already described.

*Weakly singular integrals*

These integrals are characterized by a singularity of $O(\ln r)$. The weakly singular integrals that appears for the coefficients of $u_i(x')$ and $\theta_i(x')$ in the displacement equation and the coefficients of $q_i(x')$ in the temperature equation are calculated using a Gaussian formula with singular weight functions as described e.g. in Becker (1992).

## 5.4   Evaluation of stress intensity factors

The stress intensity factors can be calculated from the boundary element solution by a number of different methods like for example by the use of special crack tip elements or the path independent integrals. A review of these methods applied to the boundary element method can be found by authors like Mukhopadhyay et al. (2000) and Aliabadi (2002). In general the J-integral is one of the most accurate methods to calculate the stress intensity factors for crack problems. However accurate results are also obtained with special crack tip elements like the discontinuous quarter point elements.

The discontinuous quarter point element has been used to calculate crack problems of both elastic and thermoelastic formulation of the boundary element method, and the derivation is summarized in this section.
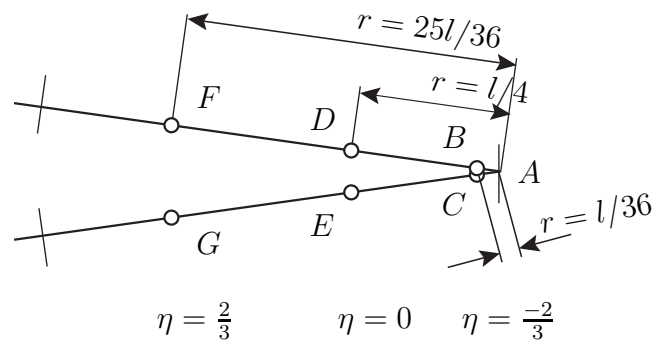


*Figure 5.3*   Discontinuous quarter point elements

By moving the mid-point node to a quarter point position, the displacement field described by the elements obtain a desired $\sqrt{r}$ dependency on the distance to the crack tip. These quarter point elements were firstly demonstrated in the finite element method by Barsoum (1976) and Henshell (1975) and for discontinuous elements, Fedelinski et al. (1995) were the first to use the quarter point configuration in the boundary element method.

Consider a crack located in the plane with $y = 0$ and with the crack tip at $x = 0$. The distance along the x-axis can be described by the crack tip element as it was the case for the thermoelastic fields (5.7), thus x is given by

$$x = \sum_{\alpha=1}^{3} N_\alpha(\eta)x^\alpha = N_1\frac{l}{36} + N_2\frac{9l}{36} + N_3\frac{25l}{36} \tag{5.17}$$

When the shape functions (5.7) are inserted into (5.17) it can be shown that

$$\eta = -1 + 2\sqrt{\frac{x}{l}} = -1 + 2\sqrt{\frac{r}{l}} \tag{5.18}$$

Substituting the above expression (5.18) into the displacement field approximation (5.7) it can be shown that

$$u_i = a_1 + a_2\sqrt{\frac{r}{l}} + a_3\frac{r}{l} \tag{5.19}$$

where $a_1, a_2$ and $a_3$ are coefficients of the approximated displacements calculated from the displacements at the element nodes. From the solution of the displacement fields in the vicinity of the crack tip (3.6) the displacements at the crack surfaces can be written as

$$u_2(\theta = \pi) - u_2(\theta = -\pi) = \frac{\kappa + 1}{\mu} K_I \sqrt{\frac{r}{2\pi}}$$

$$u_1(\theta = \pi) - u_1(\theta = -\pi) = \frac{\kappa + 1}{\mu} K_{II} \sqrt{\frac{r}{2\pi}} \tag{5.20}$$

When the expression of displacement at the crack tip element (5.19) is inserted into (5.20) it is seen that the $\sqrt{r}$ singularity cancels out and an expression independently of $r$ can be obtained when $r \to 0$. The stress intensity factor can be derived directly from the above expressions. Fedelinski et al. (1995) however used the method of minimization of the squared differences between the analytical and boundary element values of the crack opening and crack sliding displacements to give

$$K_I = \frac{6\mu}{5(\kappa + 1)} \sqrt{\frac{\pi}{2l}} (\Delta u_2^{BC} + 3\Delta u_2^{DE})$$

$$K_{II} = \frac{6\mu}{5(\kappa + 1)} \sqrt{\frac{\pi}{2l}} (\Delta u_1^{BC} + 3\Delta u_1^{DE}) \tag{5.21}$$

# Chapter 6
# Summary of results in enclosed papers

The chapter presents main results from the papers [P1]-[P4]. The papers [P1]-[P3] are based on a 2 dimensional dual boundary element formulation presented in section 5. While the last paper [P4] presents a new method to perform numerical simulation of non-planar 3D crack growth by the combination of FEM and BEM.

## 6.1   Crack growth in a piston crown [P1]

The 2D dual boundary element formulation presented in section 5 is used in [P1] to perform numerical simulation of crack growth in a simplified engine part of a large diesel engine. The analyzed engine part is the piston crown shown in figure 6.1.a which due to its placement in the combustion chamber is exposed to both high temperatures and pressures. Reasonable results are expected when analyzing crack growth in a nearly axisymmetric structure with a simplified plain strain model 6.1.b especially in the area of the crack as described in [P1].

The crankshaft rotation of $360°$ defines one pressure cycle of compression and expansion of gas above the piston crown. When one pressure cycle is modelled it is discretized into ten steady state load steps that are chosen so that load step number six represents the angular position of the crankshaft that gives exactly the maximum combustion pressure. The crack initiation is modelled by inserting a crack at the lower part of the weld shown in figure 6.1.b.

The $K_I$ and $K_{II}$ factors are calculated for the initial crack configuration and it is found that the thermal loading of the piston crown ensures a dominant mode I loading in all load steps. The lowest value of $K_I$ is obtained for the highest combustion pressure as the combustion pressure tends to close the crack. The crack growth analysis is complicated by the fact that the piston crown is subjected to non-proportional loading as demonstrated in figure 6.2 by the ratio of $K_I$ and $K_{II}$. In the figure load steps zero and eleven are included in the figure to demonstrate the beginning and end of the load cycle. The variation of the ratio during the load cycle will cause that a different crack extension angle is predicted for each load step.

A simple criterion is chosen to propagate the crack as the extension angle of only one load step is used. It is assumed that the crack grows due to the size of the loading and due to the part of the load cycle at which a given load is present. Thus to propagate the crack load step two is therefore the primary choice. This load step represents the highest mode I loading of all increments. The $K_I$ and $K_{II}$ factors are shown in figure 6.3 for crack increment 0, 3, 6. From the figure it is seen that the variations of the stress intensity factors are unchanged for the different increments of the crack. The $K_I$ values
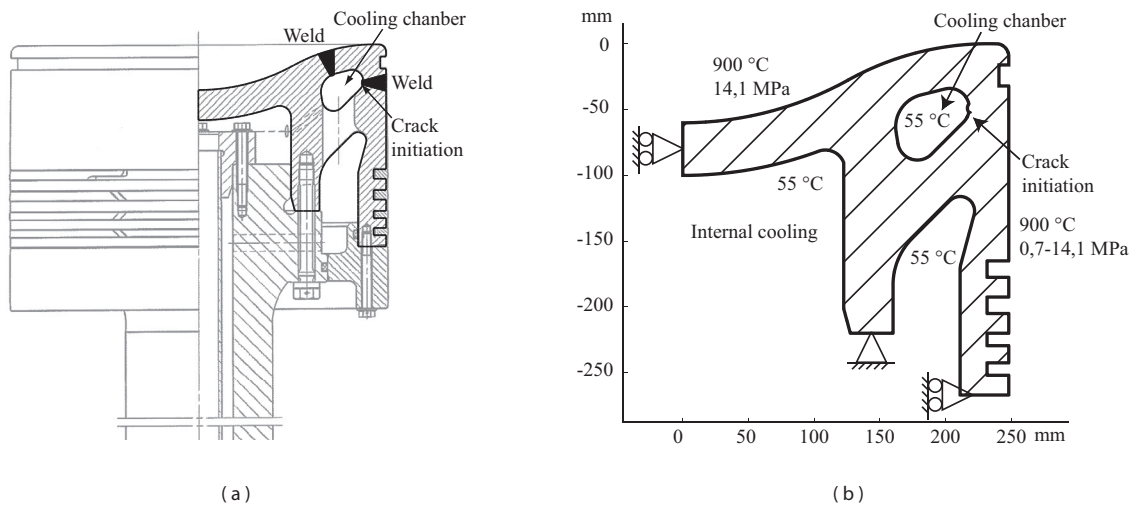
*Figure 6.1*    Model of the piston crown loaded with the maximum combustion pressure and steady state temperature field
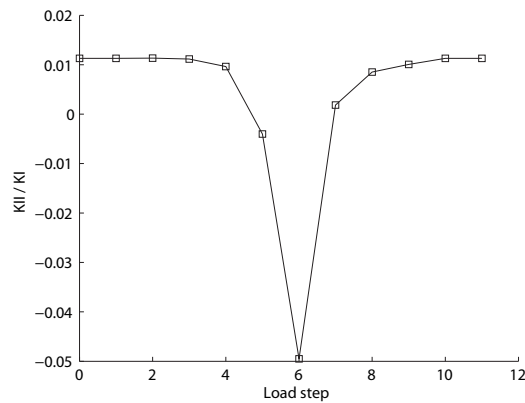


*Figure 6.2*    The ratio of $K_I$ and $K_{II}$ is calculated for a load cycle that represents a $360°$ rotation of the crankshaft

are generally observed to decrease and this is explained by the fact that the crack growth reduces the stiffness of the structure. Furthermore the reduced stiffness results in an increased variation of the $K_I$ for each crack increment and thus the crack growth rate will increase. When the crack is propagated perpendicular to the maximum principal stress direction the mode I loading will be dominant and small values of $K_{II}$ are expected. This tendency is seen to be in accordance with the results in figure 6.3.

To demonstrate the importance of choosing the correct pair of stress intensity factors to propagate the crack it is in addition chosen to perform calculations where the crack is propagated by the load step which gives the biggest deviation in the crack extension angle from the angle of load step 2. Therefore load step 6 is chosen to propagate the crack in the additional analysis. Load step 2 and 6 represents two extremes and any other prediction
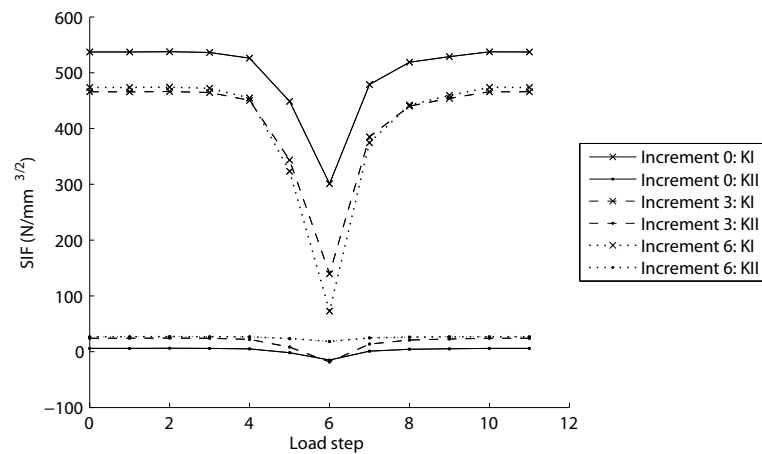
*Figure 6.3*   The stress intensity factors are calculated for load cycles that represent a $360°$ rotation of the crankshaft when the crack is propagated due to load step 2

of the crack extension angle will have values between these. The crack path predictions obtained by the two extremes are shown in figure 6.4. Comparing the crack propagated by the use of load step 2 with the crack in the micro sample it can be seen that they are in accordance with each other.

The crack propagated by load step 6 is as expected found to give the biggest deviation from the crack in the micro-sample. Thus no better choice of stress intensity factors to propagate the crack is obtained than in load step 2. The difference between the crack in the micro-sample and the crack propagated by load step 2 can be caused by the simplifications introduced in order to model the problem by a plane strain boundary element model.
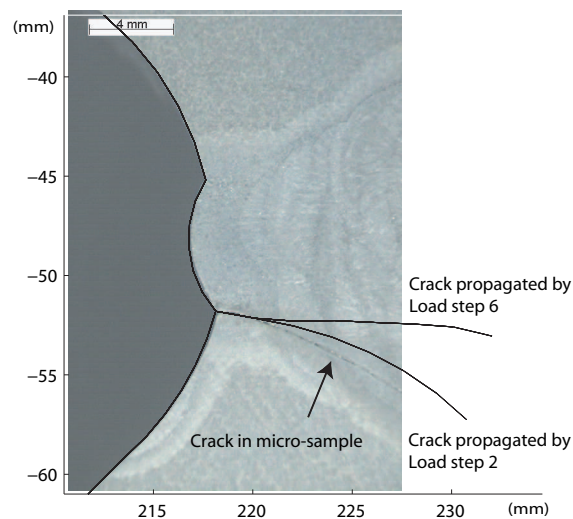


*Figure 6.4*   Micro-sample of piston crown with crack and calculations of cracks propagated by load step 2 and load step 6

## 6.2   Correction of the crack extension direction [P2]-[P3]

In order to avoid introduction of an error when a local crack growth criterion is used in an incremental crack growth formulation, each straight crack extension would have to be infinitesimal or have its direction corrected. The description of both a reference and a proposed procedure to correct the crack extension direction of a mixed mode crack path is summarized in this section together with the results of a test example. The study been performed is based on a formulation of the dual boundary element method (Portela et al., 1993). The crack extension direction is calculated by the maximum principal stress criterion (Erdogan and Sih, 1963).

The reference correction procedure presented by Portela et al. (1993) is firstly described and the expected performance is shortly discussed. In order to correct the local crack growth direction $\theta_{t(n)}$ so that it can be used to predict the crack growth direction of the $n$'th crack-extension increment a correction angle $\beta$ is introduced. This correction angle is given by $\beta = \theta_{t(n+1)}/2$ where $\theta_{t(n+1)}$ is the direction of the next crack-extension increment, also computed by the maximum principal stress criterion. For the current $n$'th crack-extension increment the i'th iteration can be summarized as follows

- For the first iteration only, evaluate the crack path tangent direction $\theta_{t(n)}$ using the maximum principal stress criterion

- Along the direction computed in the previous step, extend the crack one increment $\Delta a$ to $P^i$ and evaluate the new stress intensity factors

- With the new stress intensity factors and the maximum principal stress criterion evaluate the next crack-path direction $\theta^i_{t(n+1)}$

- Define the correction angle $\beta^i = \theta^i_{t(n+1)}/2$ measured from the increment defined in the second step

- Correct the crack extension increment, defined in the second step, to its new direction given by $\theta^{i+1}_{t(n)} = \theta^i_{t(n)} + \beta^i$

- Starting from the second step, repeat the above steps sequentially while $|\beta^{i+1}| < |\beta^i|$

This method for correcting the crack extension direction is demonstrated in figure 6.5. For each iteration the direction of the crack increment $n$ is moved towards the direction of the crack increment $n + 1$. Thus the correction angle $\beta^i$ is expected to decrease for each iteration until it changes sign at some point. Imagine that the procedure is repeated a specific number of iterations, $i = b$, until the crack tip $P^b$ is placed on the actual crack trajectory. At this point the correction angle $\beta^b$ is different from zero as shown on figure 6.5. If the correction procedure continues to run for $i > b$, the cracktip $P^i$ moves away from the actual crack trajectory until the point $P^c$ is reached. By this point the correction angle passes zero and the correction procedure will stop as $|\beta^{c+1}| < |\beta^c|$. This
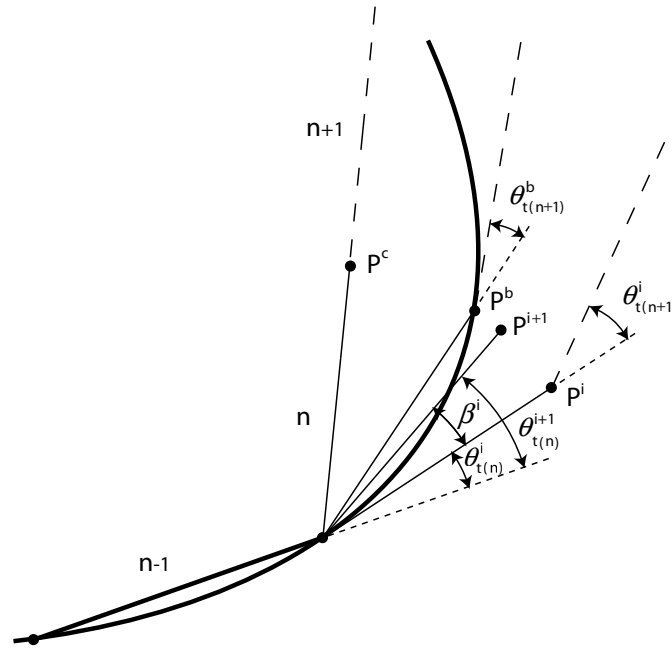
*Figure 6.5* Reference procedure for correction of the crack extension direction

postulate indicates the need for a different stop criterion for the iterative procedure. Two possibilities are either to limit the number of correction iterations that are performed or to stop the correction when the correction angle is below a certain value. However the utilization of these two stop criteria to calibrate the correction will depend on the problem that has to be solved.

In the proposed method the crack extension direction $\theta_n$ of an increment $n$ is found from the local crack growth direction at the previous crack tip $P_n$ and at the new crack tip $P_{n+1}$ combined with the assumption that the actual crack increment can be described as a second order polynomial.To illustrate the proposed crack correction procedure the actual crack path in figure 6.6 is considered. In the derivation of the expression for the corrected crack extension direction it is assumed that part of crack path u(x) describes the shape of a second order polynomial. For the iteration i an approximated value of the corrected crack extension angle $\theta_n^{i+1}$ is obtained from

$$tan(\theta_n^{i+1}) = \frac{1}{2}(tan(\theta_n) + tan(\theta_n^i + \theta_{n+1}^i)) \tag{6.1}$$

where $\theta_n$ is the local crack growth direction at the previous crack tip and $\theta_n^i$ is the corrected crack extension angle at the previous increment. Thus for the current n'th crack extension increment the i'th iteration can be summarized as follows

- For the first iteration only, evaluate the local crack growth direction $\theta_n$ by the maximum principal stress criterion and extend the crack one increment $\Delta a$ to $P_{n+1}^i$

- Calculate the stress intensity factors at $P_{n+1}^i$ and then calculate the next local crack growth direction $\theta_{n+1}^i$ using the maximum principal stress criterion

- Calculate the corrected crack-extension direction by using (6.1) and correct the crack extension increment.

- Starting from the second step repeat the above steps sequentially while $|\Delta\theta_n^i| > \beta$. The calibration constant is in this paper chosen as $\beta = 0.1°$.
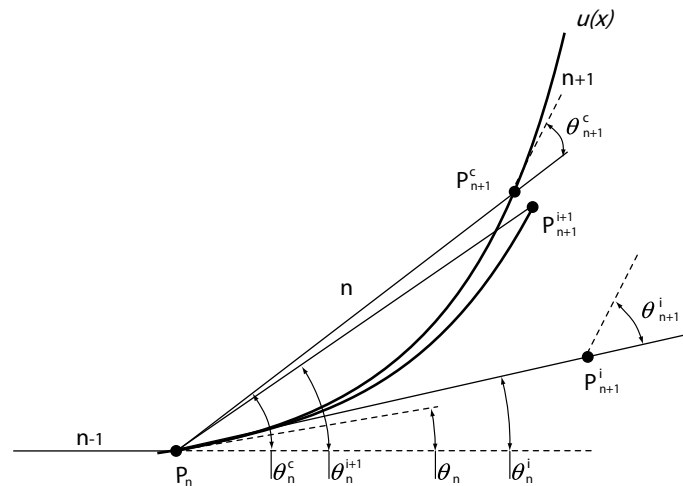


*Figure 6.6*    Proposed procedure for correction of the crack extension direction

The two methods to correct the crack extension direction have been studied in three examples described in the papers [P2]-[P3]. The results of the first and most pronounced example are summarized in this section. The results of this example are in accordance with the results of the other two examples. In the first example the regular cruciform plate (Portela et al., 1993) shown in figure 6.7.a is studied. To be able to evaluate the precision of the two correction methods it is chosen to find the actual crack path. The actual crack path can be found by the use of very small crack extensions for each increment. To assure that the size of the crack extensions are sufficiently small, several crack path analyses are performed in order to show that the crack path for each analysis converges towards the actual crack path. The crack paths are calculated with different number of increments and as shown in figure 6.7.b the difference between the crack paths increases as the cracks grow.

To illustrate the differences between the crack paths, distances are calculated between the reference crack path and a crack path calculated using another number of increments. A good representation of the actual crack path is found for this test example when 64 increments are used as discussed in [P2]. This is shown on figure 6.8.a as the actual crack path is chosen as a reference crack path.

The computations of the crack paths are performed with the use of the two crack correction methods. The computations are carried out with the two longest crack increments which give the biggest deviations from the actual crack path. The distances between the actual crack path and the crack path calculated with the crack correction methods are shown in figure 6.8.b. From the figure it appears that the crack path calculated with the
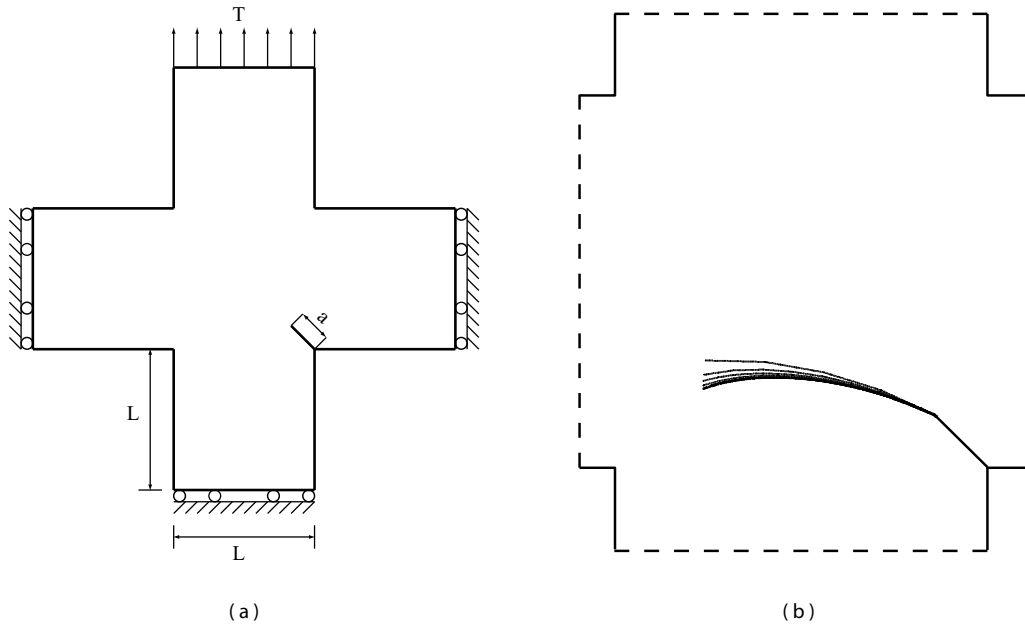
*Figure 6.7* Test example one (a) Cruciform plate with initial crack of length $a = 0.2L$ (b) Crack paths calculated without correction and with different number of increments
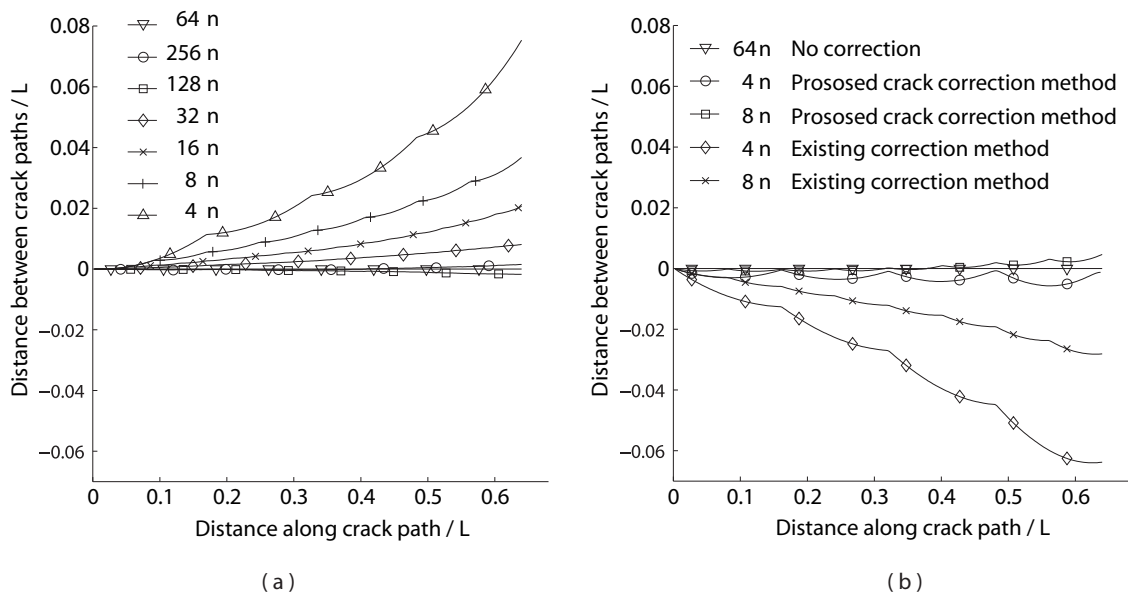


*Figure 6.8* Distance between crack paths with different number of increments (n) (a) without correction (b) with correction

reference correction method has moved to the other side of the actual crack path. This demonstrates an effect of overcorrection that was discussed in the summary of the reference correction method. The use of the reference correction method moves both crack paths closer to the actual crack path, but the crack paths are seen to deviate just as much

from each other as if no correction has been applied. Both results calculated with the proposed correction method appear to describe almost the same crack path much closer to the actual crack path. This indicates that the proposed crack correction method is less sensitive to the increment size and that it gives a much better approximation of the actual crack path.

To illustrate the two iterative crack correction methods the relation between the crack extension angles and the number of iterations is plotted in figure 6.9 for a crack path with 4 increments. The crack path with 4 increments is chosen because it deviates the most from the actual crack path when no correction method is applied. From the figure it appears that the reference correction method converges much more slowly towards the corrected crack extension angle than the proposed crack correction method. As expected, the proposed crack correction method results in angles very close to the corrected crack extension angle already after the first iteration. Thus fewer iterations are necessary for the proposed crack correction method.
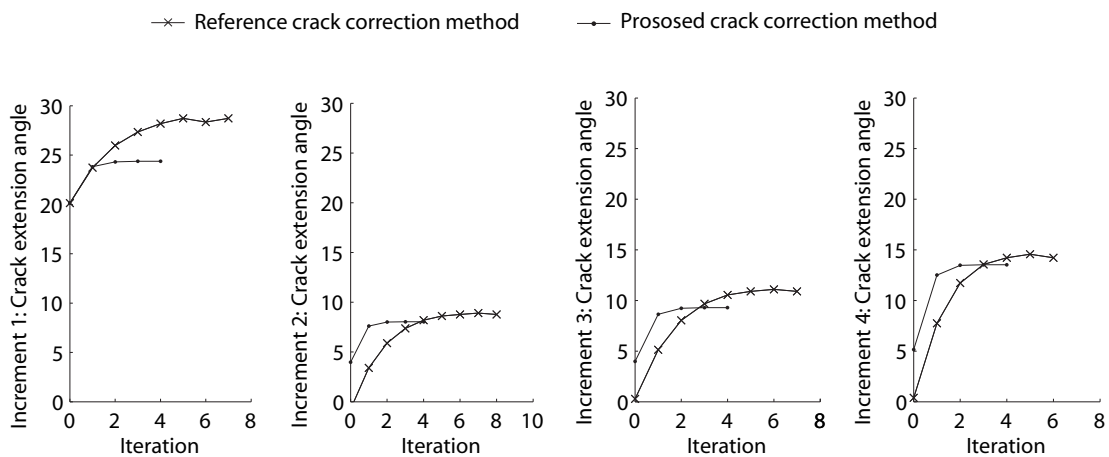


*Figure 6.9*     Relation between crack extension angle and the iteration number for each correction method

## 6.3 Analysis of non-planar 3D crack growth [P4]

A new method to analyze 3D non-planar crack growth is presented in [P4]. The proposed method takes advantage of both the boundary element method (BEM) and the finite element method (FEM). The BEM and FEM methods are linked by a submodelling strategy, figure 6.10, in which the solution of a global FE model containing an approximation of the crack is interpolated to a much smaller BE model containing a fine discretization of the real crack. In the development of the method it is found very important that the proposed method is compatible with existing FE models that have previously been developed for the complex engineering structures in terms of the commercial softwares ABAQUS.
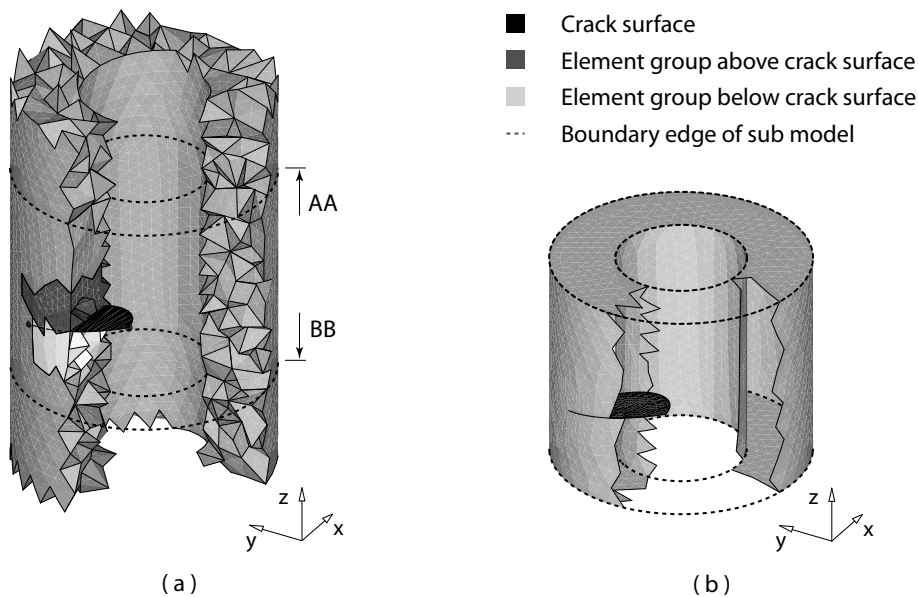


*Figure 6.10* Submodelling strategy in which part of the global model between cut AA and BB is reanalyzed by the use of a sub model (a) Global model with rough model of crack (b) Sub model with exact crack geometry

The use of the proposed method to analyze non-planar 3D crack growth is expected to be influenced by several factors such as the mesh size of the global model, the sub model size and the approximation of the crack geometry in the global model. Thus these factors have been investigated in [P4] by several analyses on a model of a test specimen for a large diesel engine. The model of the test specimen is shown in figure 6.11 and the material parameters used in this model are $E = 200 GPa$ and $\nu = 0.3$. The results obtained with the proposed submodelling strategy are evaluated by comparing to corresponding results obtained with a global cracked BE model. To ease the comparison the elements used to mesh the global BE model have the same small size as those in the BE sub model both in the vicinity of the crack and in the remaining domain. Due to the small element size and the excellent precision of the boundary element method very precise results are obtained
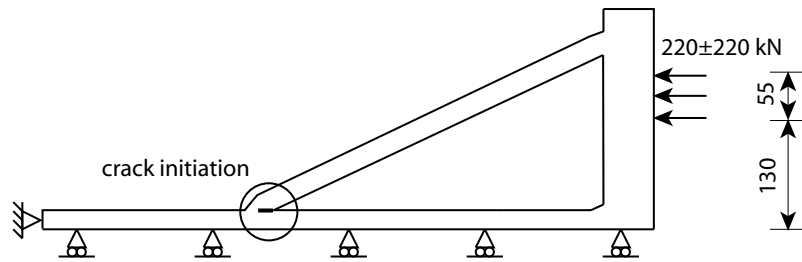
with the global BE model.



*Figure 6.11*    Model of the test specimen with pre-crack shown

The approximation of the crack in the global model is investigated together with the influence of the element size in the global model. Figure 6.12 displays six different approximations of the crack element faces in the global model. The crack surfaces (s1-s4) are obtained by two different schemes of the proposed method and different sizes of the elements in the global FE model. The crack surfaces (s5-s6) are obtained by manually meshing with two different sizes of the elements in the FE global model. By the first scheme (s1-s2) a smoothed selection of element faces as they are placed in the FE mesh represents the crack surface. In the second scheme (s3-s4) the chosen element faces are morphed to fit the real crack surface and thus a much better representation of the crack surface is obtained.

△  Crack element faces of global FE model
—  Edge of crack surface
···  Front of crack surface were visible above element faces
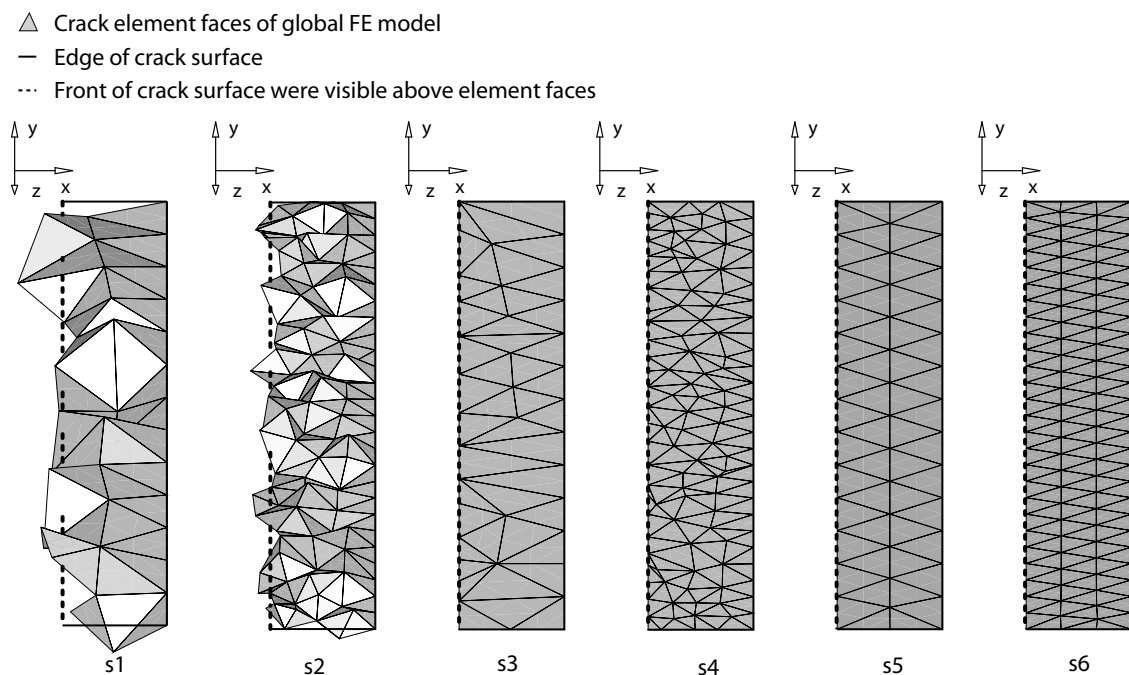


*Figure 6.12*    Crack element faces shown in perspective with average element size of 2.5 mm and 5.0 mm (s1-s2) Smoothed surfaces (s3-s4) Morphed surfaces (s5-s6) Manually meshed surfaces

The displacement field of each of the six different global models is interpolated to the boundary of the six equivalent sub models. Since the problems studied are primarily in-plane problems, figure 6.13 only display the $K_I$ and $K_{II}$ factors calculated by the use of the sub models. Comparing the values of the $K_I$ factor along the crack front it becomes obvious that the results obtained with the smoothed crack surfaces differ in the way that they have the largest deviation of approximately 4 % below the results of the global BE solution. While the results obtained with both the morphed surfaces and the manually meshed surfaces undershoot with approximately 2 %. By halving the number of elements in the vicinity of the crack in the global model the deviation is increased by approximately 1 % for the morphed and the manual meshed crack surface in the global model. The figure displaying the $K_{II}$ values shows more even results with less deviations. The results obtained with the smoothed surfaces overshoot the global solution by approximately 1.5 % while results obtained with the morphed and manually meshed surfaces are closer to the global solution with a deviation of 0 to 1 %. Almost no effect is obtained from doubling the number of elements close to the crack. From the presented results it is found that the results obtained with the morphed surfaces have such small deviations from the results obtained with the manually meshed surfaces that it can be concluded that the automatic mesh modification procedure gives just as good results as manual remeshing.
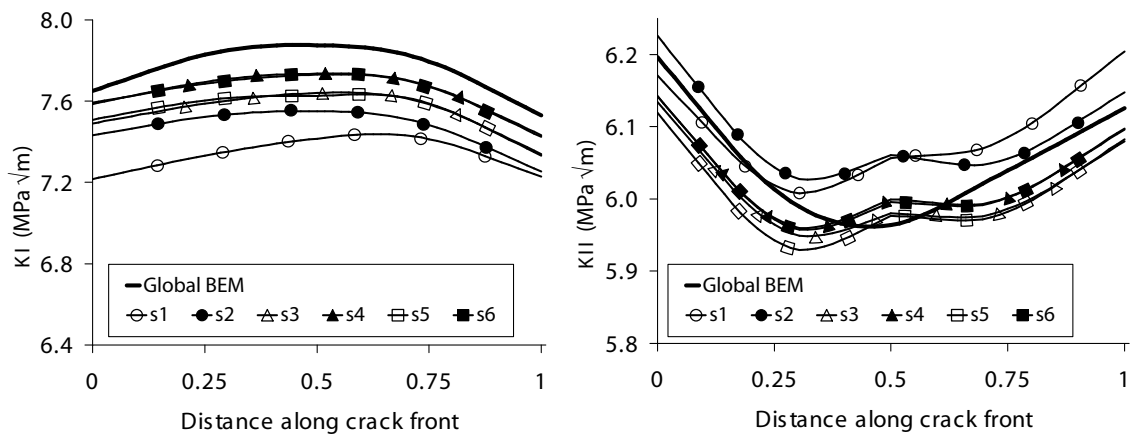


*Figure 6.13* Values of $K_I$ and $K_{II}$ along the crack front for the maximum loading

The study of the $K_I$ and $K_{II}$ along the front of the initial crack showed that very accurate results are obtained with the proposed method as compared to the global BE analysis. Calculations on fatigue crack growth in the test specimen have also been carried out to compare with experiments. Material data for the fatigue crack growth analysis is obtained by fitting of Paris law to measurements of crack growth in SENB test specimens. The crack growth has been analyzed by extending the crack in six increments and increment number six is shown figure 6.14 for both the global and the sub model. From the figure it is seen that the best representation of the crack in the sub model is clearly obtained by the morphing scheme. However as the crack grows the size of the FE elements has decreased relative to the the total crack length and since small elements yield good results the smoothing scheme is also expected to give good results.

*Figure 6.14*    Increment six of crack growth analysis (a) Crack in sub model seen along z-axis (b) Perspective view of smoothed crack element surface in global FE model (c) Perspective view of morphed crack element faces in global FE model
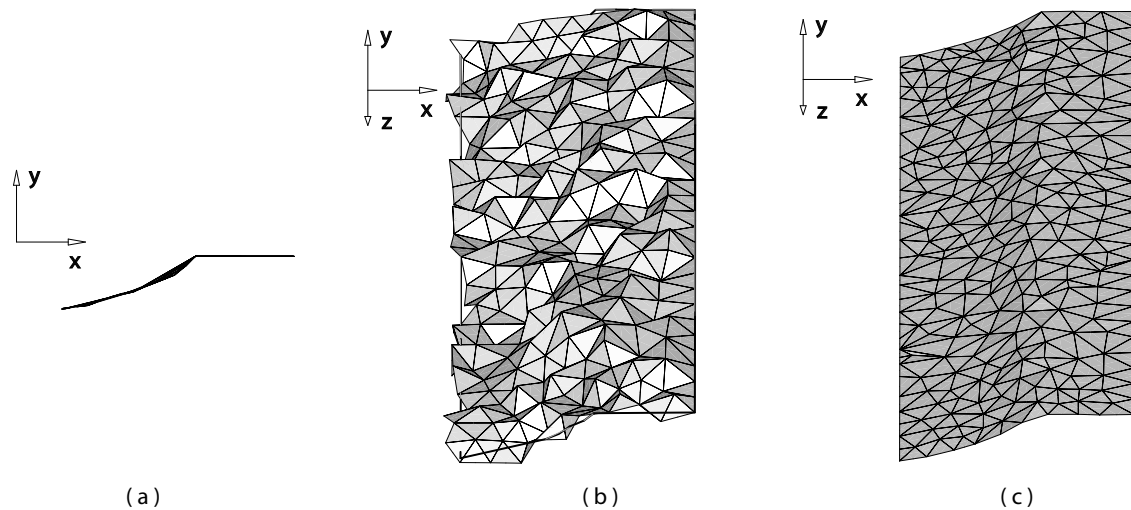
The stress intensity factors have been calculated at the center of the crack for the global BE model and for different configurations of the proposed method as shown in figure 6.15. The values shown in the figure are not directly comparable after the first crack extension since deviations of the values of the stress intensity factors result in different crack paths. The differences in crack path are however expected to be small as there is a reasonable correlation between the stress intensity factors and as the average crack extension of 2 mm is kept constant for all calculations. Comparisons of the $K_I$ values show a general increase when the crack grows as would be expected because the stiffness of the structure is reduced while the loading is held constant. The largest deviation of 6 % from the global BE solution is as expected obtained for the smoothed crack surface with an element size of 5.0 mm in the global model. From this solution it is further seen that the deviation from the global BE solution both increases and decreases, which can be explained by the dependence on the element locations in front of the crack. The solutions obtained for the proposed method using smoothing with small elements and morphing with large elements are almost the same with a maximum deviation of approximately 3%. The solution obtained with morphing and small elements has a maximum deviation of approximately 2%. Values of $K_{II}$ tend toward zero after the first crack increment as can be expected from the use of the strain energy density criterion. Small variations in the crack shape for each calculation will result in noticeable variations in the $K_{II}$ value and thus when the values are close to zero large percentage deviations are found. The existence of small deviations of the crack shape for the different analyses are indicated by the increased deviations in the $K_{II}$ values when the crack grows.

The results of the crack growth analysis are compared to the results of experiments. The predicted crack path, figure 6.14.a can be compared to the primary crack path observed in the experiment, figure 6.16.a from which it is seen that a nearly perfect match
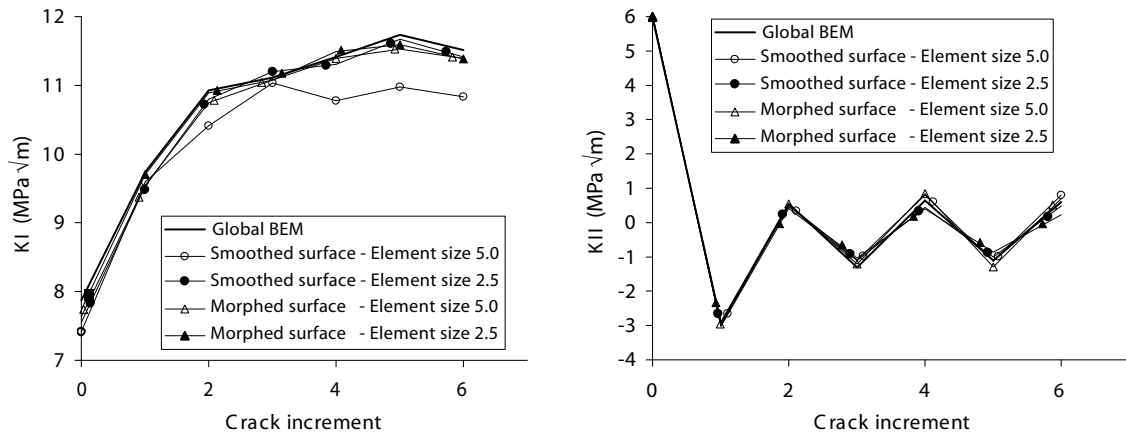
*Figure 6.15*    Values of $K_I$ and $K_{II}$ at the center point of the crack front for each crack increment

is obtained. Comparison on the crack growth rate is also performed as the experimental crack has been equipped with a crack gauge on each side of the structure. The results of the crack gauges, figure 6.16.b show as expected that the crack propagates equally fast on both sides of the structure. The average crack growth rate measured by the two gauges can be calculated by the results shown in figure 6.15 to be $4.6 \cdot 10^{-9}$ m/cycle and $6.3 \cdot 10^{-9}$ m/cycle. When these crack growth rates are compared with the results of the material testing [P4] it can be seen that $\Delta K_{eff}$ at the crack front can be expected to be in the range of $12 - 15.5 MPa\sqrt{m}$. The calculated $\Delta K_{eff}$ for the pre-crack and the first increment are 12 $MPa\sqrt{m}$ and $11.5 MPa\sqrt{m}$ respectively. Thus good agreements between the calculated and measured crack growth rates are obtained.
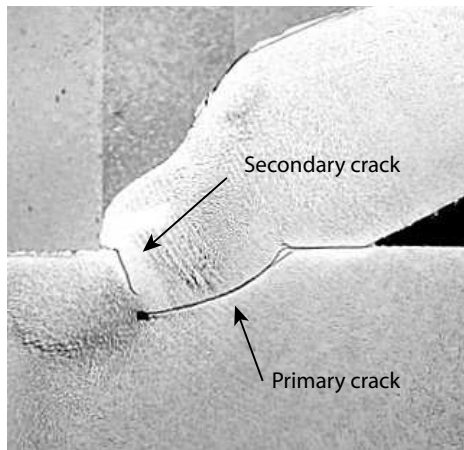
<div align="center">( a )</div>
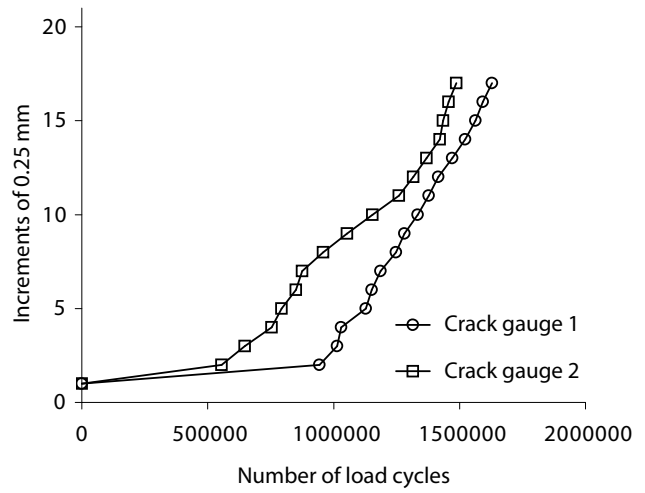


<div align="center">( b )</div>

*Figure 6.16*    Test results (a) Cracks in test specimen (b) Measured crack increments of primary crack

# Chapter 7
# Analysis of fatigue crack growth in large diesel engines

The proposed method to analyze 3D non-planar crack growth is finally demonstrated on a case of fatigue crack growth in a large diesel engine. The demonstration aims to show the capability of the proposed method on these advanced engineering structures and it further enables a discussion on additional developments that can improve the analysis of crack growth in large diesel engines. Thus the configuration used to analyze crack growth in the present section serves a demonstration purpose.



Connection surface:
 Frame - Cylinder

Piston rod

Guide planes

Guide shoe

Connecting rod

Chrank shaft

Stay bolt tubes

Connection surface:
Frame - Cylinder

Guide planes

Main bearing

Section

( a )

( b )
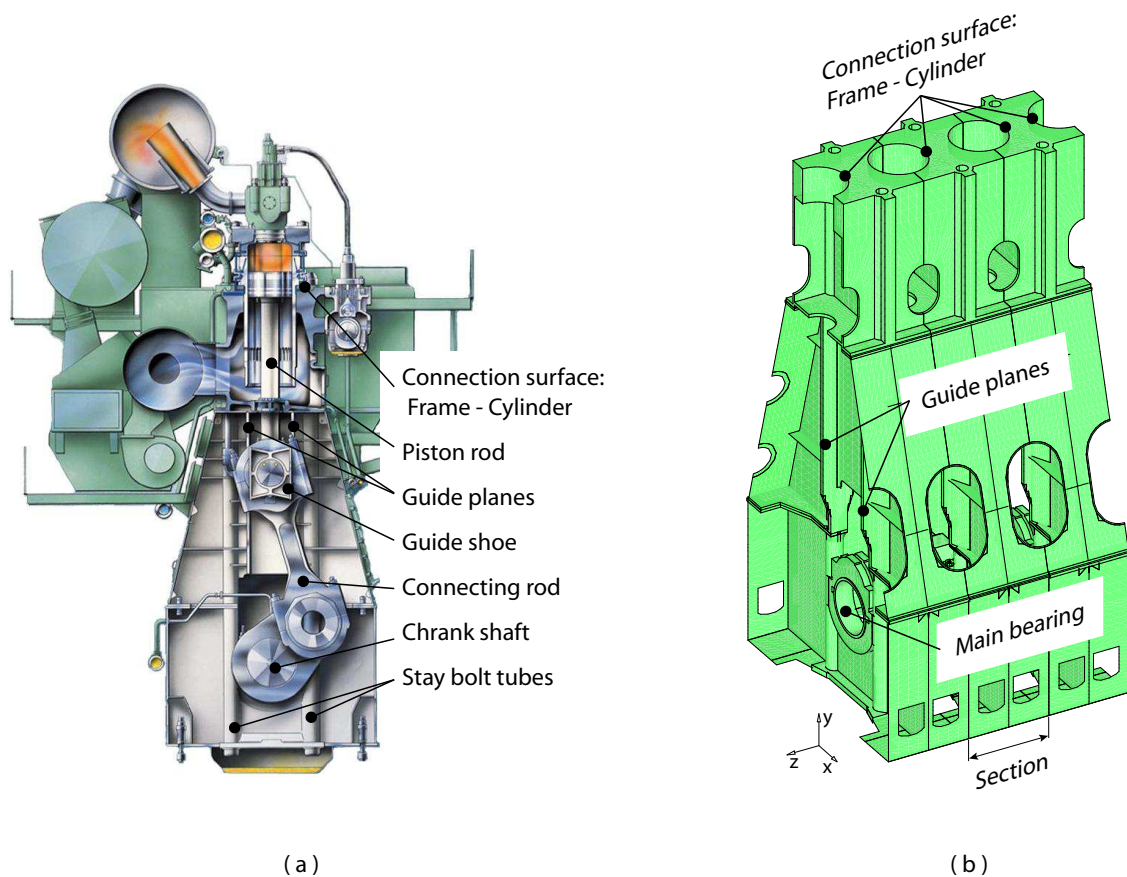
*Figure 7.1*    Large diesel engine (a) Cross section of engine (b) Model of engine frame with approximately $10^6$ degrees of freedom

The analysis of fatigue crack growth in a large diesel engine is very different from the analysis of fatigue crack growth in a test specimen such as the one studied in [P4] because the loading of the crack in an advanced engineering structure is often very complex. An example of the complexity is non-proportional loading. Thus in the present section sev-

55

eral different criteria to perform fatigue crack growth in complex loaded structures are considered.

The engine to be analyzed is a 12 cylinders two stroke engine with a cylinder bore of 90 cm for which the cross section can be seen in figure 7.1.a. The crack has been observed to grow in a small part of the engine frame and a model of part of the frame is needed in order to predict crack growth. A previously developed model of the engine frame exists and thus it is possible to take advantage of one of the main ideas of the proposed method, the ability to analyze crack growth in a previously developed computational model. The frame model used is only briefly explained in the following as it could be any other advanced engineering structure that could be studied for crack growth.

The model of the frame consists of several models of sub parts which are aligned in the global FE coordinate system to form a section of the frame between the halves of two cylinders placed next to each other. This section of the frame can then be duplicated to cover the desired number of cylinders. The frame model is shown in figure 7.1.b and it appears that it contains two duplicates one on each side of the section of interest. The connection of the parts are in general done by either prescribing continuity of displacements or by the use of a contact formulation. For the present frame model it is chosen to model the assembly of the main bearings by the use of a contact formulation while continuity of displacements are prescribed on the remaining surfaces. The stationary loading is at first applied to the frame model by pretension of the stay bolts that hold the frame together, figure 7.1.a and the studs that hold the main bearing assemblies together, figure 7.2.a.
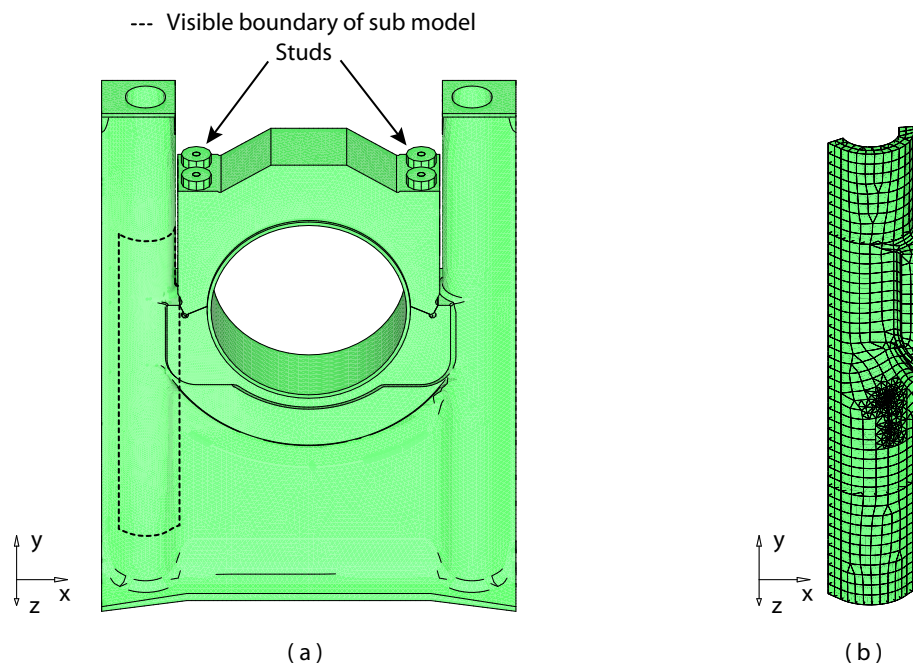


*Figure 7.2* Models of frame (a) Part of FE model that contains the crack (b) BE sub model that contains the hole area of interest for analysis of crack growth

The dynamic loads of the moving parts on the frame are obtained by a dynamic anal-

ysis of the moving parts that convert the translation of the piston crown to the rotation of the crank shaft. These loads are applied to the guide planes and the main bearings of the frame, figure 7.1.a, by either hydro dynamic or elasto hydro dynamic analyses. In addition the dynamic load of the pressure in the combustion chamber is applied to the common surface of the frame and the cylinder pointed out in figure 7.1.a. The dynamic load operating on the frame during one $360°$ cycle of the crank shaft defines one load cycle. This load cycle is analyzed by discretization into 36 load steps that represent evenly distributed angular positions of a full rotation of the crank shaft.

The area of interest for the present crack growth calculation is the stay bolt tube in the engine section in the middle of the model. If a sufficiently large material defect formed as a crack is located on the inside of the tube it is expected to be capable of growing. Figure 7.2.a illustrates the area of interest in a part of the global FE model and figure 7.2.b displays the sub model used by the proposed method to propagate the crack.
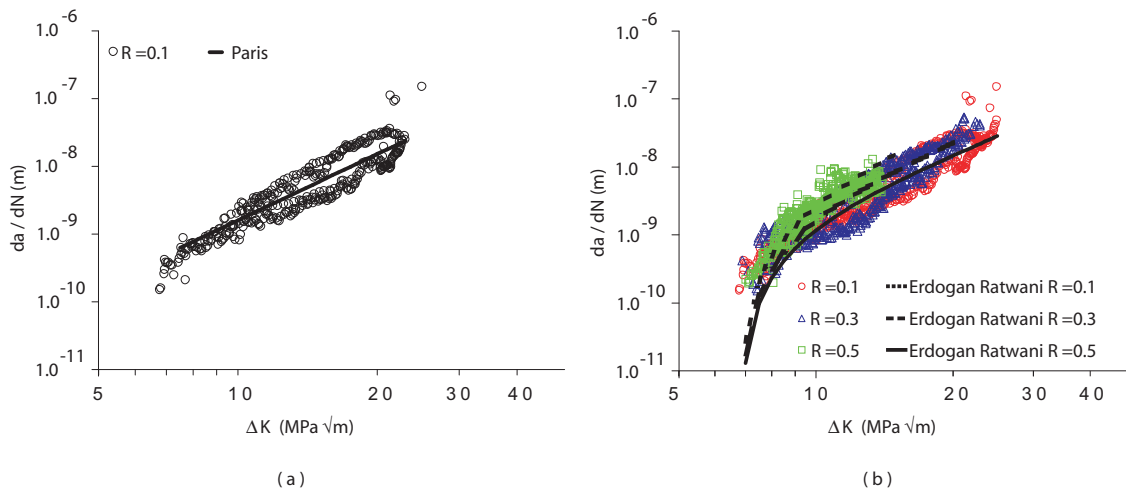


*Figure 7.3* Fitting of crack growth laws to measurements of fatigue crack growth (a) Paris law fitted to experimental results for R=0.1 (b) Erdogan and Ratwani (1970) for R equal to 0.1, 0.3 and 0.5

To analyze fatigue crack growth of the structure several material tests have been carried out for load ratios $R = K_{min}/K_{max}$ of 0.1, 0.3, 0.5 of the material of the stay bolt tube. Based on this test data crack growth laws can be fitted to describe the material. Paris law of fatigue crack growth (Paris and Erdogan, 1963) and an extension of this law proposed by Erdogan and Ratwani (1970) are considered in the present example

$$\frac{da}{dN} = C(\Delta K)^n \tag{7.1}$$

$$\frac{da}{dN} = \frac{C_0(\Delta K - \Delta K_{th})^m}{(1 - R)K_c - \Delta K} \tag{7.2}$$

The fitting of the two crack growth laws to the available material data is shown in figure 7.3. As illustrated in the figure the load ratio influence the measured relation of $\Delta K$

and $\frac{da}{dN}$. Paris law does not include the effect of changed load ratio and it is only intended for the part of the curve which is straight. On the opposite the growth law by Erdogan and Ratwani (1970) can be fitted to all regions of the curve if sufficient material data exist and the crack growth law does take the effect of R into account. In the present version of the boundary element software (BEASY, 2007) the crack growth module fails to predict a new crack front if part of the crack front is growing much slower than the rest. By the use of the crack growth law by Erdogan and Ratwani (1970) the crack growth rate drops drastically at the values of $\Delta K$ close to $K_{th}$. Thus to stabilize the prediction of the crack extension and to keep the demonstration example simple it is chosen to use Paris law to propagate the crack fitted for $R = 0.1$. As an extension of the use of Paris law one could use Walkers law (Walker, 1970) which include the effect of changed load ratio without the effect of fast changing grow rates close to the threshold values.

A penny shaped crack is chosen as the initial crack with a length six times as long as it is deep. The initiation point and direction are chosen by the best judgement of the pictures available of the real crack. The size of the initial crack is chosen as relatively small compared to the final crack length and reasonable according to the size of the elements in the global model as discussed in [P4]. The $K_I$, $K_{II}$ and $K_{III}$ factors are calculated along the crack front during one load cycle and to illustrate the results the factors calculated at the center of the crack are shown in figure 7.4 for each load step. From the figure it is seen that the inserted crack is loaded in mixed-mode since it is exposed to high values of all modes of fracture during the load cycle.
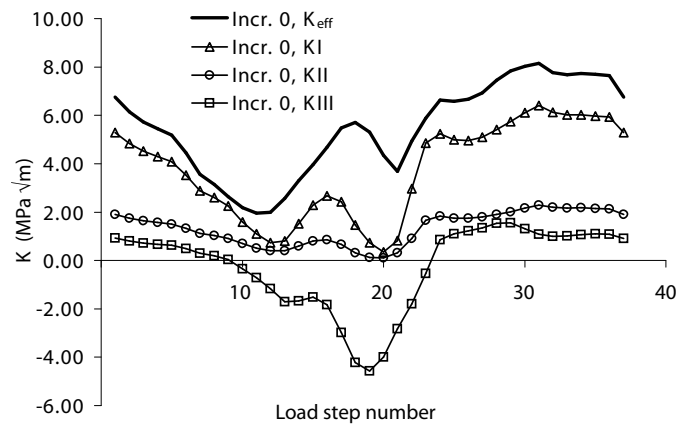


*Figure 7.4*    Stress intensity factors calculated at the center of the initial crack

Analyses of mixed-mode fatigue crack growth based on Paris law are possible by the definition of an effective stress intensity factor which takes all three modes of fracture into account. In the literature two different ways of defining this effective stress intensity factor are found

$$\Delta K_{eff} = f(\Delta K_I, \Delta K_{II}, \Delta K_{III}) \tag{7.3}$$

$$\Delta K_{eff} = K_{eff}^{max} - K_{eff}^{min} \tag{7.4}$$

The expression (7.3) does not take into account the relative variation of $K_I$, $K_{II}$ and $K_{III}$ during one load cycle. A typical example of relative variation is demonstrated for the present example in figure 7.4. Since the relative variation of the stress intensity factors is considered to be very important it is chosen to use the expression (7.4). Several expressions for the effective stress intensity factor can be found in the literature as discussed in [P4], examples of these are

$$K_{eff} = K_I \tag{7.5}$$

$$K_{eff} = \sqrt{K_I^2 + K_{II}^2 + K_{III}^2} \tag{7.6}$$

$$K_{eff} = \sqrt[4]{K_I^4 + 8K_{II}^4 + \frac{8}{1-\nu}K_{III}^4} \tag{7.7}$$

$$K_{eff} = \sqrt{(K_I + B|K_{III}|)^2 + 2K_{II}^2} \tag{7.8}$$

While the first expression can be considered to be a good approximation for mixed-mode problems dominated by mode I, the remaining expressions tend to describe $K_{eff}$ as the dominance of mode I is decreased. The sum of squares (7.6) weighs the different modes of fracture equally. (7.7) is an extension of the widely used expression by Tanaka (1974) for the two plane modes of fracture in which all three modes of fracture are included. The expression of $K_{eff}$ (7.8) is used by Gerstle (1985) and it is in accordance with the expression of Mi and Aliabadi (1995) where the empirical constant is chosen as $B = 1$. The expression of (7.8) is used in the present example as it has been used in [P4] to perform an accurate estimate of the crack growth rate. However since the properties of these expressions vary with the ratio of $K_I$, $K_{II}$ and $K_{III}$ one expression can not be considered to be generally applicable without the necessity to perform several tests. The more dominant the mode I loading is the more reliable the expression for $K_{eff}$ becomes as the results of the expressions come closer to each other and as Paris law is derived for mode I loading.

From the calculated values of $K_I$ and $K_{II}$, figure 7.4, it is seen that the ratio of $K_I$ to $K_{II}$ varies during the load cycle. Thus the initial crack is subjected to non-proportional loading which could be expected for such a complex example of both geometry and loading. Crack growth in a piston crown exposed to non-proportional loading is covered in [P1] in which good results were obtained with a simple criterion to calculate the crack growth angle $\theta$, that is

$$\theta = \theta(K_{eff}^{max}) \tag{7.9}$$

The load cycle for the present example is however more complex and thus additional criteria is considered to propagate the crack at each point along the crack front. Examples of these are

$$\theta = \frac{\theta(K_{eff}^{min})K_{eff}^{min} + \theta(K_{eff}^{max})K_{eff}^{max}}{K_{eff}^{min} + K_{eff}^{max}} \tag{7.10}$$

$$\theta = \frac{\sum \theta(K_{eff}^i)K_{eff}^i}{\sum K_{eff}^i} \qquad \text{for } K_{eff} > K_{eff}^{i-1} \tag{7.11}$$

In the expression (7.11) the extension angle is calculated for each load step that has higher value of $K_{eff}$ than the previous load step. The final crack extension angle is calculated by factoring the calculated extension angles by the size of $K_{eff}$. An expression according to this can be found in Spievak et al. (2001). A simplification of this expression can be considered (7.10), for which it is much easier to estimate the crack extension angle by looking at the $K_I$ and $K_{II}$ factors and thus this criterion is used in the present test example. Good results are expected for both (7.10) and (7.11) if used in the example described in [P1] as high values of $K_{eff}$ are obtained for the load step which gives the best results.
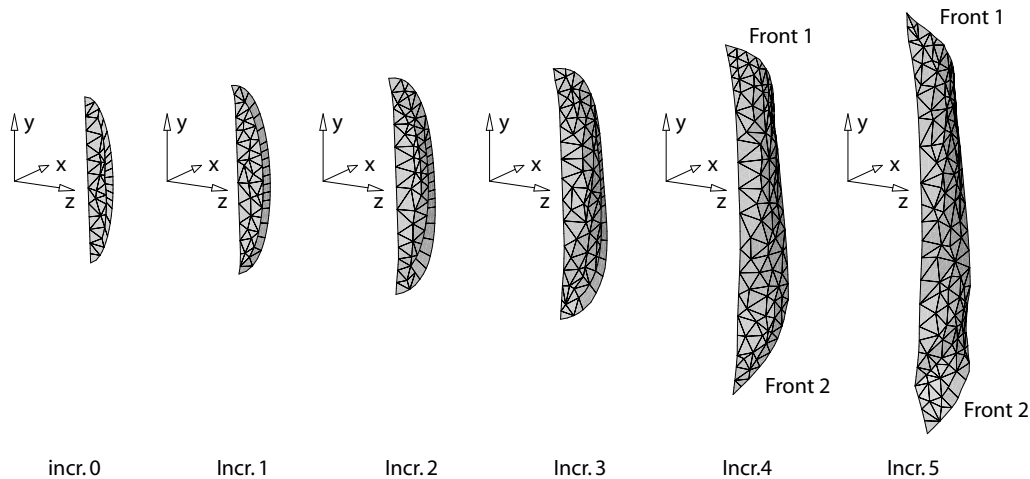


*Figure 7.5*    Growth of a crack in the frame

Based on the above choice of criteria the crack can be propagated in several increments each of these increments is shown in figure 7.5. In figure 7.6.a the calculated values of $\Delta K_{eff}$ have been shown along the crack front for the first three increments. The values of $\Delta K_{eff}$ are very close to the values $K_{th}$ observed for the material tests. As Paris law is used and the $K_{th}$ is set equal to 0 it is possible to continue the crack growth analysis. As the crack grows the values $\Delta K_{eff}$ increase except at the center of the crack.

In figure 7.6.b the values of stress intensity factors for the center point of crack increment 3 are shown. From this figure it is seen that low and almost negative values of the $K_I$ factor close to the outer surface of the stay bolt tube are obtained. Negative values of $K_I$ indicate that the crack surfaces are overlapping, which is not possible in reality. As the present version of BEASY is not capable of considering contact in connection with the dual boundary element formulation additional criteria are considered in order to continue the crack growth prediction in the best possible way. Assuming no friction between the surfaces of the crack the $K_I$ is kept equal to zero while $K_{II}$ and $K_{III}$ vary as calculated. Alternatively, we could assume full friction between the surfaces of the crack so that $K_I$ is kept equal to zero while $K_{II}$ and $K_{III}$ are kept equal to the values of the last load step with positive $K_I$. In the present example it has only been possible to carry out the calculation with the assumption of no friction. The no friction assumption can further be
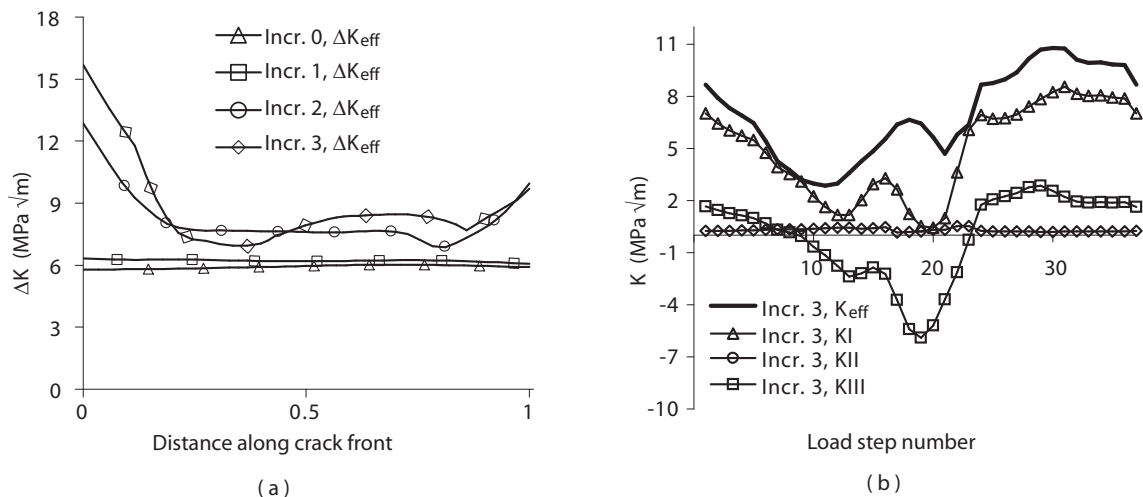
*Figure 7.6* Stress intensity factor calculated of the growing crack (a) $\Delta K_{eff}$ of increment 1-3 (b) Stress intensity factors at the center point of the crack for increment 3

considered to be the most conservative assumption as the assumption gives higher values of $K_{II}$ and $k_{III}$ and thus higher values of $\Delta K_{eff}$ and the crack grow rate.

When the crack penetrates the outer surface of the stay bolt tube then especially one end of the crack has higher values of $\Delta K_{eff}$, which causes the crack to propagate faster down along the stay bolt tube. The crack has now changed character as it is a two bay crack. The values of $\Delta K_{eff}$ for the two crack fronts and the first two increments of the two bay crack are shown in figure 7.7. From the figure it is seen that the values of $\Delta K_{eff}$ now are above the threshold values. The lower crack front has generally higher values of $\Delta K_{eff}$ and it will thus grow faster.
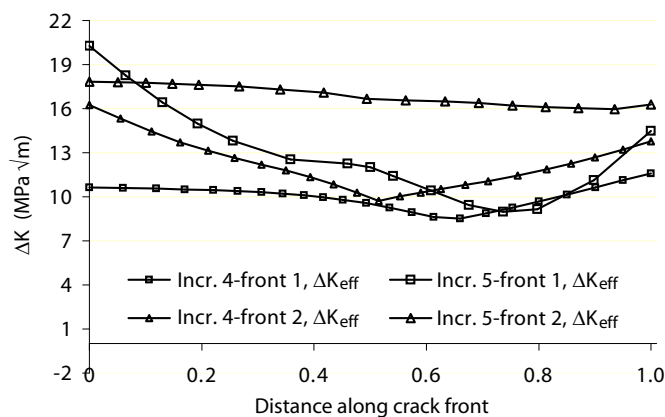


*Figure 7.7* Values of $\Delta K_{eff}$ for the two fronts of the growing crack

To illustrate the variation of the stress intensity factors over one load cycle at each crack front the calculated values are shown in figure 7.8 at the center point of each crack front. By comparing figure 7.8.a with figure 7.8.b it is seen that the variation of the stress

intensity factors follows much the same pattern with the highest values of $K_{eff}$ around load step 30 and the lowest values around load step 12. For high values of $K_{eff}$ the mode I loading is dominant for crack front 1 and the largest for crack front 2 and thus the validity of $K_{eff}$ is considered reasonable as discussed above.
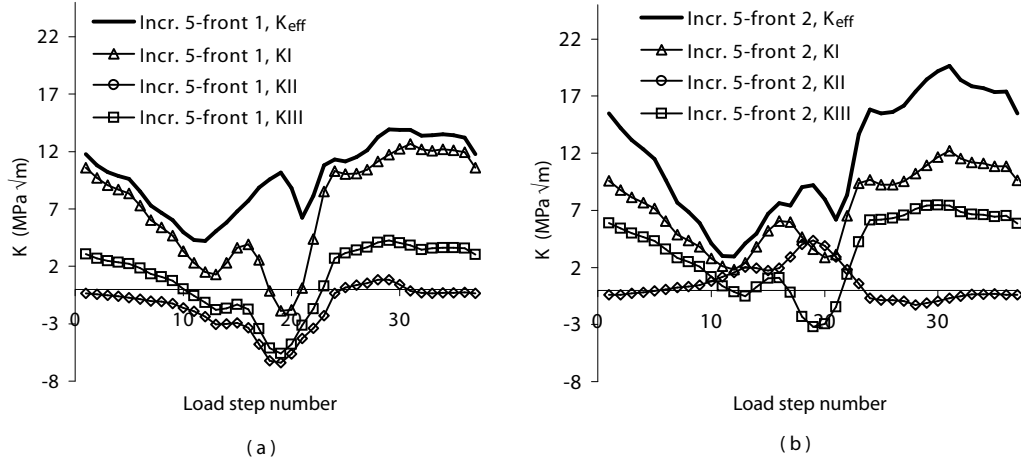


*Figure 7.8*    Stress intensity factors calculated at the center of the crack for both crack fronts of increment 5

A crack with a length of 12 cm and a depth of 2 cm was inserted in a model of an engine frame. The position and orientation of the inserted crack was based on an estimate of the initiation site and angle of a real crack. By several increments the crack grew from the inner surface of the stay bolt tube to the outer surface, a distance of approximately 3.2 cm. When the crack reached the outer surface it changed character to a two bay crack which continued to propagate along the stay bolt tube. Thus in the final increment of the calculation the crack had grown 5.3 cm upwards and 13 cm downwards. When comparing the predicted crack with a part of the real crack path as in figure 7.9 it is seen that they are in accordance with each other.
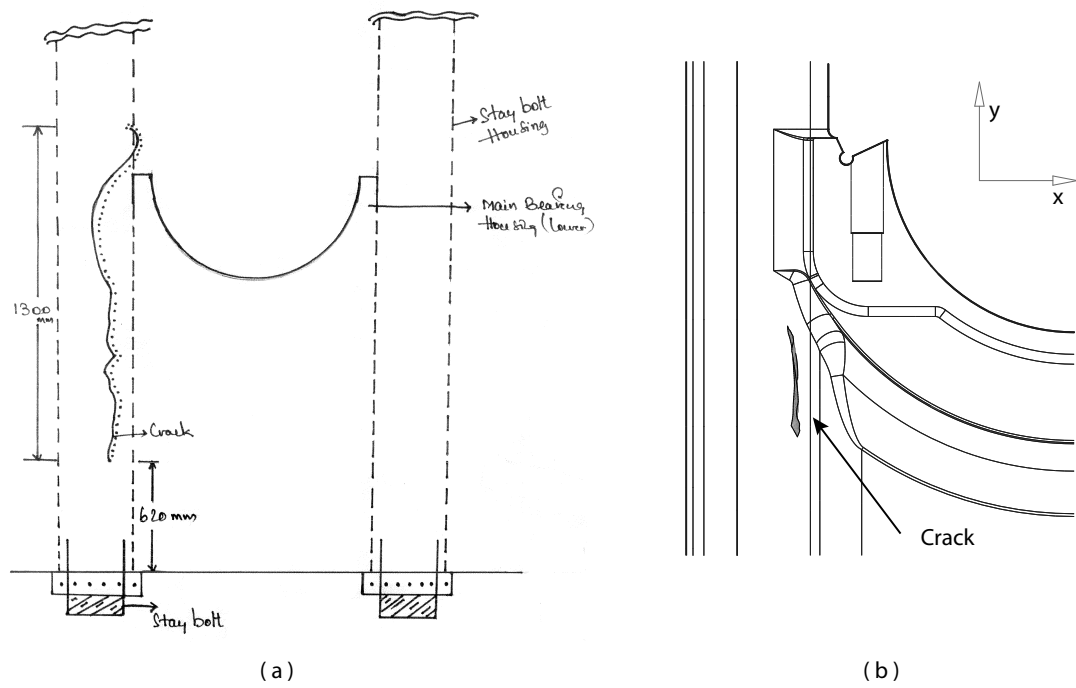
*Figure 7.9*   Crack growth in the frame of a large diesel engine (a) Sketch of real crack drawn on site (b) Model of crack growth

# Chapter 8
# Conclusion

The boundary element method has been used in this thesis to predict crack growth in several test structures and structures of large diesel engines. In the first part of the project a two dimensional boundary element program was developed by the formulation of Prasad et al. (1994). In the final part of the project three dimensional non-planar crack growth was analyzed by the development of a solution based on software from different commercial providers. Good agreements on crack paths and growth rates were found in all predictions, which motivated to an increased complexity of the analyses to be performed in the thesis. Four papers [P1] to [P4] have been included in the thesis. These papers form a base of knowledge used in the final complex fatigue growth calculation applied on a complex model of an engine frame.

The two dimensional thermoelastic dual boundary element formulation (Prasad et al., 1994) was used to analyze crack growth in a plane strain model of an axisymmetric crack in a piston crown. The thermal exposure of the piston crown gave rise to positive mean stress while the pressure in the combustion chamber resulted in cyclic load on the piston crown. The combination of these loads resulted in the propagation of the crack. The non-proportional character of the loading influences the prediction of the crack growth direction. The importance of choosing the right pair of stress intensity factors to propagate the crack in case of non-proportional loading was demonstrated. It was found that the load step with the highest $K_I$ of the dominant mode I loading was the obvious choice to be used to propagate the crack. Despite the simplified model and the challenge of non-proportional loading it was possible to obtain good correlation between the predicted crack path and a micro-sample of the cracked piston crown.

The extension of curved cracks by straight elements was studied in [P2] and [P3] by the use of the two dimensional dual boundary element formulation (Portela et al., 1992). A new correction procedure to correct the extension direction was proposed and compared to a reference procedure (Portela et al., 1993). The two procedures were compared in three examples and it was shown that the proposed method gives a much better approximation to the actual crack path. Furthermore the proposed crack correction procedure is shown to depend very little on the increment size as compared to the reference procedure. It is also demonstrated that the proposed method uses fewer iterations to obtain a better approximation of the actual crack path. The work carried out with the correction of the crack extension direction for two dimensional problems is worth keeping in mind when dealing with three dimensional crack growth predictions for which the computational cost is much larger.

To be able to analyze complex engineering structures as in large diesel engines a new method was proposed in [P4] to predict 3D non-planar crack growth. In the development of the method it was considered to be a very important feature that the method is able

to perform accurate crack growth analysis in large complex FE models that have previously been developed. The proposed method takes advantage of a submodelling strategy in which the crack in the global FE model can be described by two different approximations of the real crack in the BE sub model. The precision of the proposed method is shown to increase by adjusting three parameters, i.e. when the best approximation of the crack in the global FE model is used, when the element size in the global model is decreased and when the size of the sub model is increased. By comparisons of predictions and experiments for crack path and crack growth rate by the proposed method good agreement was found. According to all of the results presented it is concluded that the proposed method can be used to perform accurate numerical evaluations within Linear Elastic Fracture Mechanics.

The proposed method for the analysis of 3D non-planar crack growth [P4] is finally applied to a large and complex model of an engine frame. A pre-crack is inserted in the model of the frame by evaluation of the final crack path observed in a real engine frame. The complex loading of the three dimensional crack front can be analyzed by the combination of several criteria as discussed in the chapter 7. Based on a brief discussion and reference to the results of [P1] and [P4] a combination of the criteria is chosen and the crack is propagated in several increments. In the present example it was found that a contact formulation was needed to avoid that the crack surface collapses. As this was not possible within the scope of this project additional criteria were suggested as an alternative. By comparison with the crack path of a real frame it is seen that a good correlation is obtained for the part of the crack path that has been modelled. Since many criteria exist to analyze this complex example it is emphasized that several more comparisons with real cracks will increase the knowledge of choosing the optimal criteria. Thus this thesis has provided tools which will improve analyses of crack growth in complex structures.

# References

Aliabadi, M.: 2002. *The Boundary Element Method Volume 2: Applications in Solids and Structures*. John Wiley & Sons. Chichester.

Anderson, T.: 1995. *Fracture Mechanics*. CRC Press. Florida.

Barsoum, R. 1976. On the use of isoparametric finite elements in linear fracture mechanics. *International Journal for Numerical Methods in Engineering* **10**(1), 25–37.

BEASY: 2007. Beasy version 10 release 8 - documentation.

Becker, A.: 1992. *The boundary element method in engineering: A complete course*. McGraw-Hill. London.

Betti, E. 1872. Teoria dell'elasticita. *Il Nuovo Cimento* **2**, 7–10.

Blandford, G., Ingraffea, A. and J.A., L. 1981. Two-dimensional stress intensity factor computations using the boundary element method. *International Journal for Numerical Methods in Engineering* **17**(3), 387–404.

Brebbia, C. and Dominguez, J. 1977. Boundary element methods for potential problems. *Applied Mathematical Modelling* **1**(7), 372–378.

Crouch, S. 1976. Solution of plane elasticity problems by displacement discontinuity method .1. infinite body solution. *International Journal for Numerical Methods in Engineering* **10**, 301–343.

Cruse, T.: 1972. Numerical evaluation of elastic stress intensity factors by the boundary integral equation method. *The surface Crack: Physical Problems and Computational Solutions*. ASME. New York. pp. 153–170.

Cruse, T. and Rizzo, F. 1968. A direct formulation and numerical solution of general transient elastodynamic problem. *Journal of Mathematical Analysis and Applications* **22**(1), 244–259.

dell'Erba, D. 1999. Dual boundary element formulation for three-dimensional thermoelastic fracture mechanics. *PhD thesis, Wessex Institute of Technology, University of Wales*.

dell'Erba, D. and Aliabadi, M. 2000. Three-dimensional thermo-mechanical fatigue crack growth using bem. *Internal Journal of Fracture* **22**(4), 261–273.

Erdogan, F. and Ratwani, M. 1970. Fatigue and fracture of cylindrical shells containing a circumferential crack. *International Journal of Fracture Mechanics* **6**(4), 379–392.

Erdogan, F. and Sih, G. 1963. On the crack extension in plates under plane loading and transverse shear. *Journal of Basic Engineering* **85**(4), 519–527.

Eshelby, J. 1956. The continuum theory of lattice defects. *Solid state physics-advances in research and applications* **3**, 79–144.

Fedelinski, P., Aliabadi, M. and Rooke, D. 1995. A single-region time-domain bem for dynamic crack problem. *International Journal of Solids and Structures* **32**(24), 3555–3571.

Gerstle, W. 1985. Finite and boundary element modelling of crack propagation in two and three dimensions using interactive computer graphics. *PhD Thesis, Cornell University, New York*.

Henshell, R.D.; Shaw, K. 1975. Crack tip finite elements are unnecessary. *International Journal for Numerical Methods in Engineering* **9**(3), 495–507.

Inglis, C. 1913. Stresses in a plate due to the pressence of cracks and sharp corners. *Transactions of the institute of naval architects* **55**, 219–241.

Irwin, G.: 1948. Fracture dynamics. *Fractureing of Metals, ASM, Cleveland, Ohio*. American Society for Metals. pp. 175–194.

Irwin, G. 1957. Analysis of stresses and strains near the end of a crack traversing a plate. *Journal of Applied Mechanics* **24**, 361–364.

Jeng, G. and Wexler, A. 1977. Isoparametric, finite-element, variational solution of integral-equations for 3-dimensional fields. *International Journal for Numerical Methods in Engineering* **11**(9), 1455–1471.

Kanninen, M. and Popelar, C.: 1985. *The Boundary Element Method: Applications in Solids and Structures*. John Wiley & Sons. Chichester.

Kishimoto, K., Aoki, S. and Sakata, M. 1980. On the path independent integral-j. *Engineering Fracture Mechanics* **13**(4), 841–850.

Krishnasmy, G., Rizzo, F. and Rudolphi, T. 1992. Continuity requirements for density functions in the boundary integral equation method. *Computers & Structures* **9**(4), 267–284.

Lachat, J. and Watson, J. 1976. Effective numerical treatment of boundary integral-equations-formulation for 3-dimensional elastostatics. *International Journal for Numerical Methods in Engineering* **10**(5), 991–1005.

Mi, Y. and Aliabadi, M. 1994. 3-dimensional crack-growth simulation using bem. *Computers & Structures* **52**(5), 871–878.

Mi, Y. and Aliabadi, M. 1995. An automatic procedure for mixed-mode crack-growth analysis. *Communications in Numerical methods in Engineering* **11**(2), 167–177.

Mukhopadhyay, N., Maiti, S. and Kakodkar, A. 2000. A review of sif evaluation and modelling of singularities in bem. *Computational Mechanics* **25**(4), 358–375.

Orowan, E. 1948. Fracture and strength of solids. *Reports on Progress in Physics* **12**, 185–232.

Paris, P. and Erdogan, F. 1963. A critical analysis of crack propagation laws. *Journal of Basic Engineering* **85**(4), 528–534.

Paris, P., Gomez, M. and Anderson, W. 1961. A rational analytic theory of fatigue. *The Trend in Engineering* **13**, 9–14.

Polizzotto, C. 1988. An energy approach to the boundary element method .1. elastic solids. *Computer Methods in Applied Mechanics and Engineering* **69**(2), 167–184.

Portela, A., Aliabadi, M. and Rooke, D. 1992. The dual boundary element method - effective implementation for crack problems. *International Journal for Numerical Methods in Engineering* **33**(6), 1269–1287.

Portela, A., Aliabadi, M. and Rooke, D. 1993. Dual boundary element incremental analysis of crack propagation. *Computers & Structures* **46**(2), 237–247.

Prasad, N., Aliabadi, M. and Rooke, D. 1994. The dual boundary element method for thermoelastic crack problems. *Internal Journal of Fracture* **66**(3), 255–272.

Qian, J. and Fatemi, A. 1996. Mixed mode fatigue crack growth: A literature survey. *Engineering Fracture Mechanics* **55**(6), 969–990.

Raveendra, S. and Banerjee, P. 1992. Boundary element analysis of cracks in thermally stressed planar structures. *International journal of solids and structures* **29**, 2301–2317.

Rice, J. 1968. A path independent integral and approximate analysis of strain concentration by notches and cracks. *Journal of Applied Mechanics* **35**(2), 379–386.

Rizzo, F. 1967. An integral equation approach to boundary value problems of classical elastostatics. *Quarterly of Applied Mathematics* **25**, 83–95.

Saez, A. and Gallego R., D. J. 1995. Hypersingular quarter-point boundary elements for crack problems. *International Journal for Numerical Methods in Engineering* **38**(10), 1681–1701.

Sih, G. 1974. Strain energy density factor applied to mixed mode crack problems. *International Journal of Fracture* **10**(3), 305–321.

Sih, G. and Cha, B. 1974. A fracture criterion for three-dimensional crack problems. *Engineering Fracture Mechanics* **6**(4), 699–732.

Snyder, M. and Cruse, T. 1975. Boundary-integral equation analysis of cracked anisotropic plates. *International Journal of Fracture* **11**(2), 315–328.

Somigliana, C. 1885. Sopra l'equilibrio di un corpo elastico. *Il Nuovo Cimento* **3**, 17–20.

Spievak, L., Wawrzynek, P., Ingraffea, A. and D.G., L. 2001. Simulating fatigue crack growth in spiral bevel gears. *Engineering Fracture Mechanics*.

Symm, G. 1963. Integral equation methods in potential theory .2.. *Proceedings of the Royal Society* **A275**, 33–46.

Tanaka, K. 1974. Fatigue crack propagation from a crack inclined to the cyclic tensile axis. *Engineering Fracture Mechanics* **6**(2), 493–507.

Walker, K. 1970. The effects of stress ratio during crack propagation and fatigue for 2024-t3 and 7075-t6 aluminum. *ASTM STP 462* pp. 1–14.

Westergaard, H. 1939. Bearing pressures and cracks. *Journal of Applied Mechanics* **6**(2), 49–53.

Wrobel, L.: 2002. *The Boundary Element Method Volume 1: Applications in Thermo-Fluids and Acoustics*. John Wiley & Sons. Chichester.

P1

DBEM analysis of axisymetric crack growth in a piston crown.

*16th European Conference of Fracture*, On CD, 2006

# DBEM analysis of axisymmetric crack growth in a piston crown

Tore Lucht
Department of Mechanical Engineering, Solid Mechanics
Technical University of Denmark
2800 Lyngby, Denmark

## ABSTRACT

A practical engineering problem is considered in which an axisymmetric crack initiates from the inside of a piston crown due to both thermal and mechanical load from the combustion. A thermomechanical dual boundary element program is developed to analyze a plane strain model of the engineering problem. The crack growth direction is predicted using linear elastic fracture mechanics and the maximum principal stress criterion. It is found that the cyclic pressure in the piston crown results in a non-proportional load history. The stress intensity factors for a selected load step are used to predict the crack growth direction. A comparison shows that the crack growth prediction is in accordance with a cracked micro-sample of the piston crown.

## Introduction

The analyzed piston crown is used in big diesel engines installed in ships or stationary power stations. The axisymmetric fatigue crack was reported during inspection of engines with a particular piston crown design. The fatigue crack propagation occurs due to a combination of tensile stresses arising from the constant temperature change, and cyclical compressive stresses arising due to the cyclic pressure in the piston. No paper has been found which describes the use of computational fracture mechanics to predict crack growth directions in piston crowns, most likely because the crack propagation is limited to a specific piston crown design. To study the crack propagation in the piston crown the boundary element method is well suited because discretization only occurs at the boundary. The dual boundary element method has been used to analyze thermomechanical crack propagation [2,3,4].

Portela et al. [1] developed an analysis for mixed mode crack growth in two dimensions using a single region boundary element method. This method also known as the Dual Boundary Element Method (DBEM) avoids the singularity in the final system of equations by using displacement equations on one surface and traction equations on the other. Two dimensional problems, which include thermal load besides the mechanical load, have been analyzed by Prasad et al. [2]. The DBEM uses displacement and temperature equations on one crack surface and traction and flux equations on the other crack surface. The thermal load is treated as a body force term which normally requires domain integrals. By a Galerkin technique the domain integrals are transformed to boundary integrals so that all the advantages of the DBEM remain.

The stress intensity factors (SIFs) are computed by the use of a displacement method formulated for discontinuous quarter-point elements [5]. The crack growth is based on an incremental crack extension technique in which each crack extension is assumed to be straight [1]. The direction of the crack growth is predicted using the maximum principal stress criterion [6]. Because of the non-proportional load history the maximum principal stress criterion will predict a unique crack extension angle for each load step. It is not immediately obvious which load step to use as stated in [4] where three different selection methods are proposed. It is shown that the choice of load step is important for determining the crack paths and growth rates.

## Implementation of the dual boundary element method

The Boundary Element Method is based on solution of integral equations. In the derivation of the method partial differential equations describing the behavior of the unknown variables inside and on the boundary of the domain are transformed into integral equations relating only boundary variables. Analytical solution is only possible for very simple problems and for that reason the boundary element method uses numerical solution of the boundary integral equations. The central part of the numerical integration is the solution of the integrals for values where the integrated functions are singular.

The dual boundary element method for steady state thermoelastic crack problems is presented by Prasad et al. [2]. The formulation given by Prasad et al. is adopted in the present paper with the only change that an expression for heat transfer is

applied. In the derivation of the dual boundary element method a linear elastic isotropic and homogeneous body occupying a domain V enclosed by the boundary S is considered. The two governing equations for steady state thermoelasticity are the heat conduction equation and Navier's equation for equilibrium expressed in terms of the displacement. The two partial differential equations can be expressed as follows

$$\theta_{,kk} = 0 \tag{1}$$

$$\mu u_{i,jj} + \frac{\mu}{(1-2\nu)} u_{j,ij} - \frac{2\mu(1+\nu)}{(1-2\nu)} \alpha \theta_{,i} + b_i = 0 \tag{2}$$

Where $\theta$ is the temperature and $u_j$ is the displacement component, $\mu$ is the shear modulus, $\nu$ is Poisson's ratio and $\alpha$ is the coefficient of linear expansion. The above equations are written in indicial notation where a subscript 'i' preceded by a comma represents differentiation with respect to the 'i'th spatial coordinate in the Cartesian system and repeated indices represents summation. The differential equations (1) and (2) are solved subjected to temperature boundary conditions on the boundary $S_\theta$ and flux boundary conditions on the boundary $S_q$, displacement boundary conditions on the boundary $S_u$ and traction boundary conditions on the boundary $S_t$. The boundary conditions are divided on the boundary so that $S_\theta + S_q = S_u + S_t = S$. The flux and tractions are written as follows

$$q = -k\theta_{,n} \tag{3}$$

and

$$t_j = n_j \sigma_{ij} \tag{4}$$

Where k is the thermal conductivity, $n_j$ is the outward normal vector and $\sigma_{ij}$ is the stress tensor. The boundary temperature integral equation for a point x' on the non crack boundary S can be written as [2]

$$c(x')\theta(x') + \int_S q^*(x',x)\theta(x')dS(x) = \int_S \theta^*(x',x)q(x')dS(x) \tag{5}$$

Where the value of $c(x')$ depends on the smoothness of the boundary at $x'$. The functions $q^*(x',x)$ and $\theta^*(x',x)$ are fundamental solutions [2]. The functions are singular of the O(1/r) and of O(ln r), respectively, as $r = x'-x$ tends to zero. If the point $x'_c$ is on one of the crack surfaces and $x''_c$ is the point on the opposite crack surface with the same coordinates as $x'_c$, the temperature equation for $x'_c$ on a crack boundary is

$$c(x'_c)\theta(x'_c) + c(x''_c)\theta(x''_c) + \int_S q^*(x'_c,x)\theta(x')dS(x) = \int_S \theta^*(x'_c,x)q(x)dS(x) \tag{6}$$

The flux equation for a point x'<sub>c</sub> on a crack surface is [2].

$$c(x')q(x') - c(x'')q(x'') + n_i(x')\overline{\overline{\int_S}} \theta_i^{**}(x',x)q(x)dS(x) = n_i(x')\overline{\int_S} q^{**}(x',x)\theta(x)dS(x) \tag{7}$$

Where $\overline{\int}$ stands for a Cauchy principal value integral, $\overline{\overline{\int}}$ stands for a Hardamard principal value integral. The functions $q^{**}(x',x)$ and $\theta_i^{**}(x',x)$ are fundamental solutions [2]. The singularity of the fundamental solution is of O(1/r) and O (1/r²). In the general boundary element formulation described above temperature boundary conditions and flux boundary conditions are applied to the boundary of the cracked domain and the remaining values for the temperature and flux are calculated by numerical solution of (5), (6) and (7). Newton's law can be applied to describe conductive heat transfer at the boundary of the domain. Newton's law states that

$$-k\theta_{,n}(x) = -h(x)\left(\theta_f(x) - \theta(x)\right) \tag{8}$$

Where $\theta_f(x)$ and $h(x)$ are respectively the temperature of the surroundings and the heat transfer coefficient at the point x on the boundary. By the use of (8) in combination with (5), (6) and (7) the temperature and flux at the boundary of the domain are calculated when the values of $h(x)$, $\theta_f(x)$ and k are known.

The displacement boundary integral equation for the boundary point x' on the non cracked boundary S can be written as [2]

$$c_{ij}(x')u_j(x') + \overline{\int_S T_{ij}(x',x)u_j(x)dS(x)} - \int_S \overline{P_i}(x',x)\theta(x)dS(x)$$
$$= \int_S U_{ij}(x',x)t_j(x)dS(x) - \int_S \overline{Q_i}(x',x)q(x)dS(x)$$

(9)

Where the fundamental solutions $T_{ij}$ and $U_{ij}$ are singular of O(ln r) and of O(1/r). The functions $\overline{P_i}$ are singular of O(ln(1/r)) and $\overline{Q_i}$ are not singular at x= x'. If the point $x'_c$ is on one of the crack surfaces and $x''_c$ is the point on the opposite crack surface with the same coordinates as $x'_c$, then the displacement equation is singular as x passes through both points. The boundary integral equation for the point x' on the cracked boundary S can be written as

$$c_{ij}(x'_c)u_j(x'_c) + c_{ij}(x''_c)u_j(x''_c) + \overline{\int_S T_{ij}(x',x)u_j(x)dS(x)} - \int_S \overline{P_i}(x',x)\theta(x)dS(x)$$
$$= \int_S U_{ij}(x',x)t_j(x)dS(x) - \int_S \overline{Q_i}(x',x)q(x)dS(x)$$

(10)

The traction boundary integral equation for a point x'$_c$ on the crack surface is [2]

$$c_{ij}(x'_c)t_j(x'_c) - c_{ij}(x''_c)t_j(x''_c) + n_j(x'_c)\overline{\overline{\int_S T_{kij}(x'_c,x)u_k(x)dS(x)}} + \frac{\mu(1+\nu)}{1-2\nu}\alpha n_i(x'_c)\theta(x'_c)$$
$$+ \frac{\mu(1+\nu)}{1-2\nu}\alpha n_i(x'_c)\theta(x''_c) - n_j(x'_c)\overline{\int_S \bar{S}_{ij}(x'_c,x)\theta(x)dS(x)}$$

(11)

$$= n_j(x'_c)\overline{\int_S U_{kij}(x'_c,x)t_k(x)dS(x)} - n_j(x'_c)\int_S \bar{V}_{ij}(x'_c,x)q(x)dS(x)$$

Where the fundamental solutions $T_{kij}$ and $U_{kij}$ are singular of O(1/r) and of O(1/r$^2$). The functions $\bar{S}_{ij}$ and $\bar{V}_{ij}$ are singular of O(1/r) and of O(ln r).

The numerical implementation of the dual boundary element method described in [2] uses discontinuous quadratic elements on the crack surfaces and continuous quadratic elements along the remaining boundary except at the intersection between a crack and edge where another discontinuous element is used on the edge. In order to shorten the implementation time of the dual boundary element method for the present paper discontinuous elements are applied to all surfaces. In consequence the computation time is increased.

The J-integral is one of the most accurate methods to calculate the stress intensity factors for crack problems. However accurate results are also obtained with the simpler two point displacement formulation for discontinuous quarter point elements [5].

$$K_I = \frac{6\mu}{5(\kappa+1)}\sqrt{\frac{\pi}{2l}}\left(\Delta u_2^{BC} + 3\Delta u_2^{DE}\right)$$

(12)

$$K_{II} = \frac{6\mu}{5(\kappa+1)}\sqrt{\frac{\pi}{2l}}\left(\Delta u_1^{BC} + 3\Delta u_1^{DE}\right)$$

(13)

Where $\Delta u_1{}^{BC}$, $\Delta u_1{}^{DE}$ and $\Delta u_2{}^{BC}$, $\Delta u_2{}^{DE}$ are the differences in nodal displacement normal to the crack axis and along the crack axis. B, C are the two nodes closest to the crack tip on each crack surface and D, E represent the mid nodes on each crack surface. l is the length of the discontinuous quarter point element.

The crack growth direction in mixed-mode conditions is obtained by using the maximum principal stress criterion of Erdogan and Sih [6]

$$\theta = 2\tan^{-1}\left( \frac{KI}{4KII} \pm \frac{1}{4}\sqrt{\left(\frac{KI}{KII}\right)^2 + 8} \right) \tag{14}$$

**The piston crown**

The piston crown is situated in a very rough environment as the combustion loads the piston crown with high pressures and temperatures. In order to resist the load from the combustion the piston crown is cooled with oil on all internal surfaces. It is necessary to introduce an extra cooling chamber shown on figure 1 to obtain a sufficient cooling of the geometry. The cooling chamber makes it necessary to manufacture the piston crown as two separate parts which are assembled by welding. The residual stresses introduced by the welding process are removed afterwards by a weld heat treatment. Investigation of a cracked piston crown reveals that the fatigue crack has arised from an original crack at the root of the weld.

The present paper contains the first set of calculations aimed at describing crack propagation in the piston crown. In these calculations it is decided to model the piston crown as a two dimensional plane strain model. The real geometry of the piston crown can however be described as axisymmetric when neglecting the bores which supply the cooling chamber with oil. It is expected that the biggest difference between the two dimensional plane strain model and the axisymmetric model is found for small values of the radius where the curvature is largest. Because of that it is expected to obtain reasonable results with the plane strain model as the crack is growing in the part of the piston crown where the distance to the axis of symmetry is biggest.
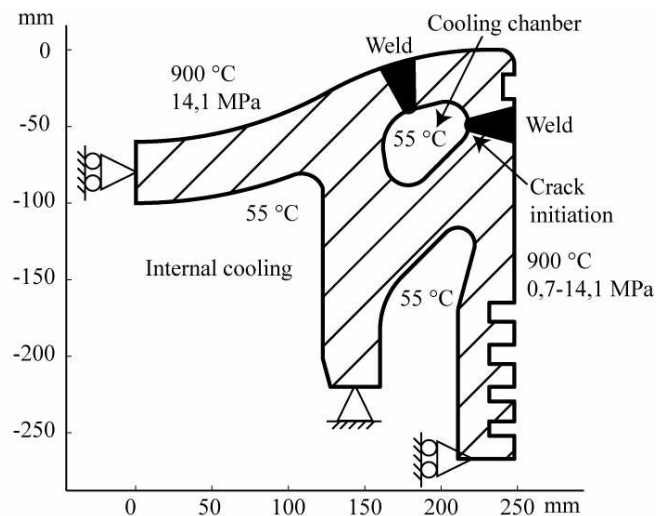


Figure 1. Model of the piston crown loaded with the maximum combustion pressure and steady state temperature field

Constrains are applied on three different surfaces as shown on figure 1. Symmetry constrains are applied to the vertical surface in the center of the piston crown as only half of the cross section is modeled. The fully constrained surface represents the connection between the piston rod and piston crown. The horizontal surface located under the piston ring grooves is constrained so that no horizontal displacement is allowed. This constrain is applied in order to obtain the stiffness of an axisymmetric geometry attached upon the horizontal surface.

The temperature distribution in the piston crown is described through interaction with the cooling oil and the inlet air which the explosion turns into a very hot combustion gas. As the engine runs most of its living time at a constant speed more than hundred rounds per minute it is assumed to be a god approximation to model the temperature distribution in the piston crown as stationary. In order to calculate the temperature distribution a set consisting of heat transfer coefficients, oil temperatures and a constant gas temperature is used. The set is known to make the calculations fit with temperature measurements in the

piston crown. The material properties are not constant within the piston crown as the temperature varies with a magnitude of about 350 $^o$C. However in the derivation of the boundary element method it is assumed that the domain is homogeneous. In some cases with simple temperature distribution this problem is solved by dividing one domain into several domains with constant material properties. In this case the temperature distribution is too complex for this method to be efficient. The piston crown is therefore modeled with the same material properties and that is expected to have minor influence on the results. In the two dimensional model the cooling bores are not modeled. This is assumed to have little influences on the results because the cooling bores have a small total area compared with the rest of the cooling surfaces and because they are situated in less exposed areas.

One pressure cycle of compression and expansion of gas over the piston is described when the crankshaft rotates 360$^o$. In order to model one pressure cycle it is discretized into ten steady state load steps that represent ten evenly distributed angular positions of a 360$^o$ rotation of the crankshaft. The relation between the angular position of the crankshaft and the load steps are chosen so that load step number six represents the angular position of the crankshaft that gives exactly the maximum combustion pressure. The pressure is applied on the top of the piston crown and down the sides where it is gradually decreased over the four piston rings. The cooling oil pressure and mass inertia of the dynamic system have been neglected because these two factors are known to have little influence on the results.

The initiation of the crack is modeled by inserting a small crack element into the geometry of the piston crown at the lower part of the weld as shown on figure 1. The angle of the inserted crack is chosen such that it agrees with micro-samples of the cracked piston crown.

**Results**

The SIFs for one load cycle described by the ten load steps is plotted on figure 3. Load steps zero and eleven are included in the figure to demonstrate the beginning and end of the cycle. Comparing SIFs for mode I and mode II it is clear that the mode I loading is dominant in all load steps. The highest values of the $K_I$ appear at the load steps where the piston crown is loaded with the lowest pressure. At these load steps where the thermal load is dominant it opens the crack which results in the highest $K_I$. However when the pressure increases the compressive load on top of the piston crown tends to close the crack which results in much lower values of $K_I$.
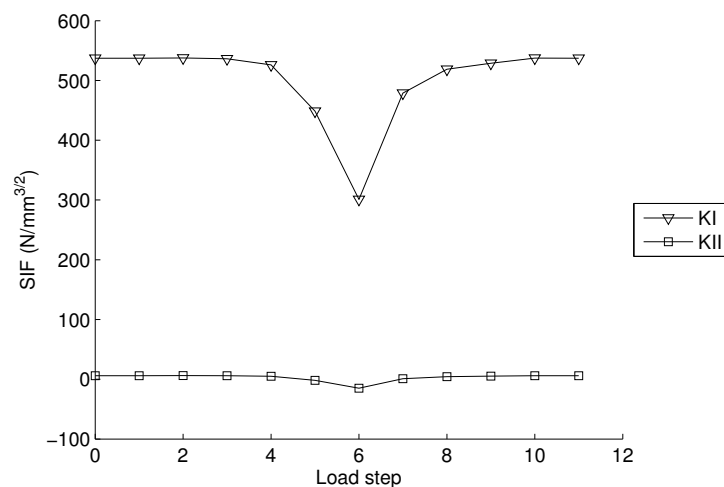


Figure 3. The stress intensity factors are calculated for a load cycle that represents a 360$^o$ rotation of the crankshaft

To demonstrate that the piston crown is subjected to non-proportional loading the ratio of $K_I$ to $K_{II}$ is shown on figure 4. The ratio is seen to change and consequently the maximum principal stress criterion would predict different propagation angles for each load increment. Only one pair of SIFs is wanted for each load cycle. Load step 5, 6 and 7 have different value of the ratio compared with the rest of the load steps. This limits the choice of SIFs to either those calculated in load step 5, 6 and 7 or to SÍFs representing the rest of the load steps. To choose an appropriate pair of SIFs it is assumed that the crack would grow due to the size of loading and due to the part of the load cycle at which the given load is present. Since the dominant mode one loading is highest and almost constant in most of the load cycles except for load step 5, 6 and 7 it is obvious to choose one of the remaining load steps to propagate the crack. Load step 2 is therefore chosen to propagate the crack as this load step represents the highest mode I loading.
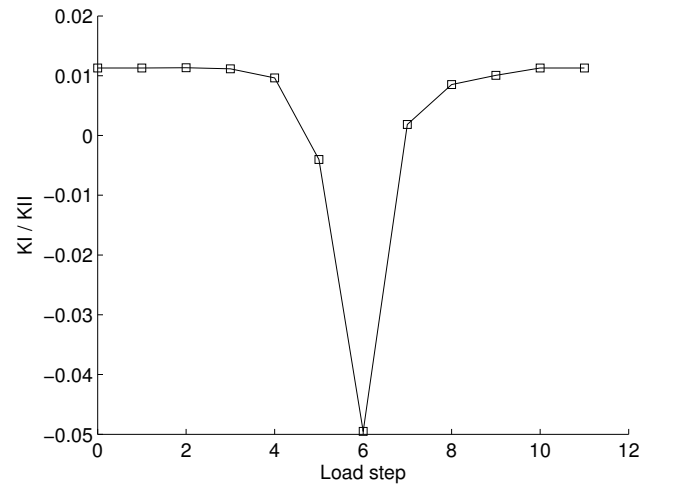
Figure 4. The ratio of $K_I$ to $K_{II}$ is calculated for a load cycle that represents a 360° rotation of the crankshaft

The crack is propagated in six increments using the SIFs from load step 2. The load steps of the initial crack, increment 3 and increment 6 are shown on figure 5. The variation in the SIFs can be seen to be unchanged for the different increments of the crack and therefore the reason retains for choosing load step 2 to propagate the crack. Generally the $K_I$ has decreased for all load steps with the biggest decrease at load step 6. This can be explained by the fact that the longer the crack becomes the easier it is to close. Furthermore the variation of $K_I$ increases for each crack increment and because of that the crack grow rate will increase as well. When the crack is propagated perpendicular to the maximum principal stress the modes one loading will be dominant and small values of $K_{II}$ are expected. This tendency is seen to be in accordance with figure 5. The difference between $K_I$ and $K_{II}$ is seen to be smallest at load step 6.



Figure 5. The stress intensity factors are calculated for load cycles that represent a 360° rotation of the crankshaft when the crack is propagated due to load step 2

To demonstrate the importance of choosing the correct pair of SIFs to propagate the crack the SIFs from a different load set than the most obvious one are now chosen. The load step which gives the biggest SIF-deviation from the SIFs of load step 2 is load step 6. Therefore this load step is chosen to propagate the crack. Figure 6 shows as above that variation in the SIFs is unchanged for the different increments of the crack. However figure 6 shows large increases in $K_{Ii}$ for all other load step than the one which are used to propagate the crack. This clearly indicates that the directions of the maximum principal stress are different for these load steps.
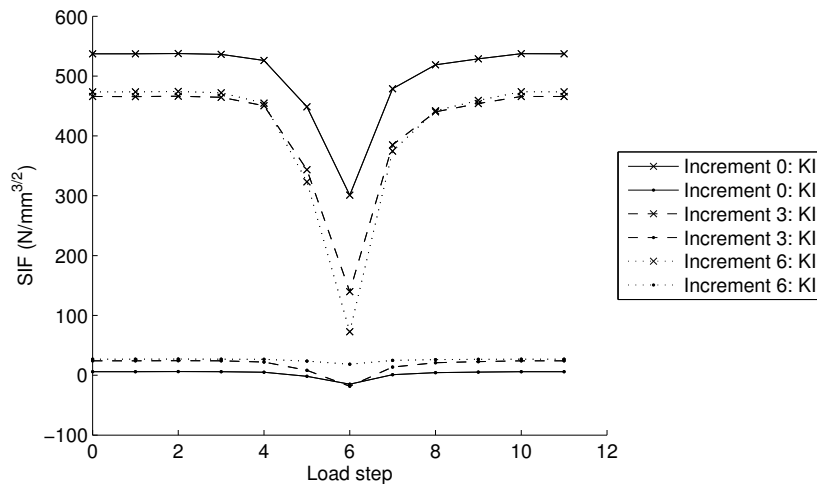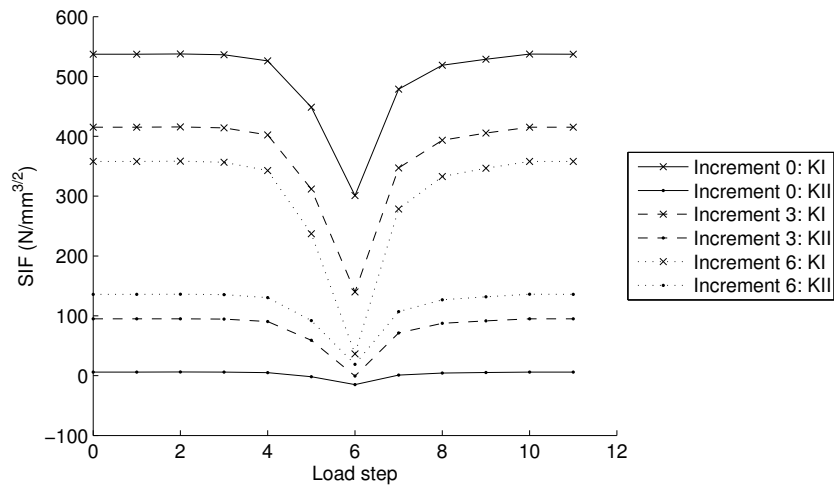
Figure 6. The stress intensity factors are calculated for load cycles that represent a 360° rotation of the crankshaft when the crack is propagated due to load step 6

The cracks propagated by load step 2 and 6 are both shown on figure 7 where they are compared with the crack in the micro-sample of the crack piston crown. Comparing the crack propagated by the use of load step 2 with the crack in the micro-sample it can be seen that they are in accordance with each other. The crack propagated by load step 6 is as expected found to give the biggest deviation from the crack in the micro-sample. A better crack prediction than the one found with load step 2 cannot be found even if another selection method is used to choose the SIFs from which the crack growth direction is predicted. Load step 2 and 6 represents two extremes and any other prediction will be in between. The difference between the crack in the micro-sample and load step 2 is expected to be caused by the simplifications introduced in order to model the problem with plane strain boundary element.



Figure 7. Micro-sample of piston crown with crack and calculations of cracks propagated by load step 2 and load step 6

**Conclusion**

A dual boundary element method has been implemented to predict the crack growth direction in a plane strain model of an axisymmetric crack in a pisto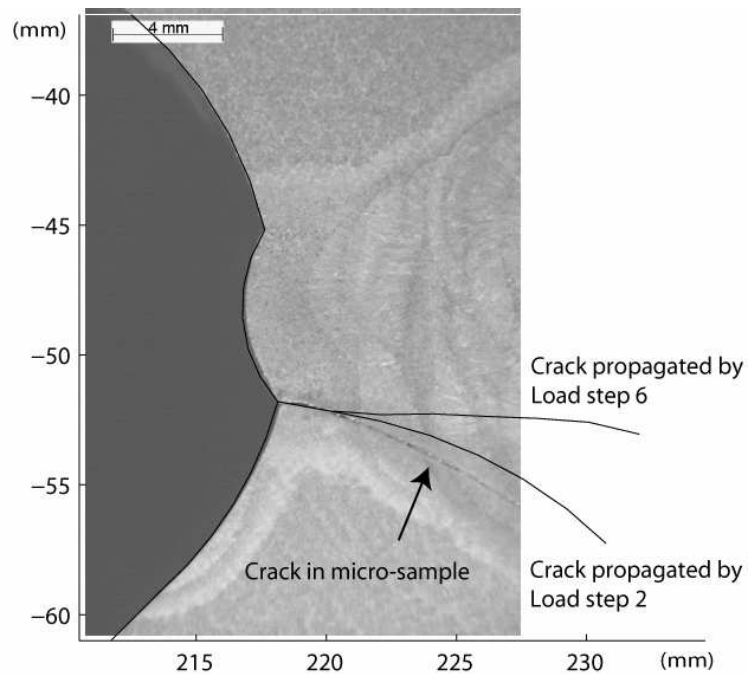n crown. The crack is propagated due to both mechanical and thermal load from the combustion. The loading of the piston crown is found to be non-proportional which causes the maximum principal stress criterion to predict unique angles for each load step. However one group of load steps which represents most of the load cycles was found to have nearly all the same ratio of $K_I$ to $K_{II}$ and the highest values of the dominant $K_I$. The SIFs from these load steps were an obvious choice to be used to calculate the crack growth direction. The predicted crack growth was shown to be in accordance with a micro-sample of the cracked piston crown despite the simplifications introduced in order to develop the model based on the plane strain boundary element method. The importance of choosing the correct pair of SIFs to calculate the crack growth direction was also demonstrated and it was found that the prediction of the crack growth direction could not be improved by another choice of SIFs.

**References**

1. Portela A., Aliabadi M.H. and Rooke D.P., "The Dual boundary element method: Effective implementation for crack problems", International Journal for Numerical Methods in Engineering, vol. 33, 1269 -1287, 1992

2. Prasad N.N.V., Aliabadi M.H. and Rooke D.P.,"The Dual boundary element method for thermoelastic crack problems" International Journal of Fracture, vol. 66, 255-272, 1994

3. Prasad N.N.V., Aliabadi M.H. and Rooke D.P.,"Incremental crack growth in thermoelastic problems" International Journal of Fracture, vol. 66,R45-R50, 1994

4. Prasad N.N.V., Aliabadi M.H. and Rooke D.P.,"Thermomechanical fatigue crack growth" International Journal of Fatigue, vol. 18, 349-361, 1996

5. Aliabadi M.H.,"The boundary element method", volume 2, John Wiley & Sons Ltd. (2002)

6. Erdogan, F. and Sih GC.," On the crack extension in plates under plane loading and transverse shear" Journal of Basic Engineering, vol. 85, 519–527,1963

P2

# Correction to the crack extension direction in numerical modelling of mixed mode crack paths.

## LETTERS IN FRACTURE AND MICROMECHANICS

# CORRECTION TO THE CRACK EXTENSION DIRECTION IN NUMERICAL MODELLING OF MIXED MODE CRACK PATHS

T. Lucht[1] and M.H. Aliabadi[2]

[1] *Department of Mechanical Engineering, Solid Mechanics, Technical University of Denmark, 2800 Kgs. Lyngby, Denmark, e-mail: trl@mek.dtu.dk*
[2] *Department of Engineering, Imperial College, University of London, UK., e-mail: M.H.Aliabadi@imperial.ac.uk*

**Abstract.** In order to avoid introduction of an error when a local crack growth criterion is used in an incremental crack growth formulation, each straight crack extension would have to be infinitesimal or have its direction corrected. In this paper a new procedure to correct the crack extension direction is proposed in connection with crack growth analyzed by the Dual Boundary Element Method (DBEM). The proposed correction procedure and a reference correction procedure already described in the literature are evaluated by solving two different computational crack growth examples. In the two examples it is found that analyses of the crack paths performed with the proposed crack correction procedure using big increments of crack extension are in excellent agreement with analyses of the crack paths performed by using very small increments of crack extension. Furthermore, it is shown that the reference correction procedure has a tendency to overcorrect the crack growth direction if the stop criterion for the iterative correction procedure is not calibrated in each new crack growth analysis.

## 1 The proposed correction method

The proposed method to correct the crack extension direction is an iterative method, for which it is important to determine the local crack growth direction. Several mixed mode fracture criteria have been proposed to determine the local crack growth direction such as the maximal energy release rate, Cotterell (1965), and the maximum principal stress criterion, Erdogan, et al. (1963). Both these linear elastic fracture criteria imply that $K_{II} = 0$ when the crack follows a path with a continuously turning tangent, Cotterell, et al. (1980) and Rubinstein (1991). Exceptions from this generally accepted assumption that the crack propagates in mode I are further discussed in Rubinstein (1991). However using the usual assumption, the choice of local crack growth criterion will not influence the final crack path. Thus the maximum principal stress criterion is used as it is easily implemented and found as one of the most commonly used criteria for 2D crack path calculation. In the proposed method the crack extension direction $\theta_n$ of an increment $n$ is found from the local crack growth direction at the previous crack tip $P_n$ and at the new crack tip $P_{n+1}$ combined with the assumption that the actual crack increment can be described as a second order polynomial. A similar approximation of the shape of the crack increment is used in the predictor-corrector method, Thielig, et al. (2005), which is

Figure 1: Correction of the crack extension direction

based on an incremental parabolic approximation of the crack path together with the modified virtual crack closure integral method.

To illustrate the proposed crack correction procedure the actual crack path in figure 1 is considered. This actual crack path is assumed to describe the shape of a second order polynomial $u(x)$. For the $n$'th crack increment, where the iterative correction method has been applied for $i = c$ iterations, the crack tip $P_{n+1}^c$ is on the curved crack path. In this case the relation between the crack extension angle $\theta_n^c$, the local crack growth direction at the previous crack tip $\theta_n$, and that at the new crack tip $\theta_n^c + \theta_{n+1}^c$, is derived with the angles measured from the previous increment

$$tan(\theta_n^c) = \frac{1}{2}(tan(\theta_n) + tan(\theta_n^c + \theta_{n+1}^c)) \qquad (1)$$

In general the crack is extended in the direction $\theta_n^i$ for a given iteration $i$ and the crack tip $P_{n+1}^i$ is placed outside the actual crack path as shown in figure 1. The direction of local crack growth at the crack tip is $\theta_n^i + \theta_{n+1}^i$ measured from the previous increment. For the $i$'th iteration (1) can be used to calculate the angle $\theta_n^c$ at which the crack tip $P_{n+1}^c$ is on the actual crack path. However, as $\theta_n^c + \theta_{n+1}^c$ is not know for the $i$'th iteration, an approximated value for this angle is used, which is $\theta_n^i + \theta_{n+1}^i$. By inserting into equation (1), an approximated value of $\theta_n^c$ is obtained

$$tan(\theta_n^{i+1}) = \frac{1}{2}(tan(\theta_n) + tan(\theta_n^i + \theta_{n+1}^i)) \qquad (2)$$

In the limit, where $\theta_n^i + \theta_{n+1}^i \rightarrow \theta_n^c + \theta_{n+1}^c$, it follows from (1) and (2) that $\theta_n^{i+1} \rightarrow \theta_n^c$ and there the crack extension angle has been found, at which the crack tip is on the

actual crack path. This limiting process can be modelled in an iterative procedure. Let the first crack extension angle be equal to the local crack growth direction at the old crack tip, $\theta_n^i = \theta_n$. If a reasonable size of the straight crack increment is used, it follows that the local crack growth direction measured from the previous increment, $\theta_n^i + \theta_{n+1}^i$, is closer to $\theta_n^c + \theta_{n+1}^c$ than $\theta_n$ and therefore by the use of equation (2) it follows that $|\theta_n^c - \theta_n^{i+1}| < |\theta_n^c - \theta_n^i|$. In this way the crack tip is moved closer to the actual crack tip and a better approximation of the local crack growth direction at the new crack tip can afterwards be calculated for $i+1$'th iteration. So for each iteration it follows that $\theta_n^i \rightarrow \theta_n^c$ when $i$ is increased. A general crack is now considered, at which it is assumed that the crack path can be described by a piece-wise sequence of second order polynomials. For the current $n$'th crack extension increment, the $i$'th iteration can be summarized as follows

- For the first iteration only, evaluate the local crack growth direction $\theta_n$ by the maximum principal stress criterion and extend the crack one increment $\Delta a$ to $P_{n+1}^i$

- Calculate the stress intensity factors at $P_{n+1}^i$ and then calculate the next local crack growth direction $\theta_{n+1}^i$, using the maximum principal stress criterion

- Calculate the corrected crack-extension direction, by using (2) and correct the crack-extension increment.

- Starting from the second step, repeat the above steps sequentially while $|\Delta \theta_n^i| > \beta$. The calibration constant is in this paper chosen as $\beta = 0.1°$.

## 2 Incremental analysis by The Dual Boundary Element Method

In the present paper a formulation of the dual boundary element method, Portela, et al. (1993), is used to analyse crack growth in different examples. Corrections are applied and each example is solved both with, the crack correction procedure, Portela, et al. (1993), and the crack correction procedure proposed in this paper. In the two following computational crack growth examples both correction methods are calibrated so that when the correction of the crack extension direction is below $0.1°$ the correction procedure is stopped. This calibration is applied in order to limit the total number of iterations and because changes of the crack extension angle below this values are considered to have negligible influence on the final crack path.

To be able to evaluate the precision of the two correction methods it is chosen to find the actual crack. The actual crack path can be found by the use of very small crack extensions for each increment. To assure that the size of the crack extensions are sufficiently small, several crack path analyses are performed in order to show that the crack path for each analysis converges towards a specific crack path. In order to reduce the influence of the element size on the accuracy that is related to the calculation of the stress intensity factors, it is chosen to use the same element

size in these crack path analyses. In that way the length of the crack increment is defined by the number of elements, and the total number of elements on each crack path is kept constant. In the test examples the actual crack path is found when the crack extension size referred to by number of increments on the crack path has the following values 4, 8, 16, ..., 256, and when the crack path is modelled with the fixed number of 256 elements. In the calculations performed with the two correction methods, larger crack elements are used in order to create a more efficient mesh that takes advantage of the correction methods. In these calculations a crack element size equal to the increment size is used.

## 3  Cruciform plate

In this first example the regular cruciform plate, Portela, et al. (1993), with an initial corner crack is studied. The dimension of the plate is defined by the length L and the initial crack has a length of $a = 0.2L$. The boundary conditions and traction are as described by figure 2(a) and the material properties used are $E = 210000MPa$ and $v = 0.3$.



(a) Cruciform plate

(b) Crack paths calculated without correction and with different number of increments
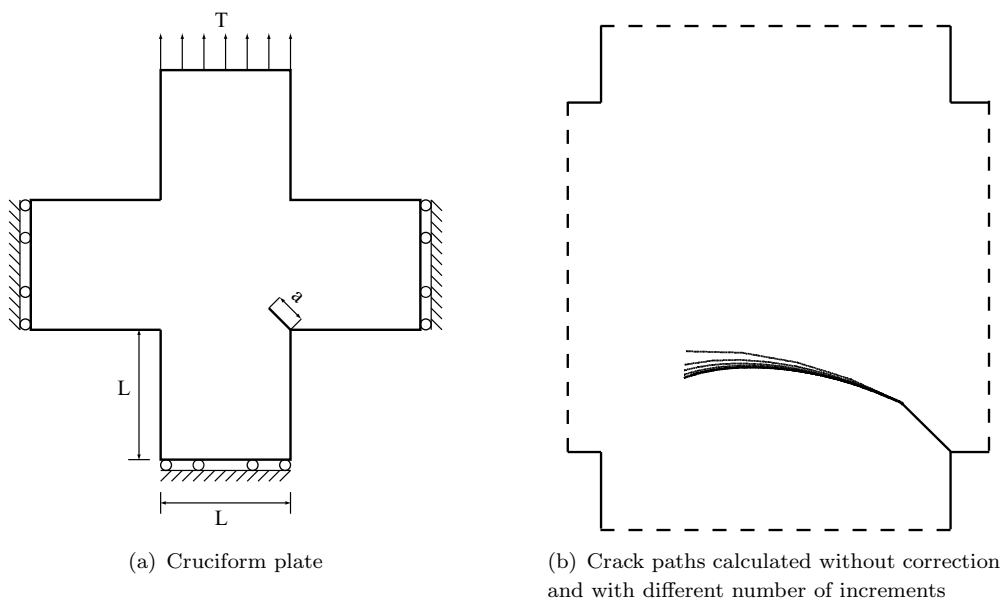
Figure 2: Test example one

The crack paths are calculated with different numbers of increments and as shown in figure 2(b) the difference between the crack paths increases as the cracks grow. In order to illustrate the differences between the crack paths, distances are calculated between the reference crack path and a crack path calculated using another number of increments. The distance is measured between corresponding points on the two crack paths. A good representation of the actual crack path is found for this test

example when 64 increments are used. This is shown on figure 3(a) as the actual crack path, chosen as a reference crack path. As expected, figure 3(a) shows that when the increment length is decreased the crack path converges towards a specific crack path. The actual crack path is expected to be found when the increment length is infinitesimal. However it appears from figure 3(a) that the crack path with 64 increments has crack paths with more increments on both sides. This is explained by the fact that the small element size used to model the increments influences the accuracy of the calculation method. These crack paths are however very close and as the crack path with 64 increments is in the middle, between two crack paths with more increments, this crack path is a good approximation of the actual crack path.
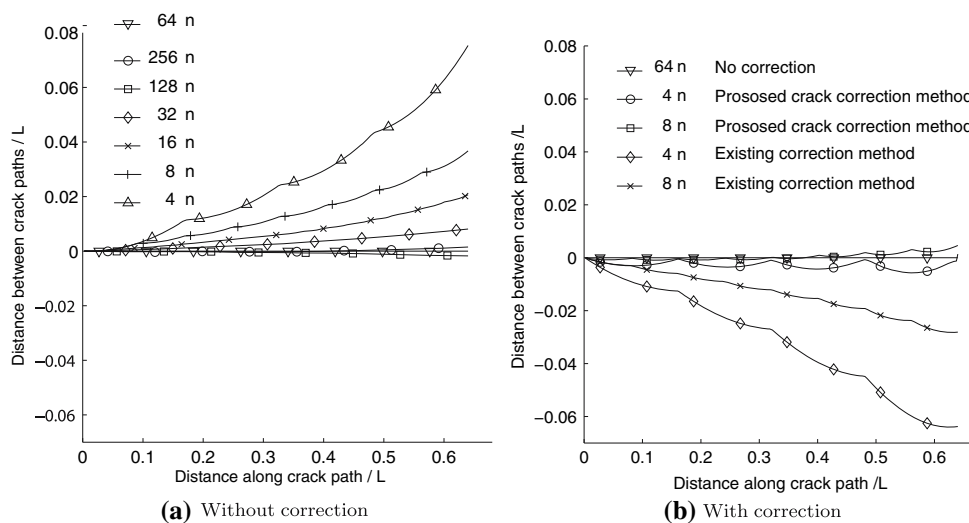


Figure 3: Distance between crack paths with different number of increments ($n$)

Computations of the crack path are now performed with the use of the two crack correction methods. The computations are carried out with the two longest crack increments, which give the biggest deviations from the actual crack path. The distances between the actual crack path and the crack path calculated with the crack correction methods are shown in figure 3(b). From the figure it appears that the crack path calculated with the reference correction method has moved to the other side of the actual crack path. This demonstrates an effect of overcorrection that can be shown from the formulation of the reference correction method if the stop criterion is not calibrated for each new crack growth analysis. The use of the reference correction method moves both crack paths closer to the actual crack path, but the crack paths are seen to deviate just as much from each other as if no correction has been applied. Both results calculated with the proposed correction method appear to describe almost the same crack path, much closer to the actual crack path. This indicates that the proposed crack correction method is less sensitive

to the increment size and that it gives a much better approximation of the actual crack path.

To illustrate the two iterative crack correction methods, the relation between the crack extension angles and the number of iterations is plotted in figure 4 for a crack path with 4 increments. The crack path with 4 increments is chosen because it deviates the most from the actual crack path when no correction method is applied. From the figure it appears that the reference correction method converges much more slowly towards the corrected crack extension angle than the proposed crack correction method. As expected, the proposed crack correction method gives angles very close to the corrected crack extension angle already after the first iteration. Thus fewer iterations are necessary for the proposed crack correction method.
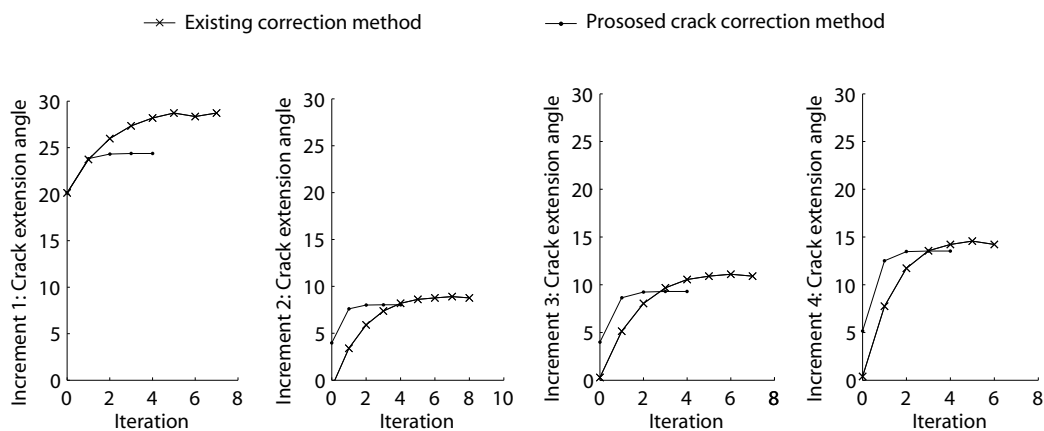


Figure 4: Relation between crack extension angle and the iteration number for each correction method

## 4   Bending specimen with hole

In this second example the crack path calculations are performed on a specially designed specimen with a hole near the crack path, Thielig, et al. (2005), as shown on figure 5(a). The specimen is loaded under lateral force bending as seen on the figure. The material used is this paper has $E = 200000 MPa$ and $v = 0.25$.

The crack path calculations are performed as in the previous examples with decreasing size of the crack extension increments in order to observe that the crack path converges towards the actual crack path. In figure 5(b) seven crack paths with the same length and a different number increments are shown. The crack path with 64 increments is used as reference crack path and it is found to give a good approximation of the actual crack path because close to it and on both sides are the crack path with 128 increments and 256 increments. The differences between the crack paths are primarily explained by the influence of the small element size on the numerical

(a) Bending specimen with hole



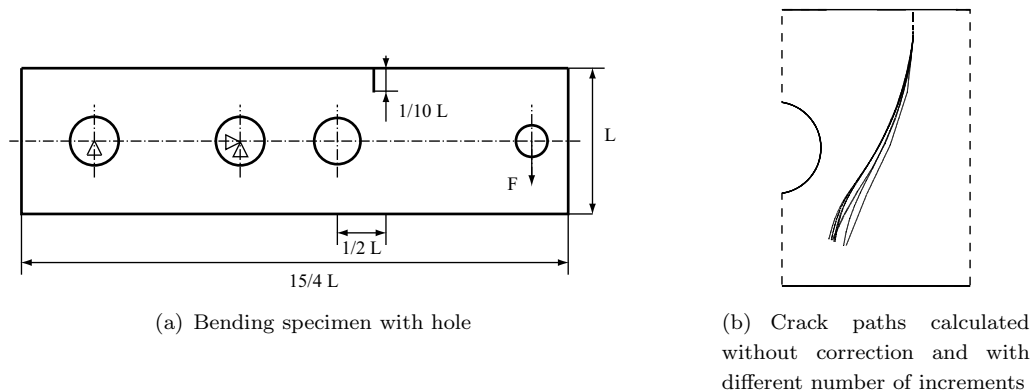(b) Crack paths calculated without correction and with different number of increments

Figure 5: Test example two

accuracy. The chosen crack path is furthermore found to be in agreement with the crack path found by experiments, Thielig, et al. (2005).

The two correction methods are applied to the crack path calculations and the results are shown in figure 6(b). In the beginning of the two crack paths the reference correction method is seen to correct the two crack paths so that they both are moved to the other side of the actual crack path. The crack paths are not quite as far away from the actual crack path as if no correction method had been used. The error introduced by overcorrection in the beginning of the crack path is however equalized by overcorrection introduced in the end of the crack path as the crack changes direction. Because of that the end of the crack path is close to the end of the actual crack path. The result of the proposed crack correction method is also displayed in figure 6(b). It is seen that both crack paths are improved remarkably by the crack correction method. The two crack paths are quite close and that demonstrates the independence of the increment size. The crack path with the smallest increment size is closest to the actual crack path.

For the bending specimen it can also be shown that the proposed crack correction method gives very precise angles only after few iterations as it was shown for the cruciform structure.

## 5   Conclusion

In order to evaluate the reference crack correction method in comparison to the proposed crack correction method crack path calculations have been performed. In test examples it has been demonstrated that the reference correction method has a tendency to overcorrect the crack path. Furthermore, it is shown that crack paths calculated with the use of the reference correction method are very dependent on the increment size as it was the case when no correction method had been used. The proposed crack correction method presented in this paper has been demonstrated in the different examples. The new method gives a much better approximation to
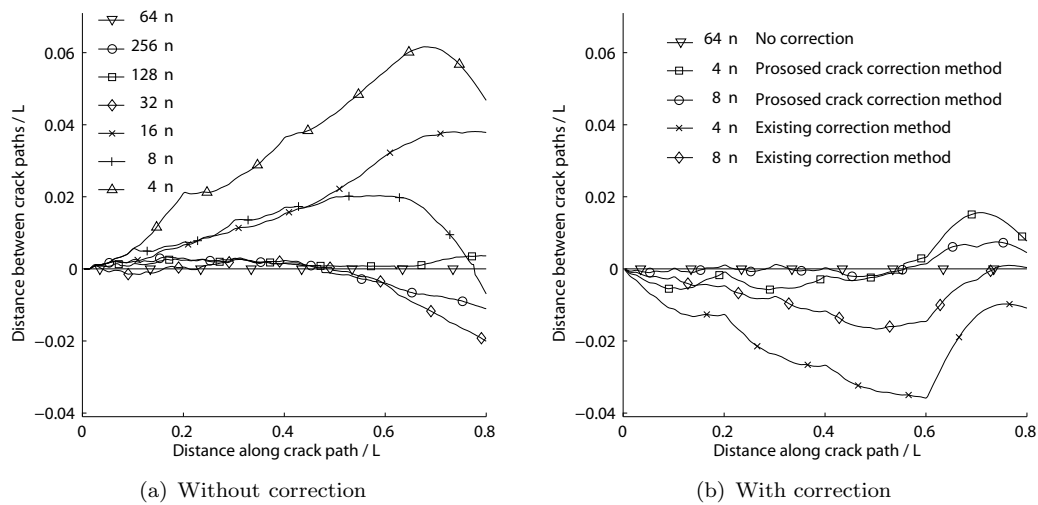
(a) Without correction  (b) With correction

Figure 6: Distance between crack paths with different number of increments ($n$)

the actual crack path, compared to the reference crack correction method. Furthermore, the proposed crack correction method is shown to depend very little on the increment size which results in good approximation of the actual crack path even for big increments. The proposed correction method uses fewer iterations to obtain a better approximation of the actual crack path than the reference method. The number of iterations for the proposed correction method can be reduced further with only a small influence on the calculated crack path. Based on the test examples a maximum of only three iterations is suggested for each increment, as only very small changes in the crack extension angle are obtained when more iterations are used.

## References

Cotterell, B., (1965) *International Journal of Fracture Mechanics* 1 , 96-103

Erdogan, F. and Sih, G. C., (1963) *J. Basic Engng* 85, 519-527

Cotterell, B. and Rice, J. R., (1980) *International Journal of Fracture* 16, 155-169

Portela, A., Aliabadi, M. H. and Rooke, D. P. (1993) *Computers and Structures* 46, 237-247

Rubinstein, A. A., (1991) *International Journal of Fracture* 47, 291-305

Thielig H., and Wünsche, M., (2005) *Advances in Fracture and Damage Mechanics* IV, 287-293

P3

A new correction procedure to correct the predicted crack extension
direction of a mixed mode crack path.

# A new correction procedure to correct the predicted crack extension direction of a mixed mode crack path

## Tore Lucht[1, a] and M.H. Aliabadi [2,b]

[1] Department of Mechanical Engineering, Technical University of Denmark, 2800 Lyngby, DK

[2] Department of Aeronautics, Imperial College London, South Kensington, London SW7 2BY, UK

[a] trl@mek.dtu.dk, [b] M.H.Aliabadi@imperial.ac.uk

**Keywords:** Boundary element method, crack extension direction, crack correction procedure

**Abstract.** In an incremental crack extension analysis each crack increment is in general modelled with a straight extension. In order to avoid introduction of an error when the local crack growth criterion is used with an incremental formulation, each straight crack extension would have to be infinitesimal as the crack growth direction changes when the crack grows. A correction procedure to correct the extension direction of the increment can however be applied to ensure that a unique crack path is achieved with different analyses of the same problem performed with different size of the crack-extension increments. A proposed correction procedure and an reference correction procedure are demonstrated by solving a computational crack growth example. The demonstration shows that analyses of the crack path performed with big crack extensions and the proposed crack correction procedure are in excellent agreement with analyses of the crack path performed with very small crack extensions. Furthermore it is shown that the reference correction procedure has a tendency to overcorrect the crack growth direction if the stop criterion for the iterative correction procedure is not specified for each new crack growth analysis.

**Proposed correction procedure.** The proposed method is an iterative method for which it is important to determine the local crack growth direction. Several mixed mode fracture criteria have been proposed to determine the local crack growth direction such as the maximal energy release rate [1] and the maximum principal stress criterion [2]. Both these linear elastic fracture criteria imply that $K_{II} = 0$ when the crack follows a path with a continuously turning tangent [3,5]. Exceptions from this generally accepted assumption that the crack propagates in mode I are further discussed in [5]. However using the usual assumption, the choice of local crack growth criterion will not influence the final crack path. Thus the maximum principal stress criterion is used as it is easily implemented and found as one of the most commonly used criteria for 2D crack path calculations.

A detailed presentation of the proposed crack correction procedure can be found in [7]. In this paper the basic idea and implementation of the proposed crack correction procedure is described. In the proposed method the crack extension direction $\theta_n$ of an increment $n$ is found from the local crack growth direction at the previous crack tip $P_n$ and at the new crack tip $P_{n+1}$ combined with the assumption that the actual crack increment can be described as a second order polynomial. A similar approximation of the shape of the crack increment is used in the predictor-corrector method [6], which is based on an incremental parabolic approximation of the crack path together with the modified virtual crack closure integral method. To illustrate the proposed crack correction procedure the actual crack path in Fig. 1 is considered. This actual crack path is assumed to describe the shape of a second order polynomial $u(x)$. For the *n'th* crack increment, where the iterative correction method has been applied for $i = c$ iterations, the crack tip $P_{n+1}^c$ is on the curved crack path and the corrected crack extension angle $\theta_n^c$ is found. For the iteration $i$ an approximated value of the corrected crack extension angle $\theta_n^{i+1}$ is obtained from

$$\tan(\theta_n^{i+1}) = \frac{1}{2}\left(\tan(\theta_n) + \tan(\theta_n^i + \theta_{n+1}^i)\right) \tag{1}$$

Where $\theta_n$ is the local crack growth direction at the previous crack tip, and $\theta_n^c + \theta_{n+1}^c$ is that at the new crack tip. Both angles are measured from the previous increment. If a reasonable size of the straight crack increment is used then $\theta_n^i \rightarrow \theta_n^c$ when $i$ increased as discussed in [7].
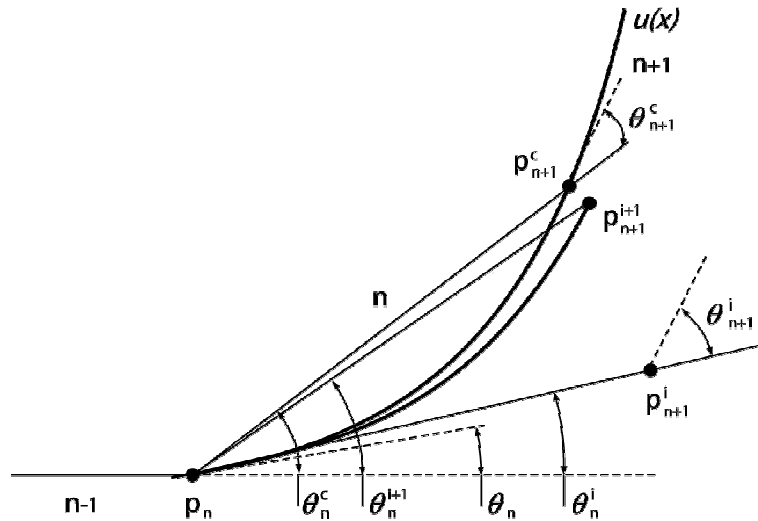


Figure 1. Correction of the crack extension direction

A general crack is now considered at which it is assumed that the crack path can be described by a piece-wise sequence of second order polynomial. For the current *n'th* crack-extension increment, the *i'th* iteration can be summarized as follows

- For the first iteration only, evaluate the local crack growth direction $\theta_n$ by the maximum principal stress criterion and extend the crack one increment $\Delta a$ to $P_{n+1}^i$

- Calculate the stress intensity factors at $P_{n+1}^i$ and then calculate the next local crack growth direction $\theta_{n+1}^i$ using the maximum principal stress criterion

- Calculate the corrected crack-extension direction by using Eq. 1 and correct the crack-extension increment

- Starting from the second step, repeat the above steps sequentially while $|\Delta \theta_n^i| > \beta$. The calibration constant is in this paper chosen as $\beta = 0.1$

**Incremental analysis by The Dual Boundary Element Method.** In the present paper a formulation of the dual boundary element method [4] is used to analyse crack growth in different examples. Corrections are applied and each example is solved both with the reference crack correction procedure [4] and the proposed crack correction procedure. To be able to evaluate the precision of the two correction methods it is chosen to find the actual crack. The actual crack path can be found by the use of very small crack extensions for each increment. To assure that the size of the crack extensions is sufficiently small, several crack path analyses are performed in order to show that the crack path for each analysis converges towards a specific crack path. In order to reduce the influence of the element size on the accuracy that is related to the calculation of the stress intensity factors, it is chosen to use the same element size in these crack path analyses. In that way the length of the crack increment is defined by the number of elements, and the total number of elements on each crack path is kept constant. In the calculations performed with the two correction methods, larger crack elements are used in order to create a more efficient mesh that takes advantage of the correction methods. In these calculations a crack element size equal to the increment size is used.

**Square plate.** In this example at square plate is loaded so that the crack initially deforms under pure mode II loading [1]. The dimension and the loading is as shown in Fig. 2 and the initial crack has the length of a=L/3. The material properties used are E=200000 MPa and v=0.25.

(a) Square plate with initial edge crack

(b) Crack paths calculated without correction
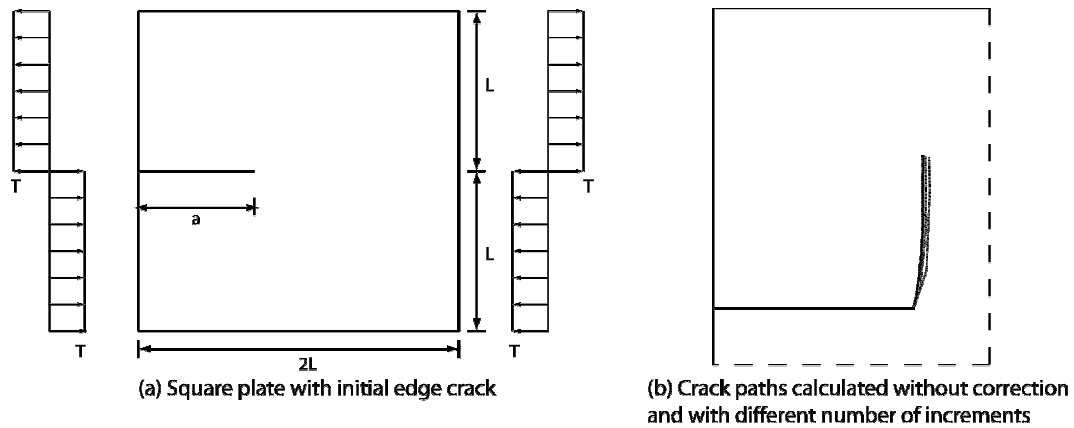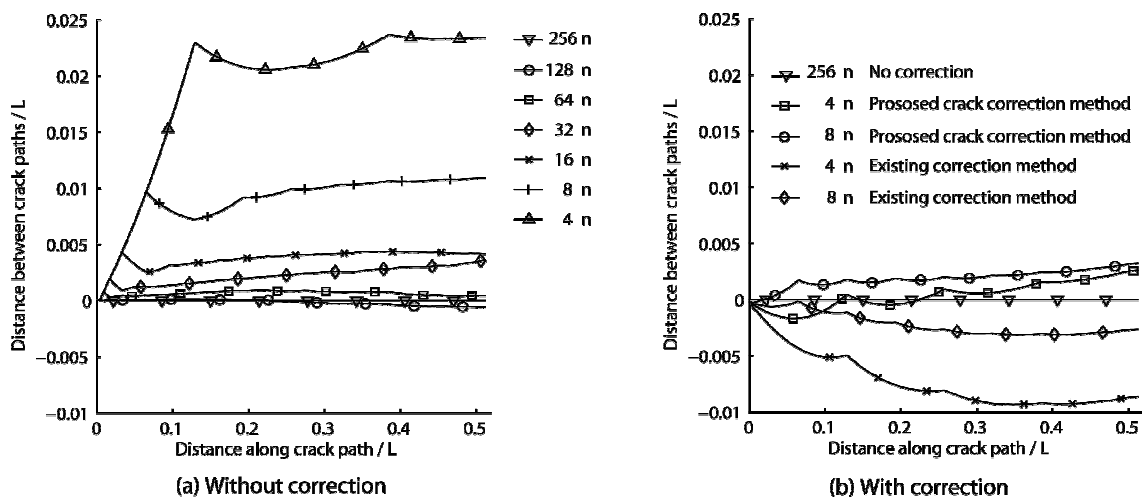and with different number of increments

Figure 2. Test example

To find the actual crack path a convergence study is performed. The crack paths calculated without correction are shown in Fig. 2 and from the figure it appears that the differences between the crack paths are introduced in the beginning of the crack growth and subsequently the differences remain nearly constant. To illustrate the differences between the crack paths the distance from a reference crack path is shown in Fig 3a. The distance between two crack paths is calculated from corresponding points on both crack paths. When the number of increments along the crack paths is increased the increment size decreases and it appears that the crack paths converge towards the crack path with the smallest increment size. From the figure it is seen that it would be a good approximation to let the crack path with 256 increments describe the actual crack path as the crack paths with 64 and 128 increments are close to it on both sides. Therefore the crack path with 256 increments is chosen as the reference crack path on Fig 3b. The differences between the crack paths with 256 increments and 128 increments are primarily explained by the fact that small element size influences the evaluation of the stress intensity factors.



(a) Without correction

(b) With correction

Figure 3. Distance between crack paths with different number of increments $n$

The reference and proposed correction methods are now applied to the crack path calculations in the two cases with the lowest number of increments. In Fig. 3b the distances from the actual crack path are plotted for the two correction methods. From the figure it is seen that the reference correction method corrects the crack paths so that they are moved to the other side of the actual crack path and that they are very different almost as if no correction was applied. The crack path with the smallest increment size gives the best approximation of the actual crack path. When the proposed correction method is used both crack paths are close to each other and to the actual crack path. This demonstrates that the crack path obtained with the proposed correction method is almost independent of the size of the crack extension increment.

The relation between the crack extension angle and the number of iterations is shown in Fig. 4 for the proposed and reference crack correction method. The slower convergence of the reference crack correction method that was demonstrated in [7] is less pronounced for this test example. This is explained by the fact that the possibility for overcorrection is limited in this specific example as the crack growth direction is almost constant. The proposed crack correction method is seen to both increase and decrease the extension angle while it converges towards the final corrected crack extension angle.
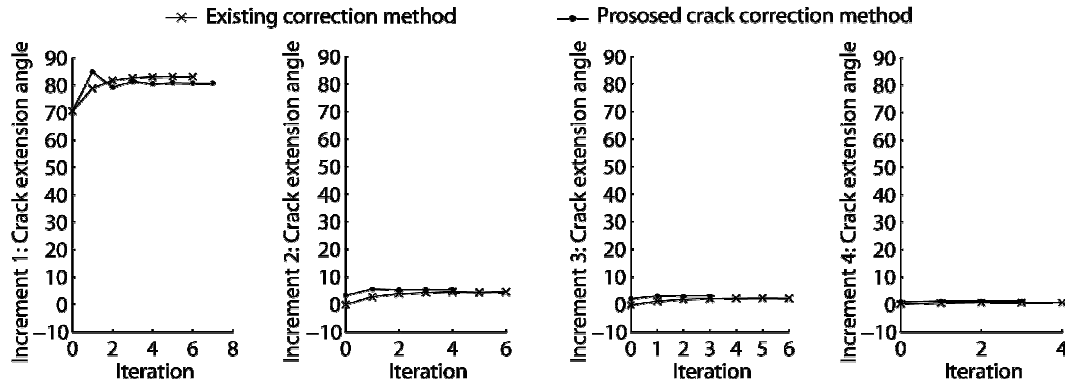


Figure 4. Relation between crack extension angle and the number of iterations

## Summary

In order to evaluate the reference crack correction method in comparison to the proposed crack correction method crack path calculations have been performed. In the test examples it has been demonstrated that the reference correction method has a tendency to overcorrect the crack path. Furthermore, it is shown that crack paths calculated with the use of the reference correction method are very dependent on the increment size as it was the case when no correction method had been used. The new method gives a much better approximation to the actual crack path, compared to the reference crack correction method. Furthermore, the proposed crack correction method is shown to depend very little on the increment size which results in good approximation of the actual crack path even for big increments. The proposed correction method uses less iterations to obtain a better approximation of the actual crack path than the reference method.

## References

[1] B. Cotterell: International Journal of Fracture Mechanics Vol. 1 (1965), p. 96

[2] F. Erdogan and G. C. Sih: J. Basic Engng Vol. 85 (1963), p. 519

[3] B. Cotterell and J. R. Rice: International Journal of Fracture Vol. 16 (1980), p. 155

[4] A. Portela, M.H. Aliabadi and D.P. Rooke: Computers and Structures Vol. 46 (1993), p. 237

[5] A.A. Rubinstein: International Journal of Fracture Vol. 47 (1991), p. 291

[6] H. Thielig and M. Wünsche: Advances in Fracture and Damage Mechanics IV (2005), p. 287

[7] T. Lucht and M.H. Aliabadi: International Journal of Fractrue (2007), in press

P4

Adaptive FE analysis of non-planar 3D crack growth by the use of a BE sub model.

*Submitted*, 2007

# ADAPTIVE FE ANALYSIS OF NON-PLANAR 3D CRACK GROWTH BY THE USE OF A BE SUB MODEL

T. Lucht[1] [2]

[1] *Department of Mechanical Engineering, Solid Mechanics, Technical University of Denmark, 2800 Kgs. Lyngby, Denmark, e-mail: trl@mek.dtu.dk*
[2] *MAN Diesel A/S, Teglholmsgade 41, 2450 Copenhagen, Denmark, e-mail: tore.lucht@man.eu*

**Abstract.** A new automated method to model non-planar 3D crack growth is proposed which combines the advantages of both the boundary element method (BEM) and the finite element method (FEM). The proposed method links the two methods by a submodelling strategy in which the solution of a global FE model containing an approximation of the crack is interpolated to a much smaller BE model containing a fine discretization of the real crack. The method is validated through several numerical comparisons and by comparison to crack growth measured in a test specimen for an engineering structure.

**Keywords: 3D crack growth, FEM, BEM, remesh, sub model**

## 1  Introduction

The increase in computer performance during the last decades has lead to large interest in optimizing structures and in predicting possible failures that can arise suddenly and cause serious problems. The developments presented in this paper are based on advanced engineering structures as in large diesel engines for propulsion of ships and for stationary power plants. From an analysis point of view these engines are ideal for fatigue crack growth analysis since they in general run at a constant cyclic loading most of their life time. Crack paths have previously been predicted in large diesel engines by a 2D BE analysis [1, 2].

As a consequence of the increased interest for modelling crack growth in advanced structures several numerical methods have been proposed recently to automated modelling of non-planar 3D crack growth. One of the main problems to be solved when simulating non-planar 3D crack growth is that the manual discretization of the domain into elements needs to be updated automatically after each crack extension so that the elements describe the shape of the arbitrary growing crack. One of the first methods presented which was able to solve this problem by reducing it by an order of magnitude was the boundary element method. In the dual boundary element method [3, 4] crack growth is analyzed by extending the crack and by performing automatic remeshing of the crack extension on the non-cracked surface. Despite the clever reduction of the remeshing problem by the order of magnitude the method has not become as wide spread as the finite element method. The boundary element method is most advantageous for linear problems and has a relative slow solution time because of the full system matrix. Several examples have however been solved

with the boundary element method during recent years as for example [5, 6, 7], using a fast BEM formulation that focuses on reducing the solution time by compression of the system matrix [8].

Also the meshless methods have been applied to model non-planar 3D crack growth and these methods solve the discretization problem as no remeshing is required. An example of this method to non-planar 3D crack growth is the Element-Free Galerkin method which is used in combination with Linear Elastic Fracture Mechanics [9]. The high flexibility of these methods is however reported to require a substantial computational cost [13]. Other methods use an enrichment of the elements which come in contact with the crack surface. By the enrichment of the element shape functions any crack configuration in the affected elements can be described. Examples of this method to non-planar 3D crack growth is the extended finite element method [10, 11, 12] and the generalized finite element method [13].

Apart from these methods which solve the remeshing problem in an elegant way there are methods which use a local remeshing of the finite element mesh. Only few applications of these methods to automate non-planar 3D crack growth are available, but some examples exist [14]. In this paper the fitting of the growing crack in terms of the discretized domain is done by splitting elements and subsequently the stress intensity factors are evaluated by the use of a submodelling strategy. In the general use of this submodelling technique the first step is to solve a problem with one mesh describing the global domain. Then another and generally finer mesh is used to reanalyze a certain sub part of the global domain which is of particular interest. Thus either the displacement field or the stress field of a global cracked domain is interpolated to the cutting boundary of a sub model having a fine mesh along the crack front.

Combinations of the presented methods also exist in the literature as is the case for the combination of the BEM-FEM [15, 16]. In these papers the BE discretization is applied to describe the local cracked domain while the FE discretization is applied to the global domain. In each method the remeshing of the FE model is avoided by either superposition of overlapping domains or coupling of FEM-BEM trough interface elements. If the remeshing problem for the FE model is solved these methods do not contain any significant advantage for crack problems compared to the general submodelling strategy.

The crack growth procedure proposed in this paper aims to solve problems of growing cracks in advanced engineering structures, such as large diesel engines [21]. Thus it is very important that the proposed method is compatible with existing FE models that have previously been built up for the complex engineering structures, typically in terms of commercial software like ABAQUS [18]. It is furthermore important that the choice of method is proven in many examples in the literature and finally that the implementation time of the method is reasonable. This leads to a combined

FEM-BEM method by the use of a submodelling strategy as illustrated in figure 1. A model describing the global domain and an approximation of the crack geometry is first solved. Then in order to obtain precise fracture mechanical parameters a sub model with a fine crack mesh is used to reanalyze a part of the global model in the vicinity of the crack. In the presented method the global model is analyzed with the finite element method (FEM) and the sub model is analyzed with the dual boundary element method (DBEM). The combined use of these methods aims to obtain the advantage of each method. The proposed method however has the disadvantage that it requires two solutions for each simulation step. Especially for large domains the submodelling technique can save time since the time spent to solve a coarse global model and a fine sub model can be less than the time spent to solve a sufficiently fine discretized model. The short implementation time for this method is obtained by the use of ABAQUS as the FEM solver, BEASY [17] as the interpolater of boundary conditions from the global model to the sub model and BEASY as BE solver and handler of the crack growth analysis. Thus the new development presented in this paper is the stable and fast updating of the crack geometry in the FE model together with the environment that combines the global and the sub model to an automated procedure.

The modelling strategy presented will undoubtedly be influenced by several factors such as the mesh size of the global model, the sub model size and the approximation of crack geometry in the global model. These factors are therefore investigated throughout this paper.

## 2   3D crack growth simulation by the proposed procedure

The proposed automated procedure to calculate 3D crack growth consists of several steps as indicated in figure 2. In the first steps data are prepared manually for the procedure to run automatically. These steps include the creation of a global finite element model used to analyze the whole domain. Furthermore a boundary element sub model is created manually based on the sub domain where the crack is supposed to grow. With the aid of the dual boundary element software BEASY an initial crack geometry is chosen and meshed into the sub model. Finally the fracture parameters are defined which are used in the crack growth analysis. These steps conclude the initial data preparation and the automated procedure is ready to be executed in batch mode.

The crack growth is modelled as an iterative procedure and for each crack extension the automated procedure activates a sequence of steps. As the crack is introduced or extended in the sub model the stiffness of both sub and global domains are changed according to the change of crack geometry. While the boundary element software takes care of the crack growth in the sub model a secondary script is needed in order to correct the stiffness of the global model. Since the sub model loading is based on the results of the global analysis the first step for each new crack increment is to update the stiffness of the global model based on the crack extension in the sub model
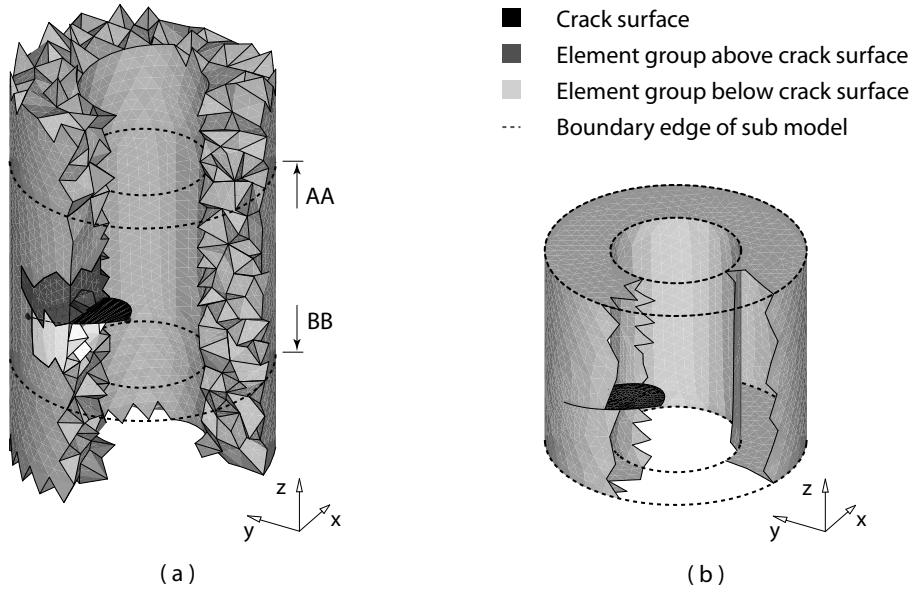
Figure 1: Submodelling strategy in which part of the global model between cut AA and BB is reanalyzed by the use of a sub model (a) Global model with rough model of crack (b) Sub model with exact crack geometry

i.e. to include a rough model of the new crack geometry in the global mesh. For this purpose an automatic modification of the global FEM mesh is carried out by an executable script to be run in the commercial mesh software named HyperMesh [19]. The advantage of using the commercial mesh software follows from the predefined routines for dealing with mesh. Furthermore the software is expected to be available in many engineering departments dealing with numerical modelling of structures. As the mesh of the global FE model is changed to describe the stiffness of the present crack configuration the next step is to solve the global FE model. In the present paper ABAQUS [18] is used as a solver. It allows to be run in batch mode and is a widely known software.

When the updated global FE model is solved the remaining steps for the current crack extension are carried out by activating the BEASY software as indicated on figure 2. The software interpolates the boundary conditions on the sub model from the solution of the global model. In this paper it is chosen to apply displacement boundary conditions to the cut faces obtained from cutting the sub model out of the global domain. Another option is to apply tractions on the cut faces but a preliminary study has shown that less accurate results were obtained. This result was explained by the fact that the traction variations were much larger over the cut faces and thus require more cut face elements to obtain the same accuracy as when
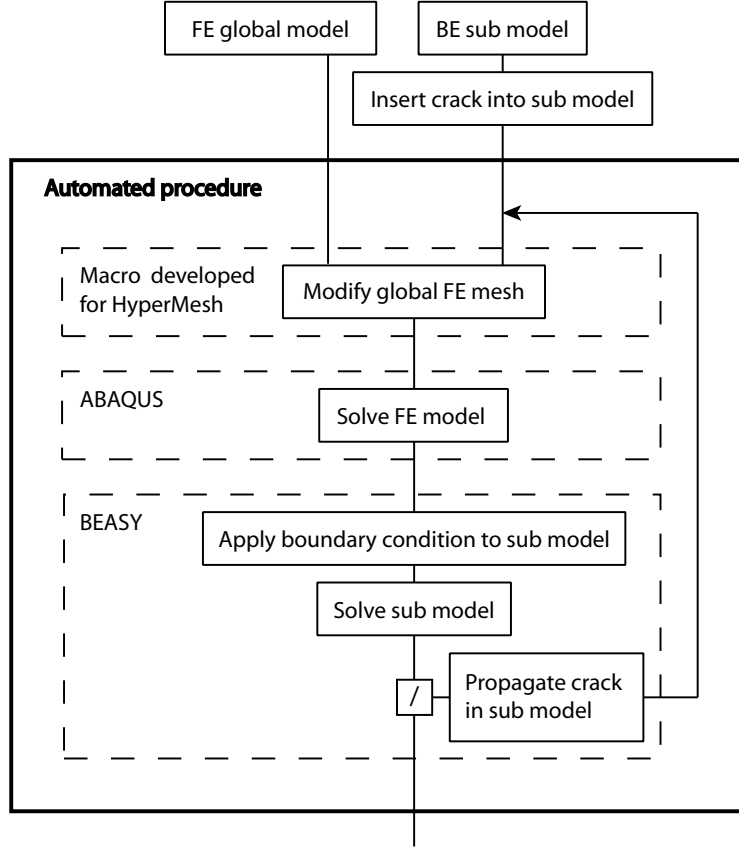
Figure 2: Automated procedure

displacement boundary conditions are applied. The sub model has now the actual load applied to it and can be solved.

Several options can be chosen for the crack growth analysis of the sub model [17] and this section only includes a brief summary of the chosen configuration used to model fatigue crack growth in a test specimen. The stress intensity factors are calculated using the J integral method by BEASY as this method is generally accepted as more precise than using the crack opening displacement (COD). To calculate the direction of the crack extension at each point of the crack front it is chosen to use the minimum strain energy density criterion [20] as this criterion has been widely used in the literature. This criterion states that the direction of crack growth at any point along the crack front is towards the minimum value of the strain energy density factor S. The strain energy density factor can be expressed as

$$S(\theta) = a_{11}(\theta)K_I^2 + 2a_{12}(\theta)K_I K_{II} + a_{22}(\theta)K_{II}^2 + a_{33}(\theta)K_{III}^2 \qquad (1)$$

where

$$a_{11} = \frac{1}{16\pi\mu}(3 - 4\nu - \cos\theta)(1 + \cos\theta)$$

$$a_{12} = \frac{1}{8\pi\mu}\sin\theta(\cos\theta - 1 + 2\nu)$$

$$a_{22} = \frac{1}{16\pi\mu}[4(1 - \nu)(1 - \cos\theta) + (3\cos\theta)(1 + \cos\theta)] \qquad (2)$$

$$a_{33} = \frac{1}{4\pi\mu}$$

in which $\mu$ is the shear modulus of elasticity and $\nu$ the Poisson's ratio. The average crack extension for each crack increment is chosen and thus in case of fatigue crack growth several crack growth laws can be used to predict the growth rate and required number of load cycles. In the present paper Paris law [22] of fatigue crack growth has been found sufficient to cover crack growth in the test specimen

$$\frac{da}{dN} = C(\Delta K)^n \qquad (3)$$

in which $\Delta K = K_{max} - K_{min}$. This equation is generally intended for mode I loading but in case of mixed-mode crack growth the value of $\Delta K$ can be replaced by $\Delta K_{eff}$ the effective stress intensity factor. Several expressions of the effective stress intensity factor have been proposed in the literature. Expressions of $K_{eff}$ by the combination of $K_I$ and $K_{II}$ were compared with experiments by Tanaka [23] and the best fitting was obtained by one expression which have been widely used. But several other expressions exist as for example by the Maximum Tangential Stress (MTS) criterion [24]. For all three modes of fracture several expressions of $K_{eff}$ also exist. The expression by Tanaka was extended [23] to cover all three modes and further Gerstle [25] proposed an expression which if the imperical constant is chosen as $B = 1$ will be equal to the expression used in [4] which is

$$K_{eff} = \sqrt{(K_I + B|K_{III}|)^2 + 2K_{II}^2} \qquad (4)$$

A more recent comparison of other expressions to predict the crack extension direction and the effective stress intensity factor can be found in [26]. In the present paper the expression (4) is adopted since it has previously been used in connection with the strain energy density criterion and good agreements with the experiments presented in the present paper are found.

## 3   Modification of finite element mesh

The mesh modification procedure has been developed for tetrahedral elements with ten nodes. These elements cause a more random placement of the element faces in the global mesh than the hexagonal elements and they will therefore better describe the shape of arbitrary cracks.
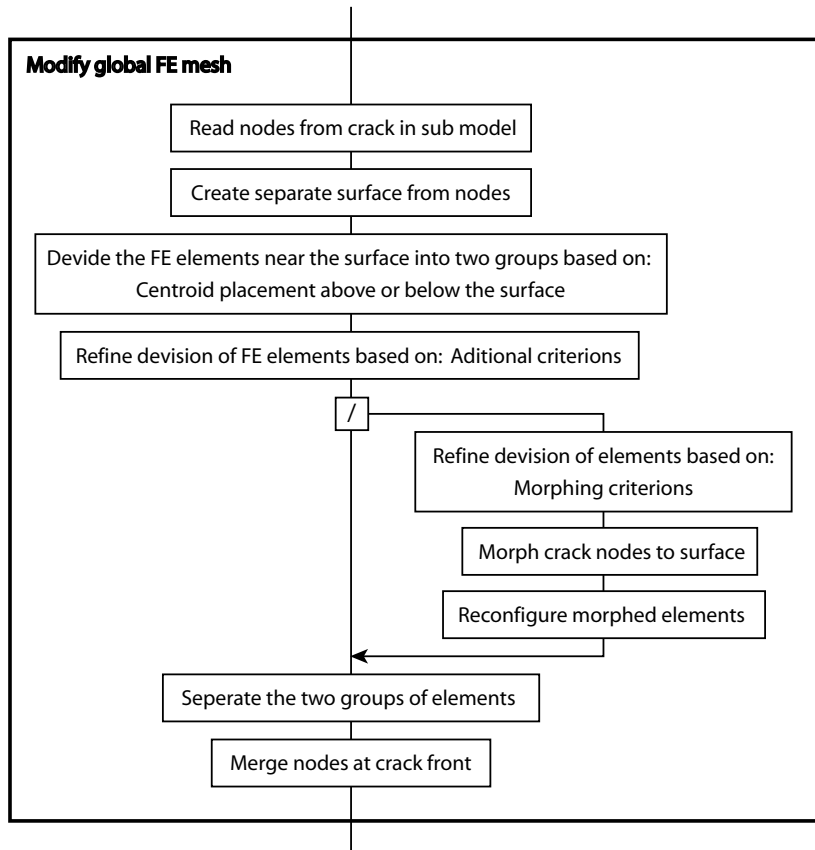
**Modify global FE mesh**

Read nodes from crack in sub model

Create separate surface from nodes

Devide the FE elements near the surface into two groups based on:
Centroid placement above or below the surface

Refine devision of FE elements based on: Aditional criterions

/

Refine devision of elements based on:
Morphing criterions

Morph crack nodes to surface

Reconfigure morphed elements

Seperate the two groups of elements

Merge nodes at crack front

Figure 3: Automated modification procedure with two different options to modify the finite element mesh

A flow chart of the script is shown in figure 3 and from this it is seen that the first step in the script is to import the crack geometry into the global model. In the BE sub model the crack is discretized by a mesh consisting of 2D discontinuous second order straight elements as illustrated in figure 4. To import this geometry crack nodes are placed in the coordinate system of the global model and from these nodes a standard command in HyperMesh can be used to generate a surface. A tolerance measure can be set to decide how closely the surface in the global model should match the nodes from the crack in the sub model. When comparing the crack surfaces in the global model and the sub model illustrated in figure 4 it is seen that a good match can be obtained for the rather advanced crack geometry.

With the crack surface imported into the global finite element model the next step is to modify the finite element mesh so that it also contains the crack. As shown in figure 3 two schemes are proposed to modify the global FE mesh. The starting point of both schemes is to divide elements around the imported crack surface into
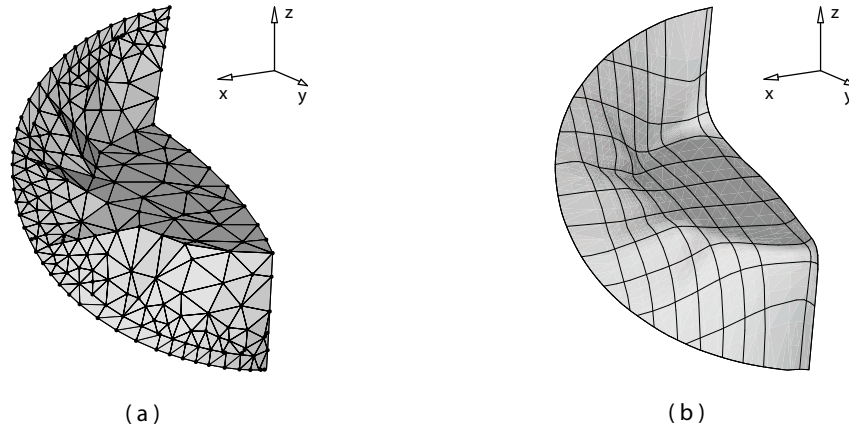
7

Figure 4: Creation of crack surface in global FE domain from the sub model crack nodes (a) Crack in sub model with only corner nodes shown (b) Created surface

two groups.

- *Divide elements in the vicinity of the crack into two groups.* The division of elements into the two groups is done by deciding whether the elements are located above or below the imported crack surface. Such a check is easily carried out by locating the centroid of the element and projecting it to the imported surface along a normal to the surface. When no surface point can be found with a normal passing trough the centroid then the element is outside the crack surface and therefore not included in either of the two groups.

In some cases such as a crack growing from a notch, elements which are not directly above or below the crack surface need to be added to one of the two groups, which requires an additional criterion.

- *Free surface crack nodes must only be connected to elements above and below the crack surface.* Elements connected to the free surface crack nodes are forced to be part of either of the group above or below the crack surface based on the placement of the element center relative to the surface.

This criterion disregards the crack front nodes. In the general case of crack growth modelling it does soon become obvious that a crack surface obtained by separation of elements due to their centroid placements will only generate a rough approximation of the crack surface in the sub model as illustrated in figure 5.a. Thus additional criteria are applied in order to refine the division of elements into the two groups and thereby create a smoother surface. The first smoothing criterion applied is

- *Smooth boundary between element groups above, below and nearby elements.* If

8

a nearby element has its four corner nodes attach to elements above or below the crack it is added to one of these groups

A typical example of this criterion can be illustrated by comparing figure 5.a with figure 5.b where it appears that an additional element face is present in the middle of the crack front after that the smoothing criterion has been applied. The next smoothing criterion applied is used to generate a more planar crack surface. This criterion considers a group of nodes which lie on the border between the element groups above and below the crack surface, called the crack nodes.

- *Smooth crack surface.* A subroutine runs through each crack node to find the distance from each crack node to the center of crack nodes on connected element corners. When the distance is found it is checked wether this distance can be minimized by moving elements connected to the present node to either the group of elements above or below the surface.

This criterion will remove peaks on the crack surface, e.g. when three faces of a tetrahedron belongs to the crack surface instead of just one of the four faces. The effect of this criterion is directly seen when comparing figure 5.a with figure 5.b, where a much more smooth surface is obtained.

In the general use of the submodelling strategy the global model is analyzed with a coarse mesh of the whole domain while the sub model is analyzed with a fine mesh of part of the domain. Based on this strategy one could argue that reasonable results can be obtained with the smoothed approximation of the crack figure 5.b in the global model and the original crack in the sub model figure 4.a. Thus when elements on both sides of the smoothed crack surface are detached the first scheme for modifying the global FE mesh is concluded.

A second scheme is now proposed as the approximation of the crack in the global model can be improved remarkably by further modification of the FE mesh. By the HyperMesh morph ability crack nodes in the FE model are moved to the imported crack surface. However, before morphing of the nodes to the crack surface an additional refinement of the element division is needed in order to avoid element collapse. One of two criteria applied ensures that none of the tetrahedral elements will have three corner nodes moved to the crack front line since this will force the element to collapse.

- *Elements are not allowed to have three corner nodes among the crack front nodes.* If an element has three corner nodes among the crack front nodes this element and its connected elements will be separated into twice the number of elements such that the three crack front nodes are divided on to two element faces as demonstrated in figure 6

△ Crack element faces of global FE model
— Boundary of crack surface were visible above element faces
⋯ Lines on crack surface were visible above element faces
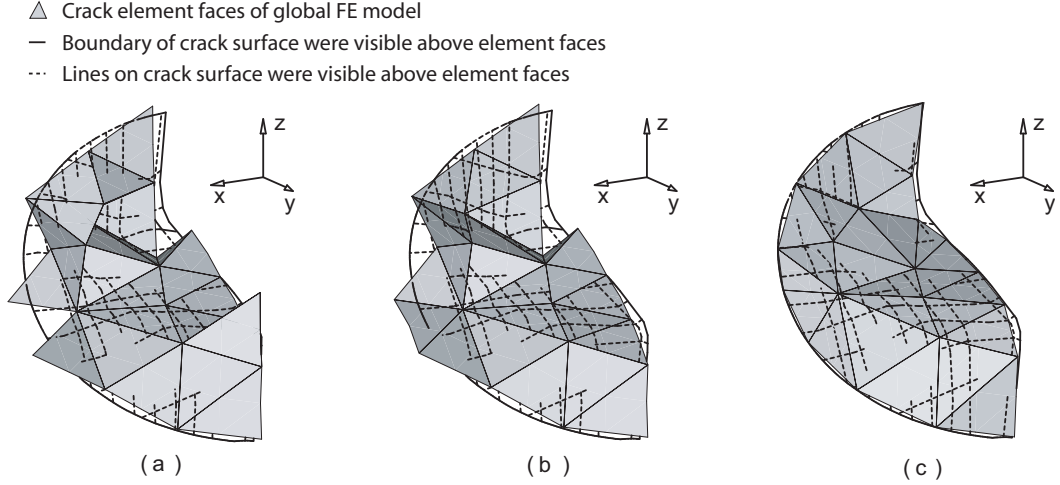
( a )          ( b )          ( c )

Figure 5: Crack element faces compared to crack surface in global FE domain (a) Rough crack (b) Refined crack after smoothing (c) Refined crack after morphing

Furthermore, a criterion is defined to avoid that all four corner nodes of a tetrahedral element lie on a planar surface, as this would cause the element to collapse.

- *Elements are not allowed to have all the four corner nodes among crack nodes* If an element after the smoothing criterion has been applied has four corner nodes among the crack nodes, this element and connected elements are separated into twice the number of elements leaving an extra non-crack node in the center as demonstrated in figure 6.

After these pre-morph criteria have been applied the morphing of crack nodes to the crack surface and the crack front nodes to the crack front line are carried out. At the present stage in the development of the morphing procedure in HyperMesh the mid-nodes of the ten noded tetrahedral elements can be misplaced. These nodes are replaced by aligning them between the corner nodes of the elements or by using the HyperMesh remesh command on the element groups above and below. The remesh command further makes it possible to remove nearly collapsed elements. The effect of these morphing criterions has not been illustrated graphically but it is shown in the remaining calculations of this paper that it has been possible to carry out the calculations purely automatically. The result of the morphed crack surface is illustrated in figure 5.c.

## 4 Test specimen from engine part of large two stroke engine

To validate the proposed method to analyze 3D crack growth a structure containing a crack will be analyzed with the proposed method and important parameters will be varied.
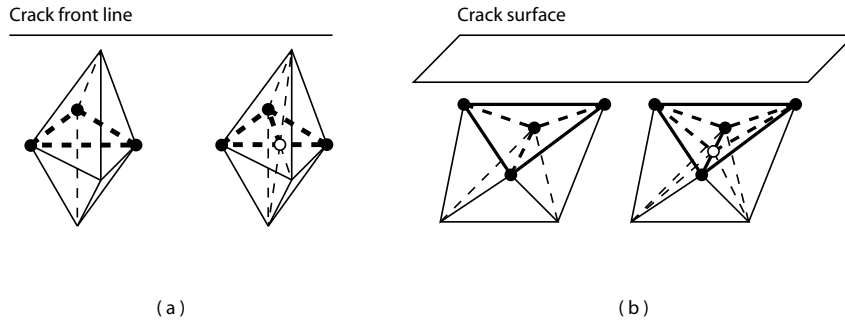
10

Figure 6: Illustration of the cutting procedure to avoid that an element has four corner nodes among crack nodes.

The results obtained with the proposed submodelling strategy are evaluated by comparing to the corresponding results obtained with a global cracked BE model. Because of the simplicity of the model analyzed in the present paper it is still within a reasonable time limit to mesh and solve the global BE model than compared to the global FE model. The elements used to mesh the global BE model have the same small size as those in the BE sub model both in the vicinity of the crack and in the remaining domain. Thus due to the small element size and the excellent precision of the boundary element method very precise results are obtained with the global BE model.

In connection with the introduction of a new welded design in the large two stroke diesel engines several experiments and numerical calculations related to fatigue crack growth were performed on parts of the new welded structure [21]. The test specimen which is illustrated in figure 7 is part of the new structure which supports the crosshead bearing so that it only moves laterally. The crosshead bearing connects the piston rod with the connecting rod and it is thereby part of the mechanism which converts the vertical oscillation of the piston to a rotation of the crank shaft. Test specimens have especially been tested for fatigue crack growth at the welds marked by B and C in figure 7. To estimate the effect of residual stresses remaining from the welding process half of the test specimens received a post weld heat treatment. Fatigue crack growth in these specimens can be evaluated using Linear Elastic Fracture Mechanics in connection with the proposed method.

This paper treats crack growth in area B illustrated in figure 7. To investigate crack growth in this area a crack notch of 8 mm is introduced by a careful welding process which leaves part of the contact surface unbound. The crack front is expected to develop from this notch when the structure has been exposed to several load cycles. The oscillating load is applied to the glide plane of the structure as demonstrated in figure 8. When modelling the test specimen it is chosen to use a symmetry approximation which would actually require that cracks were growing simultaneously
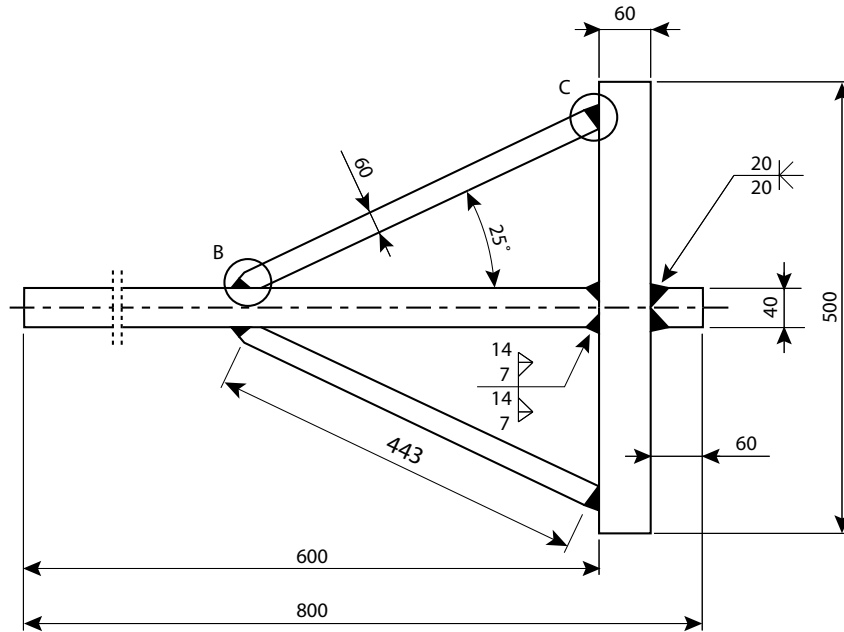
11

Figure 7: Test Specimen with thickness of 65 mm

on both sides of the middle plate. This assumption is not practically imaginable but a preliminary study has shown that the symmetry assumption gives little difference from separate growth of one of the cracks. The oscillating load applied to the test
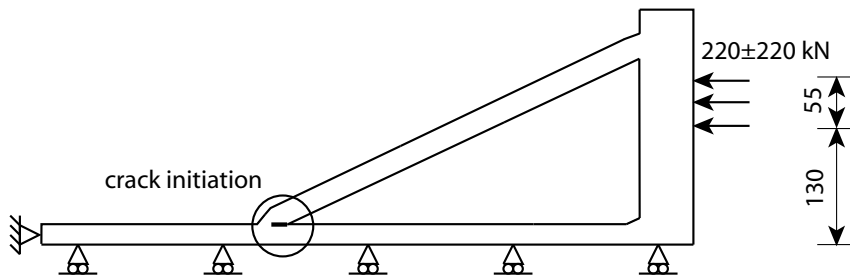


Figure 8: Loaded model of the test specimen

specimen will result in an in-plane mixed mode loading of the crack front. Due to this loading a curved crack path is expected to develop. In the following two sections dealing with the crack in the test specimen the parameters influencing the proposed method will be studied for the initial crack. Finally, the predicted crack path is compared with the crack path observed in the experiments.

12

## 5  Influence of the global element size on the analysis of the initial crack

The present section studies the influence of the global element size on the proposed method for evaluation of stress intensity factors along the crack front of the initial crack. To perform this study two questions are of primary interest. One is how well does the submodelling strategy perform in the case of crack growth and the other is how does the mesh modification procedure perform? To answer these two questions each of six different global FE models is used to load the corresponding cracked BE sub model figure 12.a.

The mesh modification procedure is developed for ten noded tetrahedral elements and thus this type of elements are placed in the area of the global model where the crack is supposed to grow as shown in figure 9. The connections between tetrahedral elements and hexagonal elements are made with constrained relations on the nodes of the common surfaces [18]. Two of the global FE models each with different element size have a manually created crack represented in the mesh which perfectly matches the crack in the sub model. The four other global models have a random mesh in the area around the crack as illustrated in figure 9. For these four models the crack representation is obtained from the mesh modification procedure. It is chosen to produce two models with a smoothed surface and two models with a morphed surface. The random tetrahedral mesh is created with an average element edge size of 2.5 mm or 5.0 mm, respectively, to ensure that the initial crack of 8.0 mm would not fit directly into the global mesh.
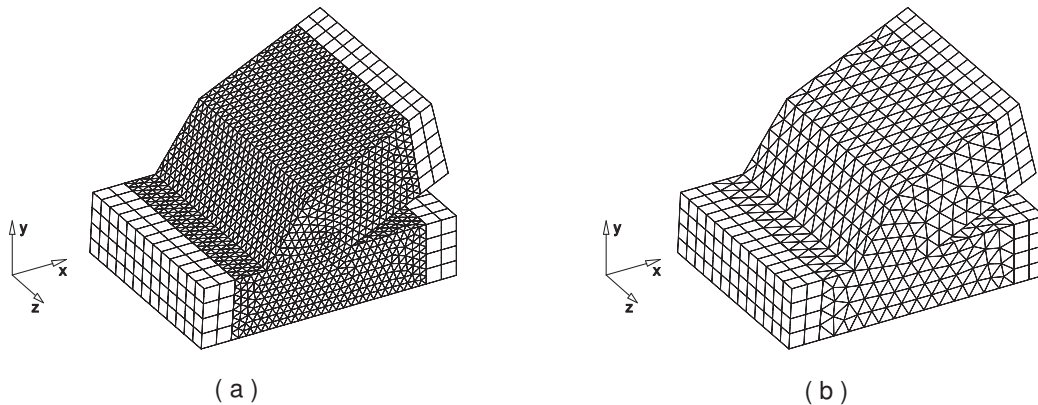


Figure 9: Global mesh in the vicinity of the crack (a) Average tetrahedron size 2.5 mm (b) Average tetrahedron size 5.0 mm

The crack surfaces introduced in the six different global models can now be compared as shown in figure 10 where the element faces between the elements above and below the crack surface have been plotted. It appears clearly that the crack surfaces created from the smoothed element faces on figure 10 s1 and s2 deviate the most from the original crack surface in the sub model. A better approximation of the original crack

13

surface is obtained when increasing the number of elements. The two crack surfaces created by the mesh modification procedure when using morphing on figure 10 s3 and s4 both describe the exact shape of the original crack. For both surfaces it is seen that while the element edges before morphing were of almost equal length their lengths differ after morphing. The crack surfaces obtained by manual modifications of the mesh match the original crack surface perfectly. Furthermore the element configurations are kept much more constant than is the case of the morphed surfaces.
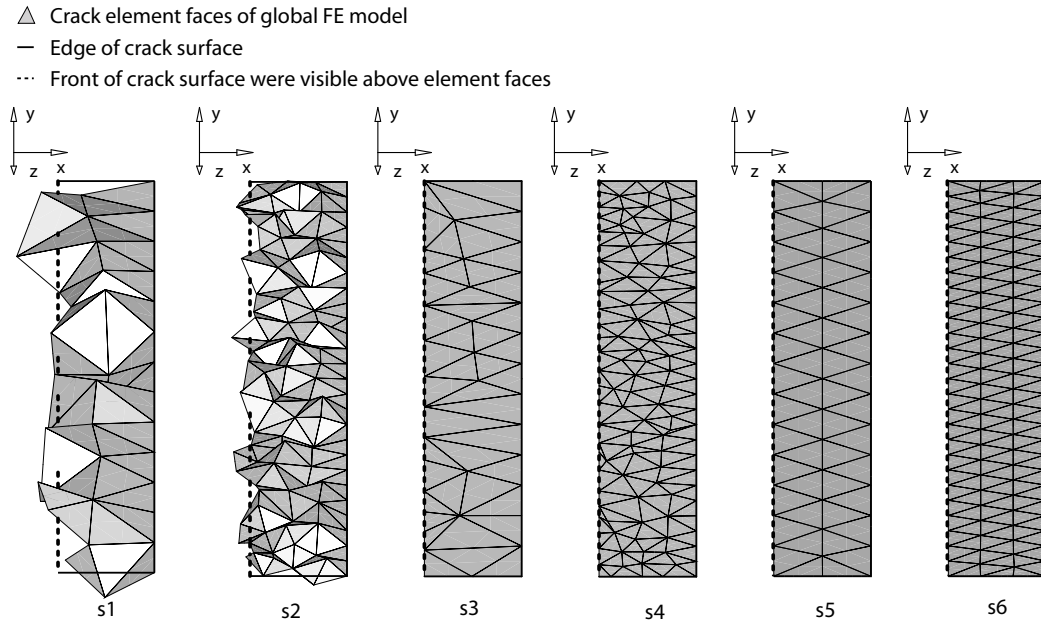


Figure 10: Crack element faces shown in perspective with average element size of 2.5 mm or 5.0 mm (s1-s2) Smoothed surfaces (s3-s4) Morphed surfaces (s5-s6) Manually meshed surfaces

The displacement field of each of the six different global models is used to interpolate to the boundary conditions on a sub model. For each sub model the same LEFM parameters have been used to ease the comparison of the results. Since the problems studied are primarily in-plane problems, figure 11 only shows the $K_I$ and $K_{II}$ factor along the crack front. Comparing the values of the $K_I$ factor along the crack front it becomes obvious that the results obtained with the smoothed crack surfaces differ in the way that they have the largest deviation of approximately 4 % below the results of the global BE solution. While the results obtained with both the morphed surfaces and the manually meshed surfaces undershoot with approximately 2 %. By halving the number of elements in the vicinity of the crack in the global model the deviation is increased by approximately 1 % for the morphed and the manual meshed crack

surface in the global model. For the smoothed surface it is interesting to observe that while the results calculated with different element sizes deviate noticeable in one end of the crack front they match in the other end. The matching results can clearly be explained by the crack front configuration in the global model figure 10 since the crack surface with large elements ($s1$) has a larger crack length in one end of the crack front and thus larger values of $K_I$.

The figure displaying the $K_{II}$ values shows more even results with less deviations. The results obtained with the smoothed surfaces overshoot the global solution by approximately 1.5 % while results obtained with the morphed and manually meshed surfaces are closer to the global solution with a deviation of 0 to 1 %. Almost no effect is obtained from doubling the number of elements close to the crack.
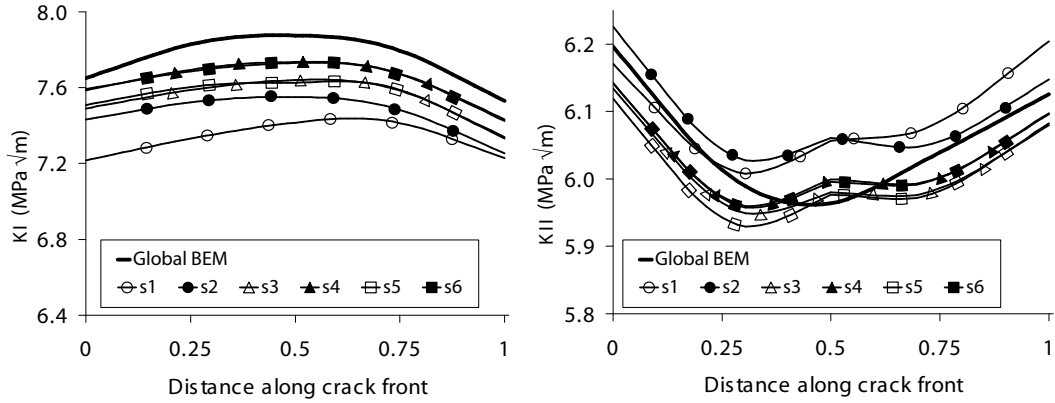


Figure 11: Values of $K_I$ and $K_{II}$ along the crack front for the maximum loading

The larger and more consistent deviations for the $K_I$ values compared to the $K_{II}$ values can be explained by the fact that these two factors express different properties of the structure. The opening of the crack expressed by the $K_I$ factor depends on the global stiffness of the structure relative to the loading. The sliding of the crack faces relative to each other expressed by the $K_{II}$ factor depends on the relative stiffness of the structure. Based on this interpretation of the $K_I$ and $K_{II}$ factors the results suggest that the global stiffness of the FE models are larger than for the global BE model. The results further suggest that the relative stiffness of the two global models is much the same which correlates with the equal geometry and loading.

From the presented results it is found that the results obtained with the morphed surfaces have such small deviations from the results obtained with the manually meshed surface that it can be concluded that the automatic mesh modification procedure gives just as good results as manual remeshing.

15

## 6 Influence of the sub model size on the analysis of the initial crack

When varying the size of the sub model it is expected that this will influence the evaluation of stress intensity factors along the crack front of the initial crack. One of the reasons for this influence can be found from the different displacement and stress fields predicted with an even FE mesh compared to a BE mesh refined in the area of the crack. A small sub model with boundary conditions interpolated from the global FE mesh would then have displacement and stress fields corresponding mostly to the FE model. By contrast a large sub model with boundary conditions interpolated from the global FE mesh will have displacement and stress fields more in agreement with the BE mesh. To study the effect of the sub model size the results from the sub model used in previous calculations are compared with results obtained with a much smaller sub model as illustrated in figure 12b.
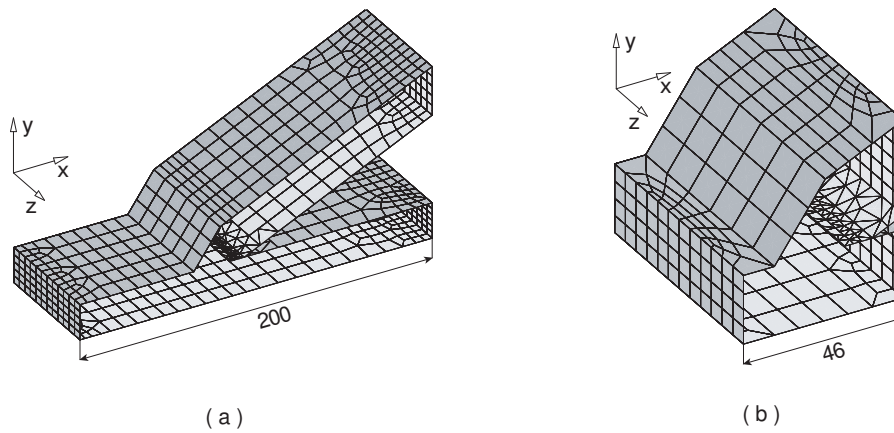


Figure 12: Boundary element sub models with one side removed (a) Model used for most analyses (b) Small sub model (s.s.m.)

The results obtained with different size of the sub model and different modifications of the global mesh are illustrated in figure 13. When comparing the results of $K_I$ along the crack front it is generally seen that the $K_I$ calculated with the small sub model undershoot the values calculated with the larger sub model. For the smoothed and morphed formed surface the deviation from values obtained with the global BE model are 8% and 3.7 % which is roughly twice the deviation obtained with the large sub model. When comparing the values of $K_{II}$ it is much more difficult to express a general trend. The maximum deviation between results obtained with the two sub models is approximately 1.5 % and the maximum deviation from results obtained with the global BE model is approximately 4 %.

The results obtained in this section support the results from the previous section, i.e. the global FE model is more stiff than the global BE model and the deviations are doubled as the sub model size is decreased. The deviations also were doubled
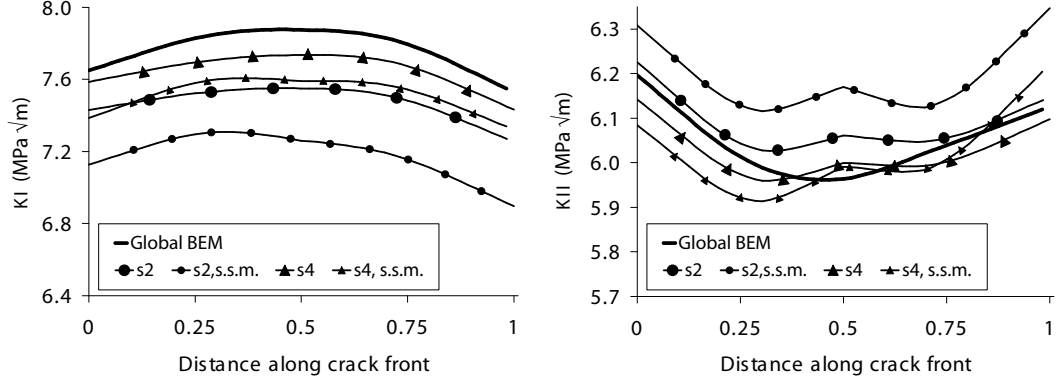
Figure 13: Values of $K_I$ and $K_{II}$ along crack front for the maximum loading

with the results obtained for the morphed surface, which was unexpected. Other effects can also influence the results such as the cut surfaces on which the boundary conditions are applied are moved much closer to the crack front as the sub model size is decreased. Any approximation introduced in the interpolation of the boundary conditions may affect the stress field around the crack.

## 7    Analysis of crack growth from the initial crack

The comparison of stress intensity factors from the different calculations for the initial crack configuration demonstrates that accurate results are obtained with the proposed method. In the present section the study on the initial crack is extended to demonstrate the capabilities of the proposed method to analyze crack growth. The calculations have been carried out both by a global boundary element model and by the proposed method. For the proposed method the large sub model and the two different sizes of tetrahedral elements in the global model have been applied.

To perform the fatigue growth analysis of the structure several material tests have been performed for a load ratio of $R = K_{min}/K_{max} = 0.1$. Figure 14 illustrates test results obtained for three different Single Edge Notched Bend specimens (SENB). Since the crack growth in the welded design remains within the regime of a constant slope between the crack growth rate and variation of the stress intensity factors, Paris law [22] has been fitted to the test results. Based on this fitting it is found that $C = 9 \cdot 10^{-13}$ and $n = 3.25$ in Eq. (3) when the unit of $\Delta K$ is MPa$\sqrt{m}$ and the crack growth distance is calculated in meters. These values are in agreement with values of standard construction steel.

The crack growth analysis is performed by extending the crack in six increments and for each of the crack increments the FE mesh is modified to describe the stiffness change for the new crack configuration. The two different schemes for modifying the FE mesh have been applied to the crack growth analysis as illustrated for every second crack increment in figure 15. The figure illustrates the differences in ap-
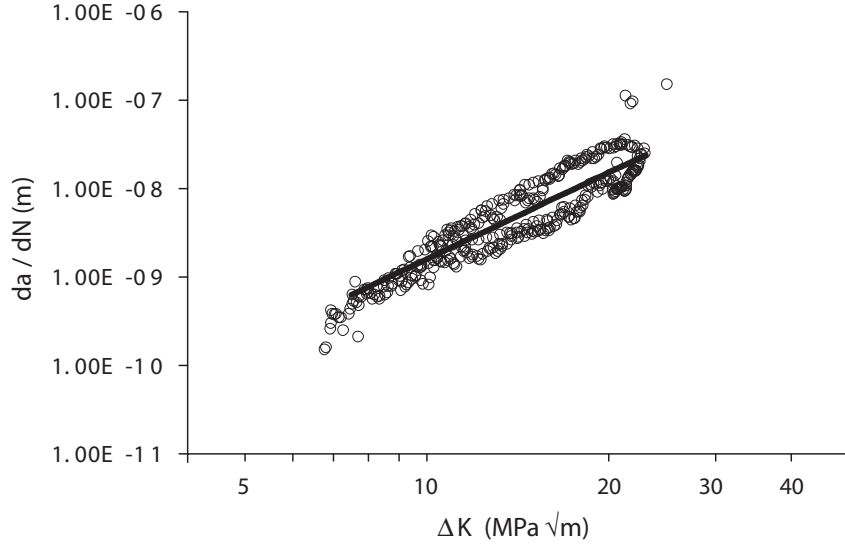
17

Figure 14: Fitting of Paris law to measurements of crack growth in SENB test specimens

proximations of the actual crack geometry by the two schemes. For a crack surface obtained by separation of elements it is seen that the extension of the crack front is done in jumps dependent on the element location at the actual crack front. For this surface it is further observed that as the crack grows the size of the FE elements in the global model decreases compared to the total crack length. For this reason it could be expected that less deviations are obtained in the results as the crack grows. A better match of the crack in the sub model is obtained when the FE-mesh is modified using morphing as illustrated in the figure 15 d, e and f. It is observed that the crack surface is not completely smooth as the mid-nodes of the elements are placed directly in between the corner nodes. Morphing of the mid-nodes to the crack surface is however expected to have no influence on the results.

The evaluation of the proposed method to analyze crack growth is carried out by comparing results of the $K_I$ and $K_{II}$ factors for each crack increment. In previous sections it was shown that variations of the $K_I$ and $K_{II}$ were rather limited along the crack front and thus to ease the comparison the values are only compared for the center point on the crack front. The calculated values of $K_I$ and $K_{II}$ are shown in figure 16 for the global BE model and for the proposed method. The values shown in the figure are not directly comparable after the first crack extension since deviations of the values of the stress intensity factors result in different crack paths. The differences in crack path are however expected to be small as there is a reasonable correlation between the stress intensity factors and as the average crack extension of 2 mm is kept constant for all calculations. Comparisons of the $K_I$ values shows
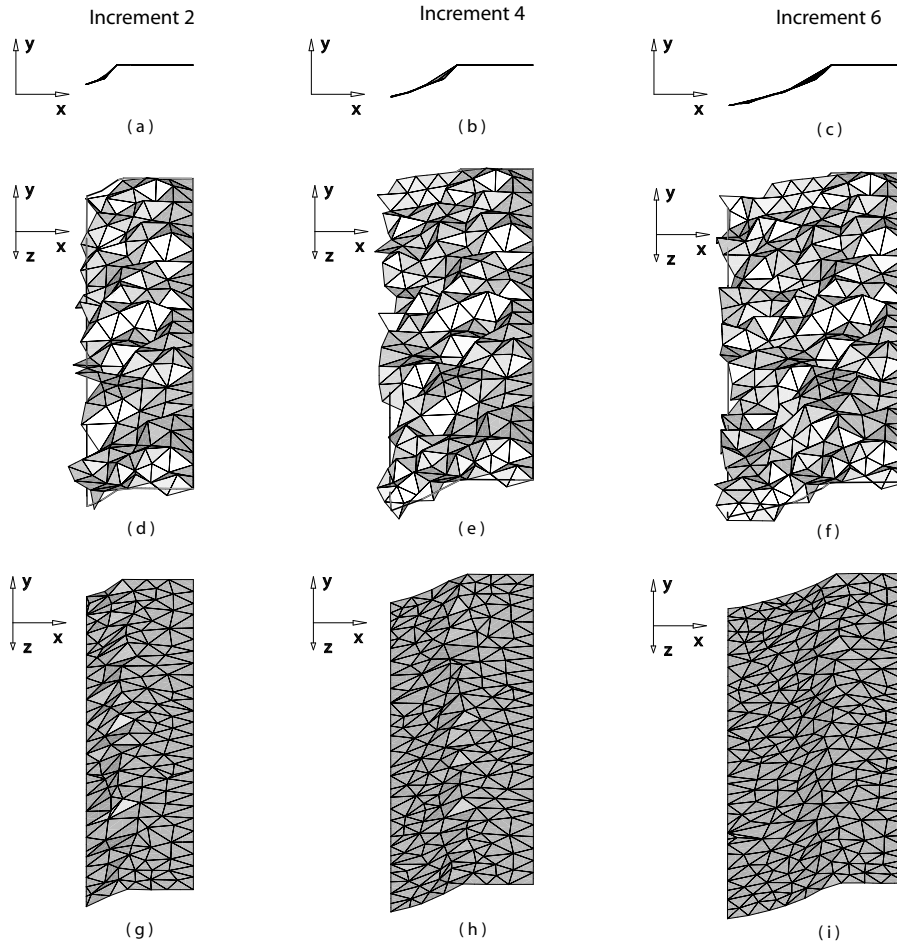
18

Figure 15: Growth of the crack (a-c) Crack in sub model seen along z-axis (d-f) Perspective view of smoothed crack element faces in global FE model (g-i) Perspective view of morphed crack element faces in global FE model

a general increase when the crack grows as would be expected because the stiffness of the structure is reduced while the loading is held constant. The largest deviation of 6 % from the global BE solution is as expected obtained for the smoothed crack surface with an element size of 5.0 mm in the global model. From this solution it is further seen that the deviation from the global BE solution increases and decreases, which can be explained by the dependence on the element locations in front of the crack. The solutions obtained for the proposed method using smoothing with small elements and morphing with large elements are almost the same with a maximum deviation of approximately 3%. The solution obtained with morphing and small elements has a maximum deviation of approximately 2%. Values of $K_{II}$ tend toward zero after the first crack increment as can be expected from the use of the crack

growth criterion. Small variations in the crack shape for each calculation will result in noticeable variations in the $K_{II}$ value and thus when the values are close to zero large percentage deviations are found. The existence of small variations in the predicted crack shapes are indicated by the increased deviations in the $K_{II}$ values when the crack grows.
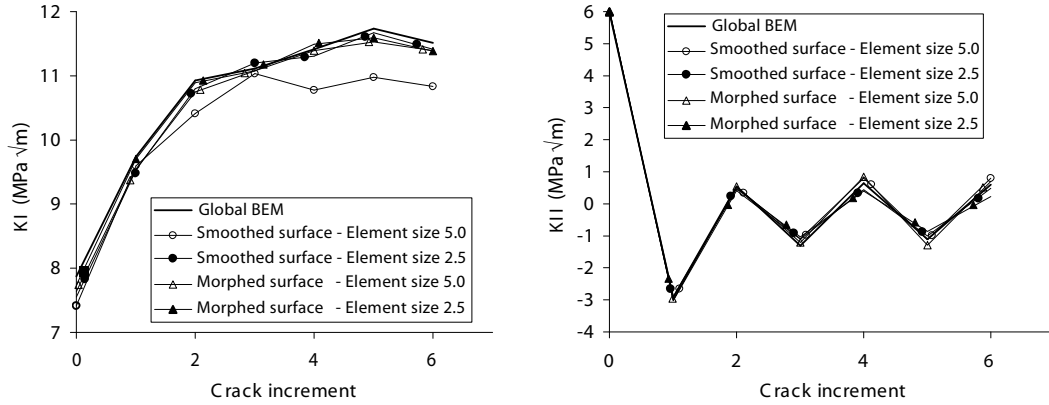


Figure 16: Values of $K_I$ and $K_{II}$ at the center point of the crack front for each crack increment

## 8   Comparison with experiments

In the present paper the global BE model has been used as a reference to evaluate the validity of the proposed method. Since the reference is only a model one could question the comparison if no relation was drawn to real observations. Therefore, comparison of crack path and crack growth rates are done for the calculations and an experiment. Results from the experiments [21] are shown in figure 17. When comparing the crack path obtained in the experiment with the calculated crack path represented by the sub model crack in figure 15.c a nearly perfect match is observed. The test specimen is observed to have a secondary crack which might be caused by a non linear effect but that would not be discussed further in this paper. During the fatigue loading of the test specimen crack propagation gauges have been mounted on each side of the structure perpendicular to the pre-crack just at the crack front. These gauges are able to detect 20 crack increments of 0.25 mm when the crack grows perpendicular to the gauge. Thus for the present test specimen the crack growth has been monitored for the first 5 mm in which the crack roughly grows with an angle of 30° to the initial crack. The results of the crack gauges show as expected that the crack propagates equally fast on both sides of the structure. The average crack growth rate measured by the two gauges can be calculated by the results shown in figure 17 to be $4.6 \cdot 10^{-9}$ m/cycle and $6.3 \cdot 10^{-9}$ m/cycle. When these crack growth rates are compared with the results of the material testing figure 14 it can be seen that $\Delta K_{eff}$ at the crack front can be expected to be in the range of

20

$12 - 15.5 MPa\sqrt{m}$. The calculated $\Delta K_{eff}$ for the pre-crack and the first increment are 12 $MPa\sqrt{m}$ and $11.5 MPa\sqrt{m}$ respectively. Thus good agreements between the calculated and measured crack growth rates are obtained.
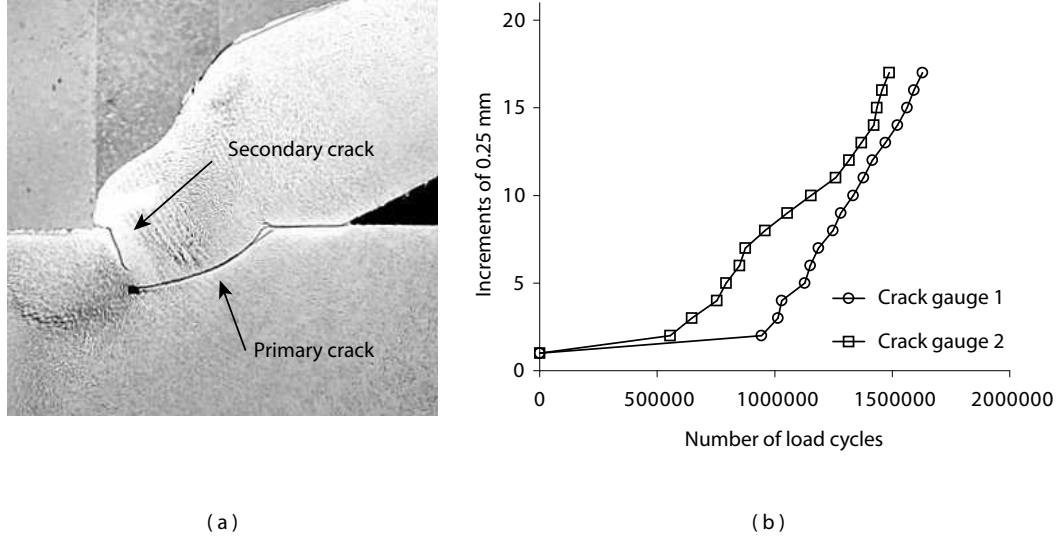


(a)

(b)

Figure 17: Test Results (a) Cracks in test specimen (b) Measured crack increments of primary crack

## 9    Conclusion

A new procedure to analyze non-planar 3D crack growth has been proposed. The proposed method takes advantage of a submodelling strategy in which the crack in the global model can be described by two different approximations of the real crack in the sub model. It has been shown by numerical evaluation of the method that precise results are obtained by either separating the elements in the global model as they are or by morphing them to fit the geometry of the real crack surface before they are separated. A much smaller number of elements is needed around the crack in the global model in cases where the morphing procedure was used. Investigations of the element size in the global model and the size of the sub model both showed an influence on the results as expected. By increasing the number of elements in the global model or by increasing the size of the sub model the precision could be increased. The proposed method was further used to analyze a case of crack growth on a test specimen which is part of a large diesel engine. The proposed method shows a good agreement with the experiments for the predicted crack path as well as the crack growth rate. According to the results it can be concluded that

21

the proposed method can be used to perform accurate numerical evaluations within linear elastic fracture mechanics. An important feature of the proposed method is that an accurate crack analysis can be incorporated in a large FE computation that has been previously developed for a complex engineering structure such as a big ship diesel engine.

**Acknowledgements**

**References**

[1] Lucht T, Aliabadi MH. Correction to the crack extension direction in numerical modelling of mixed mode crack paths. International journal of fracture 2007; 143(2): 195-202

[2] Lucht T. DBEM Analysis of axisymetric crack growth in a piston crown. 16th European Conference of Fracture 2006; (On CD)

[3] Mi Y, Aliabadi MH. 3-Dimensional crack-growth simulation using BEM. Computers & Structures 1994; 52(5): 871-878.

[4] Mi Y, Aliabadi MH. An automatic procedure for mixed-mode crack-growth analysis. Communications in Numerical Methods in Engineering 1995; 11(2): 167-177.

[5] Carter BJ, Wawrzynek PA, Ingraffea AR. Automated 3-D crack growth simulation International Journal for Numerical Methods in Engineering 2000; 47(1-3): 229-253

[6] Spievak LE, Wawrzynek PA, Ingraffea AR, et al. Simulating fatigue crack growth in spiral bevel gears. Engineering Fracture Mechanics 2001; 68(1): 53-76

[7] Cisilino AP, Aliabadi MH. Dual boundary element assessment of three-dimensional fatigue crack growth Engineering Analysis with Boundary Elements 2004; 28(9): 1157-1173

[8] Kolk K, Weber W, Kuhn G. Investigation of 3D crack propagation problems via fast BEM formulations Computational Mechanics 2005; 37(1): 32-40

[9] Krysl P, Belytschko T. The element free galerkin method for dynamic propagation of arbitrary 3D cracks. International Journal for Numerical Methods in Engineering 1999; 44: 767-800.

[10] Moes N, Gravouil A, Belytschko T. Non-planar 3D crack growth by the extended finite element and level sets - Part I: Mechanical model. International Journal for Numerical Methods in Engineering 2002; 53(11): 2549-2568

[11] Gravouil A, Moes N, Belytschko T. Non-planar 3D crack growth by the extended finite element and level sets - Part II: Level set update. International Journal for Numerical Methods in Engineering 2002; 53(11): 2569-2586

[12] Areias PMA, Belytschko T. Analysis of three-dimensional crack initiation and propagation using the extended finite element method. International Journal for Numerical Methods in Engineering 2005; 63(5): 760-788

[13] Duarte CA, Hamzeh ON, Liszka TJ, W.W. Tworzydlo. A generalized finite element method for the simulation of three-dimensional dynamic crack propagation. Computer Methods in Applied Mechanics and Engineering 2001; 190(15-17): 2227-2262

[14] Schöllmann M, Fulland M, Richard HA. Development of a new software for adaptive crack growth simulations in 3D structures. Engineering Fracture Mechanics 2003; 70(2): 249-268

[15] Han ZD, Atluri SN. SGBEM (for cracked local subdomain) - FEM (for uncracked global structure) alternating method for analyzing 3D surface cracks and their fatigue-growth. Computer Modeling in Engineering & Sciences 2002; 3(6): 699-716

[16] Frangi A, Novati G. BEM-FEM coupling for 3D fracture mechanics applications Computational Mechanics 2003; 32(4-6): 415-422

[17] BEASY version 10 release 8 Documentation 2007

[18] Abaqus version 6.5-1 Documentation 2004

[19] HyperMesh version 8.0sr1 Documentation 2007

[20] Sih GC. Strain energy density factor applied to mixed mode crack problems, International Jounal of fracture 1974; 10(3): 305-321

[21] Hansen AV, Olesen JF, Agerskov H. An investigation on the influence of root defects on the fatigue life of the welded structure of a large two-stroke diesel engine. Welding in the World, Journal of the International Institute of Welding 2004; 48(5): 46-55

[22] Paris PC and Erdogan F. A Critical Analysis of Crack Propagation Laws. Journal of Basic Engineering 1963; 85(4): 528-534

[23] Tanaka K. Fatigue crack propagation from a crack inclined to the cyclic tensile axis. Engineering Fracture Mechanics 1974; 6(II): 493-507

[24] Erdogan F, Sih G. On the crack extension in plates under plane loading and transverse shear. Journal of Basic Engineering 1963; 85: 519-527

[25] Gerstle WH. Finite and boundary element modelling of crack propagation in two and three dimensions using interactive computer graphics. PhD Thesis, Cornell University, New York, 1985

[26] Richard HA, Fulland M, Sander M. Theoretical crack path prediction. Fatigue & fracture of engineering materials & structures 2005; 28(1-2): 3-12